-

University of Cape Town

Non-isothermal dynamics of thin-film free-surface and channel flows of non-Newtonian nanofluids

IDREES KHAN

University of Cape Town

Supervisor

Dr: Tiri Chinyoka

Thesis submitted for the degree of

DOCTOR OF PHILOSOPHY

Department of Mathematics and Applied Mathematics

February 2022

The copyright of this thesis vests in the author. No quotation from it or information derived from it is to be published without full acknowledgement of the source. The thesis is to be used for private study or non-commercial research purposes only.

Published by the University of Cape Town (UCT) in terms of the non-exclusive license granted to UCT by the author.

University of Cape Town

The copyright of this thesis vests in the author. No quotation from it or information derived from it is to be published without full acknowledgement of the source. The thesis is to be used for private study or non-commercial research purposes only.

Published by the University of Cape Town (UCT) in terms Of the non-exclusive license granted to UCT by the author.

Abstract

Numerical modelling of the dynamic behaviour of generalized-viscoelastic-fluid-based nanofluids (GVFBNs) and viscoelastic-fluid-based nanofluids (VFBNs) has a number of industrial applications such as in new battery technologies and phase-change heat transfer devices. The computational results have shown that for certain flow parameters values, some of the non-Newtonian fluids also known as complex fluids (e.g. worm-like micellar solutions, granular flows, polymer solutions and some polymer melts) reveal flow instabilities within the flow field, such as the emergence of regions of different shear bands due to the flow induced material non-homogeneities. It has also been observed that it is becoming increasingly clear that the thermal run-way phenomenon should not be ignored in polymers or other complex fluids since it may, in some instances, be as important as the complex rheology in differentiating susceptibility order for different types of nanofluids, for instance Newtonian fluid Based Nanofluids (NFBN), Generalized Newtonian Fluid-Based Nanofluids (GNFBN), Viscoelastic-fluid based nanofluids (VFBN) and Generalized viscoelastic fluid based nanofluids (GVFBN). These computational observations laid the foundation of this thesis.

We have investigated the improvement of heat transfer for GVFBN and VFBN by homogenously mixed spherical shape nanoparticles. To incorporate the nanoparticles in the governing equations we use a single phase nanofluid modelling approach. Our mathematical models are governed by a system of non-linear, highly coupled, time-dependent Partial Differential Equations (PDEs). We developed computational solutions in Matlab software for the resulting system of equations by using an efficient semi-implicit finite-difference method, combined with a Crank-Nicolson scheme. In addition, the effects of nanoparticles on fluid velocity, extra stresses, temperature, and thermal conductivity are explored. Comparisons of the numerical results for the nanofluids with those from the literature without nanoparticles show excellent agreement.

Dedicated to my lovely wife, Daughter (Yousra Bibi) and son (Mohammad Hanzala Khan Safi).

Acknowledgements

In the name of ALLAH, the Most Gracious and the Most Merciful, all praise is for ALLAH; we praise Him, seek His help, and ask for His forgiveness. I am thankful to ALLAH, who gave me the courage, wisdom, guidance, knowledge and helped me throughout in completing this research. Also, I cannot forget the ideal man of the world and most respectable personality for whom ALLAH created the whole universe, Prophet Muhammad (Peace Be Upon Him).

Foremost, I would like to express my heart-felt gratitude to the most cooperative and great communicator, my supervisor Dr.Tiri Chinyoka and for his consistent tireless support and assistance throughout the course of this work. The doors towards my supervisor were always open. His guidance helped me throughout the research and writing of this thesis. He has always helped me out and tolerated my untimely disturbances.

I express my deepest sense of gratitude and sincere feelings of reverence and regard to my Co-supervisor Dr.Andrew Gill, whose encouragement helped to put me on the right track for achieving my goal.

My special thanks goes to the Mechanical Engineering department, Foundation Contingency as well as the National Research Foundation (NRF) for awarding me a scholarship that financed my studying and living expenses throughout the course of this study.

My sincere thanks go to the staff at the Department of Mathematics at the University of Cape Town (UCT) for their willingness to help with all the administrative processes.

I am very thankful to the effort of my honorable teachers and close friends, who updated my thinking, vision, knowledge, and efficiency. This improved me on a mental, physical, emotional and cultural level. Dr.Taza Gul, who give me great support and courage towards the completion of my research work. I would also like to especially express my deep indebtedness and cordial thanks to my friend Dr.Arif Ullah Khan, whose cooperation helped in resolving every difficult situation I con-

fronted.

I also wish to express my earnest gratitude to my father Haji Dost Muhammad Khan and my sweet mother, for their support and prayers. I am extremely thankful to my elder brother Dr.Muhammad Zahid Shah, for his support and source of encouragement during my studies and for his incessant support to my family during this time.

Finally I enjoyed the study with my beloved Wife, the Queen of my heart and cute children Yousra Bibi and Muhammad Hanzala Khan Safi.

Author's declaration

I Idrees khan, declare that this Ph.D thesis entitled "Non-isothermal dynamics of thin-film free-surface and channel flows of non- Newtonian nanofluids" is original and my own work. It is being submitted for the degree of DOCTOR OF PHILOSOPHY at the University of Cape Town. It has not submitted by me before for any degree or examination at the University of Cape Town, South Africa or anywhere else in the country/abroad.

SIGNED:..... Signed by candidate .....

DATE: ..... 14/02/2022 .....

"I confirm that I have been granted permission by the University of Cape Town's Doctoral Degrees Board to include the publication(s) (Chapter2, Chapter3, Chapter4, Chapter5) in my PhD thesis, and where co-authorships are involved, my co-authors have agreed that I may include the publication(s):"

SIGNED:..... Signed by candidate .....

DATE: ..... 14/02/2022 .....

Table of Contents

Chapter 1 Introduction

1.1 Nanofluid

For the development of industrial applications and research, the fluid and heat transfer (HT) carry's great importance. To enhance the order of the process is one of the main themes of the scientists and physicists; this is possible to design the process in which the energy can be transferred effectively. Heat transfer (exchange of thermal energy from one body to another at various temperatures) performance of a system is limited, due to the relatively poor thermophysical properties, of the conventional working fluids (e.g, water, engine oil, ethylene glycol, propylene glycol (PG), viscoelastic and generalized viscoelastic etc.). Therefore to enhance the thermophysical properties (i.e thermal conductivity, density, viscosity etc.) of the conventional fluids seems to be the best way to obtain the efficiency in heat transfer applications. The dispersion of uniformly tiny size particles having advance thermophysical properties into regular fluids called "base fluids" to form a suspension having improved thermophysical properties, thus show enhancement in the heat transfer characteristics. The first research on nanofluids dates back to 1993 by Masuda et al. [1]. Significant changes in the thermophysical properties like thermal conductivity and viscosity of the based fluid (water) with the addition of 27 (nm) TiO2, 13 (nm) Al2O3, and 12 (nm) SiO2 nanoparticles were measured. The term "nanofluids" was introduced a couple of years later by [2] in Argonne National Laboratory (ANL) in USA, and can be defined as the mixture of nanometre(nm) sized particles (in between 1 to 100 nm size, called nanoparticles) which is stably and uniformly suspended in conventional heat transfer fluids [3], as designed in Fig 1-1. This newly obtained nanofluids has improved thermal conductivity compared to those used heat transfer base fluids and hence shows best hope for heat transfer.

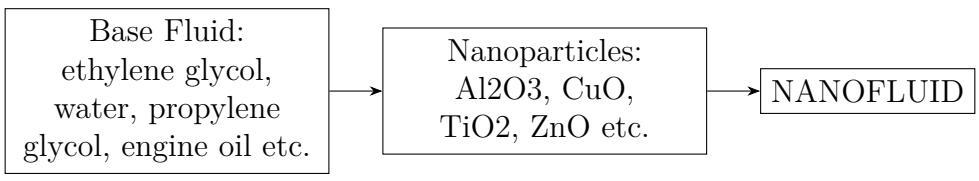

Fig. 1-1 Schematic description of base fluid in combination with nanoparticles[4]

The nanoparticles are used to enhance the thermal conductivity of the regular liquids can be chemically stable metallic (i.e. copper, gold, silver) or non-metalic. In fact, the thermal conductivities of the nanoparticles are one or more order(s) in magnitude is higher than those of conventional heat transfer liquids, even at low concentration. Choi et al. [5] stated that addition of less than 1% volume fraction of nanoparticles increases the thermal conductivity of the base fluids approximately two times. The following Table1-1: shows the relevant liquids and solids thermal conductivities [6].

It is clear from the Table1-1: that non-metallic liquids have lower thermal conductivity then those of non-metallic and metallic solids. This is the main purpose of suspending nanoparticles having enhanced thermophysical properties into commercial heat transfer fluids to develop superior thermal conductivity and advance heat transfer properties [6, 7].

Diamond, SiC, Fe3O4, SiO2, BaZrO3, ZnO, CuO, Al2O3, Cu, Al, TiO2, Au, Ag etc. are the frequently used nanoparticles for the production of nanofluids. In addition to the above-named, carbon nanotubes (CNTs) (e.g. multi walled carbon nanotubes (MWCNTs) and single walled carbon nanotubes (SWCNTs)) and titanate nanotubes (TNT) are used, as well[4].

The trends towards smaller sized suspenpended particles base fluids have now improved its heat transfer capability and increased thermal conductivity. Previously macro particles were under use with some improvements in heat transfer. Faster sedimentation of particles, corrosion and packing of channels were the drawbacks and difficult to manage. Smaller particles nanosized in base fluids came into use in commercial use for improved heat transfer, so these proved superior to macro particles and led to era in the base fluids prodigma. Nanosized particles are more stable [8] than micro being with bigger surface to volume ration approximately thousand times more than micro particles. As a result, nanoparticles have an advantage over microparticles in terms of stability [7].

It is necessary to mention here that the production of nanofluids is not simply introducing nanoparticles into the base liquid, and mixing the mixture to form a homogeneous mixture, but it involves different chemical and physical processes to disperse the particles uniformly and effectively. There are mainly two methods used for the preparation of nanofluids in the laboratory, namely the one-step method and the two-step method [3]. The two-step method is often used in research because of its low cost and simplicity. This method includes two steps. First, the nanoparticles, nanofibers, or nanotubes are converted into a powder form by physical or chemical operations (e.g. chemical vapor deposition (CVD) and inert gas condensation (IGC)

solids/liquids	Material	Thermal conductivity (W/mK)
Metalic Solids	Silver	429
	Copper	401
	Aluminum	237
Nonmetalic Solids	Diamond	3300
	Carbon nanotubes (CNTs)	3000
	Silicon	148
	Alumina (Al2O3)	40
Metallic liquids	Sodium (at 644 K)	72.3
Nonmetallic liquids	Water (H2O)	0.613
	Ethylene glycol (EG)	0.253
	Engine oil (EO)	0.145

Table 1-1 Thermal conductivities of various solids and liquids [7]

[9]). Second, the resulting powder is mixed with the base liquid by strong magnetic force, ultrasonic stirring or homogenization [10]. The main problem with the two-step process is the aggregation of nanoparticles in conventional fluid. The two-step process works pretty well for oxide nanoparticles, but not as well for metalic nanoparticles. In the one-step process, the mixing and synthesis of nanoparticles take place simultaneously. This method reduces the aggregation of nanoparticles and avoids the transformation of the raw materials into powder, desiccation etc. [11]. But one-step method is relatively expensive and cannot be applied on a large scale [12]. The main methods for the preparation of nanofluids are shown in Fig 1-2 [13].

1.2 An overview on the thermophysical properties of nanofluids

In this segment, some of the main theoretical and experimental models available for thermophysical properties of nanofluids are presented.

1.2.1 Thermal conductivity (κ_{nf})

The measure of ability of a material to conduct heat is known as thermal conductivity with W/mK is the measured of unit. Thermal conductivity is the most important variable specifying the enhancement potential of nanofluids. As mentioned earlier, generally thermal conductivity of the base fluid is lower than the nanofluids. There are different theoretical and experimental models in literature for thermal conductivity but the most used ones are discussed here.

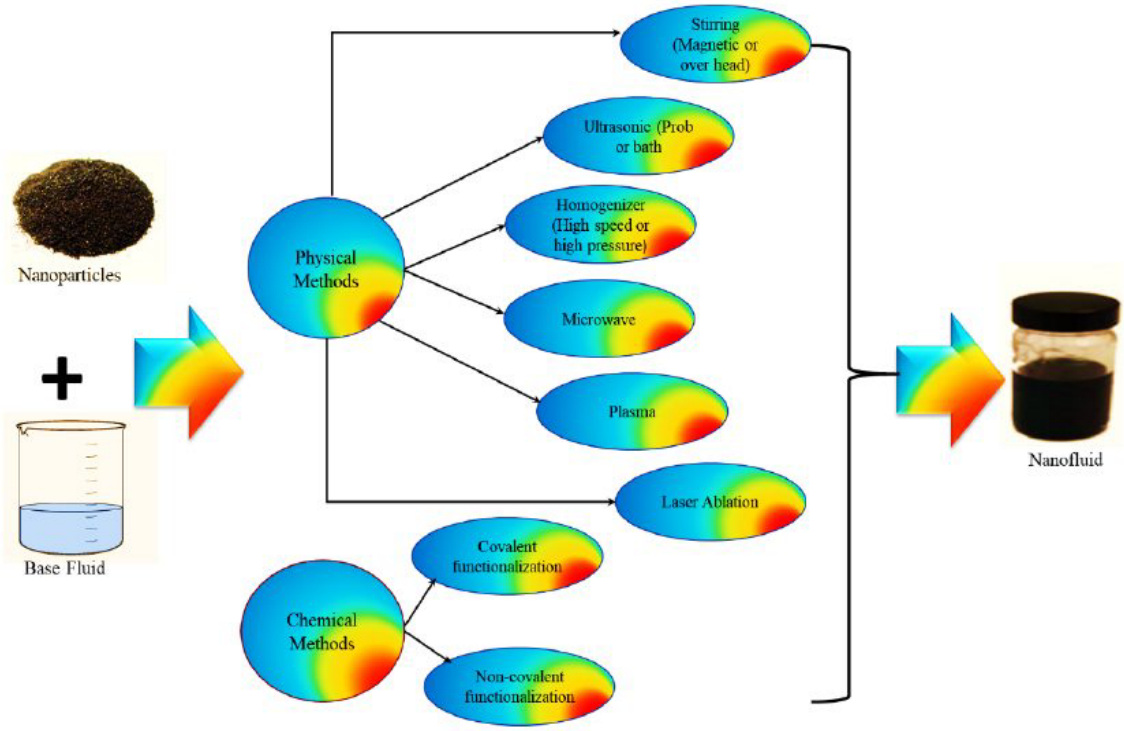

Fig. 1-2 A schematic of the chemical and physical processes for the preparation of nanofluids [13].

1.2.1.1 Theoretical models of (κ_{nf})

The Maxwell model for the theoretical study of thermal conductivity (κ_{nf}) is probably the first and frequently used theoretical model [14] given as.

$$\kappa_{nf} = \frac{\kappa_s + 2\kappa_f + 2\varphi(\kappa_s - \kappa_f)}{\kappa_s + 2\kappa_f - \varphi(\kappa_s - \kappa_f)}\kappa_f. \tag{1-1}$$

where κ_s and κ_f both are thermal conductivities of the nanoparticles as well as base fluids accordingly. Spherical particles with smaller concentration ($\varphi << 1$) can well make use of this model. Hamilton and Crosser [15] further expend the Maxwell model by the addition of shape factor for nanoparticles to it as,

$$\kappa_{nf} = \frac{\kappa_s + (\aleph - 1)\kappa_f + (\aleph - 1)\varphi(\kappa_s + \kappa_f)}{\kappa_s + (\aleph - 1)\kappa_f - \varphi(\kappa_s - \kappa_f)}\kappa_f. \tag{1-2}$$

In the Eq.(1-2) $\aleph$ is the empirical shape factor of nanoparticles. It is calculated by $\aleph = 3/\hbar$, where $\hbar$ is the particle sphericity. Spherical particles have a sphericity parameter as 1 and come to 0.5 for cylindrical shape particles. Bruggman [16] worked out on the following model while studying interactions in between spherical particles.

$$\kappa_{nf} = \frac{(3\aleph - 1)\frac{\kappa_s}{\kappa_f} + \{3(1 - \aleph) - 1\} + \sqrt{\Delta}}{4}. \tag{1-3}$$

where $\Delta = [(3\aleph - 1)\frac{\kappa_s}{\kappa_f} + \{3(1-\aleph) - 1\}]^2 + 8\frac{\kappa_s}{\kappa_f}$.

It is worth mentioning that the old models used for calculation of larger size(dimensions of micrometer/milimeter) particles generally underestimated the thermal conductivity value as against the experimental data. Apart from this they can still be implied for numerical computations of nanofluids flows. These old models have been reassembled and revamped during several trials to avoid these biases and discrepancies in calculations while making use of phenomenon involved in heat conduction of nanofluids exemplified by aggregation, nanoparticle interaction, nanolayer (i.e. liquid layering at molecular level between the liquid and particle interface) and Brownian motion (also known as Pedesis, is defined as the random movement of solid particles in a liquid due to the collision of the solid particles with the liquid molecule [13]) of nanoparticles. Which are the major factors influence the heat transfer enhancement of nanofluids.

The Brownian motion of the large size nanoparticles in the conventional approach is neglected. As the nanoparticles size decrease to nanometre scale, the Brownian motion of the nanoparticles and its effect on the neighbour liquid particles involve heat transfer.

Xuan et al.[17] suggested a thermal conductivity model by considering the effect of aggregation structure of nanoparticle clusters and Brownian motion. The suggested model is expressed as,

$$\kappa_{nf} = \kappa_f \left\{ \frac{\kappa_s + 2\kappa_f + 2\varphi(\kappa_s - \kappa_f)}{\kappa_s + 2\kappa_f - \varphi(\kappa_s - \kappa_f)} + \frac{\rho_s \varphi c_{p,f}}{2\kappa_f} \sqrt{\frac{2C_b T_{ave}}{3\pi d_s \mu_f}} \right\}. \tag{1-4}$$

The model given in Eq.(1-4) to include the Brownian motion effect is among the pioneer models. where C_b , T_{ave}, d_s are the Boltzmman constant, average temperature of the nanofluid and diameter of the nanoparticles respectively. This model depends on the size of nanoparticles, base fluid and nanoparticles thermal conductivity, nanoparticles volume fraction, temperature of the nanofluid, specific heat capacity.

When nanoparticles are mixed uniformly in a based fluid, a thin layer of liquid is formed around the surface of nanoparticles which is known as liquid nanolayer. A thermal resistance known as "Kapitza resistance" is present at the interface of base fluid and nanoparticles. According to Yu et al.[18], the layered molecules are in an intermediate physical state between a base fluid and nanoparticle. Therefore, the nanolayer of liquid molecules would be expected to lead to a higher thermal conductivity than that of the base fluid. This means that the nanolayer acts as a thermal bridge between a nanoparticle and a base fluid, and so it is the key to enhancing

thermal conductivity Yu and Choi.[19].

Yu and Choi.[19] modified the Maxwell model (in Eq.(1-1)) to calculate the effective thermal conductivity by considering the effect of nanolyer as follows,

$$\kappa_{nf} = \kappa_f \left\{ \frac{\kappa_s + 2\kappa_f + 2\varphi(\kappa_s - \kappa_f)(1+\wp)^3}{\kappa_s + 2\kappa_f - \varphi(\kappa_s - \kappa_f)(1+\wp)^3} \right\} \tag{1-5}$$

Where $\wp$ referred to the ratio of thickness of liquid nanolayer to the radius of oxide nanoparticle which is normally used to 0.1. They assumed that the particles and the nanolayer around each particle could be combined to form an equivalent particle and there is no overlap of those equivalent particles because of the low particle volume concentration. The models given in Eqs.(1-4, 1-5) are also developed for spherical shape metallic and oxide nanoparticles.

1.2.1.2 Experimental Models of (κ_{nf})

With regard to experimental correlations, they were mostly obtained for Spherical metal and oxide nanoparticles. Maiga et al.[20] showed two correlations based on experimental data. Thermal conductivity of Al2O3/EG and Al2O3/ water nanofluids as follows:

Al2O3/EG:

$$\kappa_{nf} = \kappa_f(28.905\varphi^2 + 2.8273\varphi + 1) \tag{1-6}$$

Al2O3/water:

$$\kappa_{nf} = \kappa_f\,(4.97\varphi^2 + 2.72\varphi + 1) \tag{1-7}$$

The correlations in Eqs.(1-6, 1-7) were developed for nanoparticles of size 28 nm. Khanafer and Vafai [21] suggested a general model for the thermal conductivity of Al2O3 / water and CuO / water nanofluids such as:

$$\kappa_{nf} = \kappa_f\,(1 + 1.0112\varphi + 2.4375\varphi(\frac{47}{d_s}) - 0.0248\varphi\,(\frac{\kappa_s}{0.613})) \tag{1-8}$$

The above model applies to nanoparticle sizes from 13 (nm) to 80 (nm) and up to 15% of volume fractions. Ho et al.[22] give the following empirical model for the thermal conductivity of aluminum oxide / water nanofluids, taking the size of the nanoparticles 33 (nm).

$$\kappa_{nf} = \kappa_f\,(1 + 2.944\varphi + 19.672\varphi^2) \tag{1-9}$$

The above relationship applies up to 4% of volume fraction.

In conclusion, most literature about nanofluids shows that thermal conductivity increases with increase in temperature and volume concentration while it decrease

with increase in the size of particles [23]. There is many other theoretical and experimental correlations in literature, but they are specific to the type of nanofluid tested, nature of the nanoparticles and base fluid, shape and size of the nanoparticles [13, 23]. To date, a remarkable challenge to the nanofluid research is that there is no general model which predicts thermal conductivity of nanofluids. For more experimental and theoretical models of thermal conductivity see [13, 23, 24].

1.2.2 Viscosity (η_{nf})

Resistance of a liquid to flow is known as viscosity and it is measured in terms of pascal second (Pa s) or newton second per square metre (Ns/m^2). Viscosity of the base fluids is generally lower than that of nanofluids. With increase in the concentration of nanoparticles, viscosity increases and the liquid may become non-Newtonian liquid. The following is an overview of suitable models for the viscosity of nanofluids based on Newtonian behaviour or fixed shear rate. The first models as considered for thermal conductivity are derived from the theory of suspension large spherical particles. However, it is also not possible to predict an increase in viscosity of nanofluid by volume fraction [13].

1.2.2.1 Theoretical based Models of viscosity (η_{nf})

Based on Kinetic theory Einstein [25] proposed a model for the nanofluid viscosity with volume fraction, φ of nanoparticles less then 1% as,

$$\eta_{nf} = \eta_f(1 + 2.5\varphi). \tag{1-10}$$

Brinkman [26] proposed viscosity equation for spherical shape nanoparticles which is applicable upto 4% volume concentration as,

$$\eta_{nf} = \frac{\eta_f}{(1-\varphi)^{2.5}}. \tag{1-11}$$

For hybrid nanofluid Hussain et al. [27] and Farooq et al. [28] amend the Brinkmann model [26] in the following form:

$$\eta_{hnf} = \frac{\eta_f}{(1-\varphi_{hnf})^{2.5}}. \tag{1-12}$$

Where $\varphi_{hnf} = \varphi_1 + \varphi_2$.

1.2.2.2 Experimental based Models of viscosity (η_{nf})

Using experimental data of Al2O3/water nanofluids, Singh et al. [29] change as an Einstein model in Eq.(1-10)

$$\eta_{nf} = \eta_f(1 + 10\varphi). \tag{1-13}$$

Maiga et al.[20] showed two experimental correlations for the viscosities of water/Al2O3 and Ethylene glycol(EG)/Al2O3 nanofluids respectively as

$$\eta_{nf} = \eta_f\,(123\,\varphi^2 + 7.3\,\varphi + 1). \tag{1-14}$$

$$\eta_{nf} = \eta_f\,(306\,\varphi^2 - 0.19\,\varphi + 1). \tag{1-15}$$

Ho et al. [22] experimentally investigated the natural convective heat transfer of Al2O3 / water nanofluids in three different sized vertical square enclosures and give the following model based on experimental data for the viscosity of alumina (Al2O3)/ water nanofluids. Here, the size of the nanoparticles is 33 nm (valid at $\varphi \leq 4\%$).

$$\eta_{nf} = \eta_f\,(4.93\,\varphi^2 + 222\,\varphi + 1). \tag{1-16}$$

It is notable from most articles on nanofluids that increase in volume fraction, φ, increases the viscosity, while increase in particle size and temperature reduce viscosity. As the literature is rich about this topic, only a few theoretical and experimental models were discussed. For complete overview, the reader can be refer to recent review papers [13, 24] and the references there in.

1.2.3 Density

The ratio of mass to volume is term as density and measured in terms of kg/m^3. With volume fraction φ, the nanofluid density can be calculated in the following form [30].

$$\rho_{n_f} = \rho_f(1 - \varphi) + \rho_s\varphi. \tag{1-17}$$

This formula, generally accepted by most researchers.

1.2.4 Specific heat capacity

The amount of heat required to increase the temperature of one kg of a substance by one degree (1^o) Kelvin (K) is term as specific heat capacity and having SI

unite $J/kg.K$. The equation for specific heat capacity of nanofluids can be defined as [21].

$$c_{p_{nf}} = \frac{\rho_f c_{p_f}(1-\varphi) + \rho_s c_{p_s}\varphi}{\rho_{n_f}}. \tag{1-18}$$

Where c_{p_s}, is the specific heat capacity of nanoparticles and c_{p_f}, specific heat capacity of base fluid. When the base fluid density is similar to that of nanoparticle [13] the following common simplified equation is valid,

$$c_{p_{nf}} = c_{p_f}(1-\varphi) + c_{p,s}\varphi. \tag{1-19}$$

Contrary to viscosity and thermal conductivity, only a few models are obtainable and useful for density and specific heat capacity of nanofluids. However, to date, no universal model has been possible to accurately predict the properties of nanofluids for any combination of independent variables (nature of particles, diameter of particles, etc.). Various models are available in the literature leading to the results are conflicting [31] and it is not clear which is the best for a certain situation [32].

In literature different types of approaches are available for the modling of governing equations corresponding to nanofluids. Fig 1-3 dispenses the major approaches for nanofluid flow modelling. This can be categorized as a single phase or two phase approach.

1.2.5 Single phase

Essentially a nanofluids is a two phase fluid (solid–liquid), but for numerical solutions under precise conditions some appropriate suppositions can be made to model nanofluids as single phase fluids [13]. To get accurate results with single phase modeling, it is very important to use the most appropriate correlations for the effective properties of the nanofluid. The governing equations in case of single phase model are solved for specific liquid phase. Compare to two phase model this approach requires less computation space/time and has been used for several theoretical studies of nanofluids. This model can be further divided into three, including homogeneous, Buongiorno [33] and thermal dispersion models [34]. We limit our self in this thesis to homogeneous approach which is described in detail.

1.2.5.1 Homogeneous Model

From a practical point of view, most nanofluids used to improve heat transfer consist of very fine particles, typically smaller than 40 nm. Because of these small

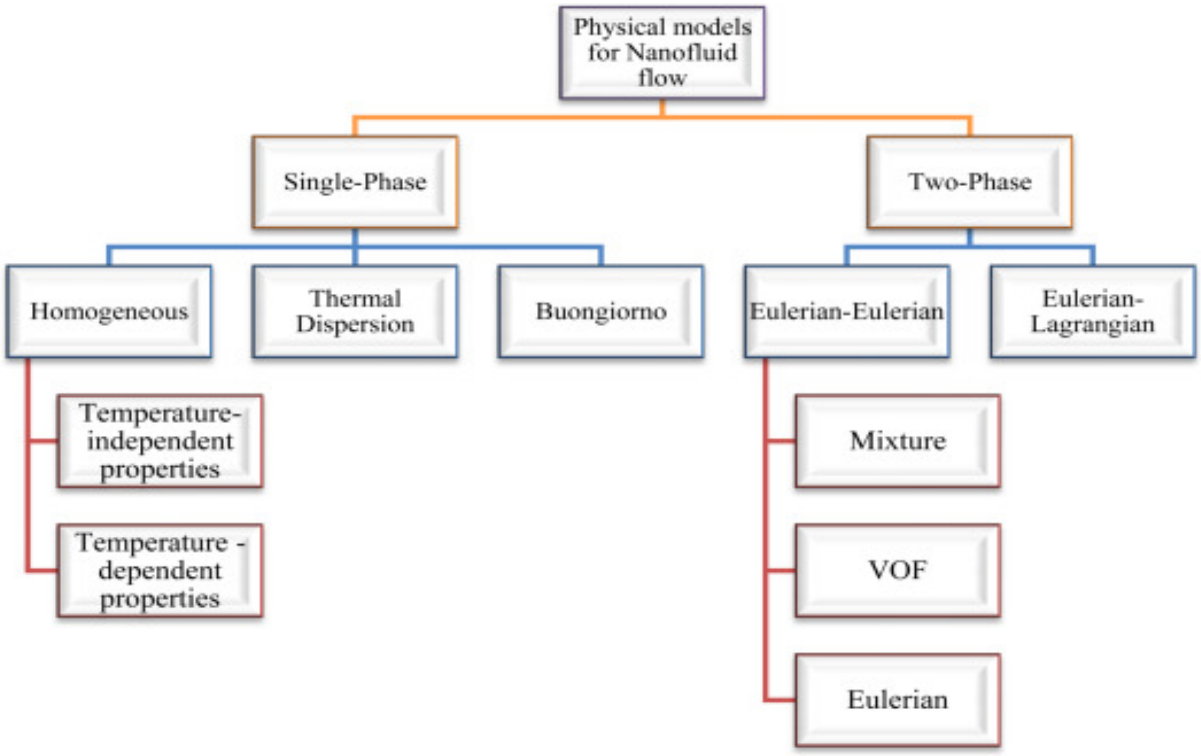

Fig. 1-3 Different approaches for the modeling of nanofluid flow [13]

dimensions, it is assumed that they can be easily fluidized and, therefore, can be considered to behave like a fluid [31]. Homogeneous model is the simplest and frequently used theoretical approach for the modelling of nanofluid flows. The main suppositions in this model are given below [13]:

◇ The slip velocity between the nanoparticles and the conventional liquid is zero.

◇ Solid particles are ultra fine and disseminate uniformly in the conventional fluid.

◇ Solid and fluid phases are in thermal equilibrium.

The above suppositions suggest that any thermal exchange and inter phase forces between the solid particles and continuous liquid phase can be neglected. Therefore, the resulting mixture can be considered as a classical mixture homogenous single phase liquid, having certain effective properties. Fig 1-4 designated the single phase flow approximation in a tube for nanofluid flow.

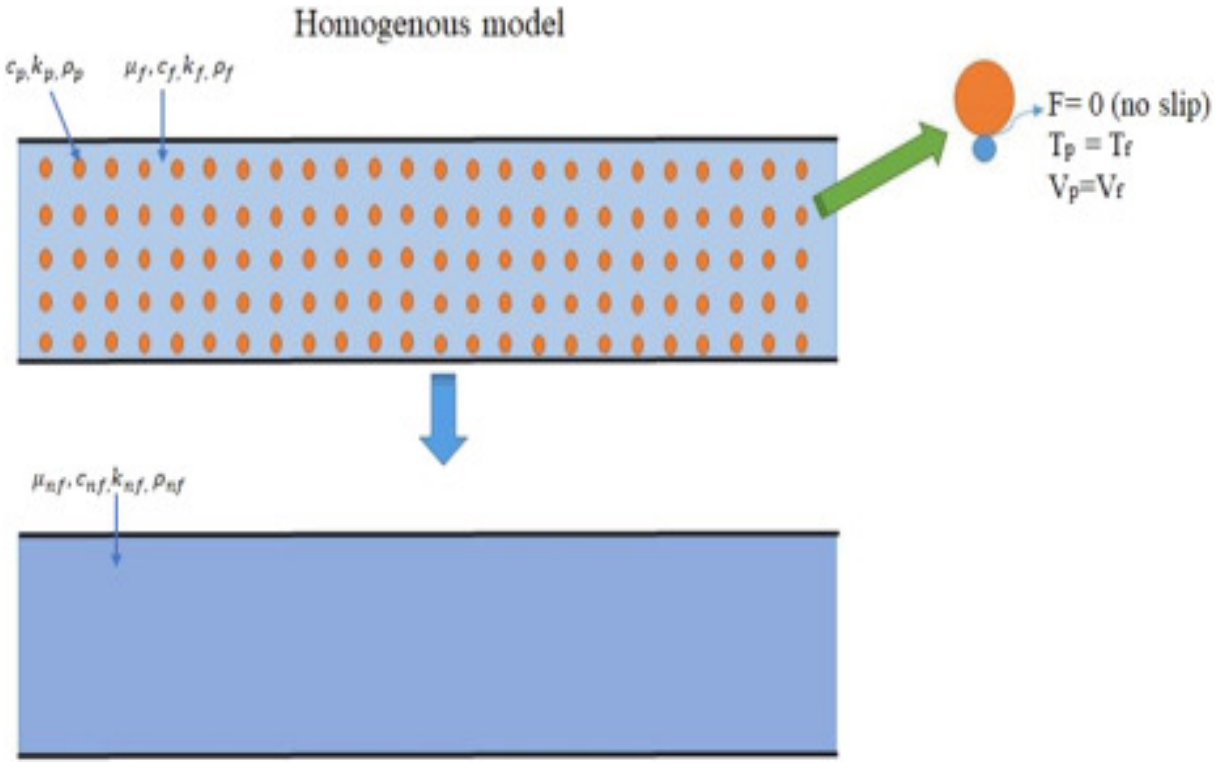

Fig. 1-4 A schematic of the single-phase homogeneous model [13].

The transport equation can be recast for nanofluids, taking into account the application of homogeneous model is as follows:
Continuity equation:

$$\nabla \cdot (\rho_{n_f} \boldsymbol{u}) = 0, \tag{1-20}$$

Momentum equation for nanofluids[13]:

$$\rho_{n_f} (\boldsymbol{u} \cdot \nabla)\boldsymbol{u} = -\nabla p + \nabla \cdot \{\eta_{nf} (\nabla \boldsymbol{u} + (\nabla \boldsymbol{u})^T)\} + F, \tag{1-21}$$

In the above equation, $\rho (\boldsymbol{u} \cdot \nabla)\boldsymbol{u}$ is the convection term, $-\nabla p$ is the pressure gradient, and $\nabla \cdot \{\eta_{n_f} (\nabla \boldsymbol{u} + (\nabla \boldsymbol{u})^T)\}$ is the viscous diffusion term. All sources indicate that the properties of nanofluids depend on the volume fraction of the particles as well as on the respective properties of the base liquid and of the solid particles. Since the properties of the base fluid depend on temperature (see Table:1-2 some of them we will discuss in the coming chapters), the properties of the nanofluid also depend on the temperature. Therefore, in this study, all the properties of nanofluids are expressed as a function of volume fraction and temperature (which we will discuss in the coming chapters).

Energy equation [13]:

$$\nabla \cdot (\rho_{n_f} c_{p_{nf}}) \boldsymbol{u} T = \nabla \cdot (\kappa_{n_f} \nabla T) + Q \tag{1-22}$$

The left side of Eq.(1-22) represents heat convection, $\nabla \cdot (\kappa_{nf} \nabla T)$ is heat conduction, and Q is viscous dissipation function resulting from work done on viscous force [13]. The selection of a suitable model for the thermophysical properties of nanofluids (especially viscosity and thermal conductivity) is the biggest challenge with the single phase homogeneous approach. These properties can be thought about as constant (temperature dependent) or temperature independent, depending on the problem and the characteristics of the mixture [13].

A lot of theoretical research has been done to model nanofluids using a homogeneous (uniform) single phase model. Here is a brief description of some studies using homogeneous model. Maïga et al.[35] consider the problem of forced convection flow of water/ Al2O3 and ethylene glycol(EG)/ Al2O3 nanofluids in a uniformly heated tube exposed to a constant uniform heat flow (flux) in the wall. Roy et al.[36] considered hydrodynamic and thermal fields of water/ Al2O3 nanofluids in a radial laminar cooling system. Saha and Paul[37] used homogeneous single phase model and temperature dependent properties to simulate turbulence of water based $Al2O3$ and $TiO2$ nanofluids in a horizontal tube under constant heat flow (flux) boundary conditions. Demir et al. [38] simulated forced convection of Al2O3 and TiO2-based nanofluids in a double-tube heat exchanger. A homogeneous single-phase model was used to solve this problem. Numble et al.[39] investigated turbulence in (EG) / water nanofluids containing Al2O3, CuO and SiO2 nanoparticles in a tube using a homogeneous (uniform) single phase model with temperature dependent properties. Morave et al. [40] carried out the study of convective heat transfer of water-Al2O3 nanofluids as a single-phase liquid in the area of tube development with constant heat flow. Manca et al. [41] used a uniform (homogeneous) single phase approach to analyze forced convection of alumina / water nanofluids in a two-dimensional channel with uniform heat flow by assuming that the properties (i.e. thermal conductivity, density etc) were temperature independent. Ahmed et al.[42] investigated laminar convection heat transfer from a tube bank under the conditions of constant wall temperature in cross-flow with Al2O3 nanofluids. Vajjha et al. [43] numerically investigated the flow and heat transfer performance of water/ ethylene glycol (EG) based CuO and Al2O3 nanofluids in the tubes of a radiator. Mansour et al.[31] applied a "homogeneoussingle phase fluid" approach to be able to study the thermo-hydraulic behavior of nanofluids.

1.2.5.2 Thermal dispersion model

The thermal dispersion model was investigated by Xuan and Roetzel [34] by modifying the homogeneous single phase model. The Random and irregular movements of nanoparticles accelerates the speed of energy exchange in nanofluid, and causes small disturbances in both velocity and temperature. The intrinsic phase mean value is defined similar to turbulence and is as follows:

$$\boldsymbol{u} = \overline{\boldsymbol{u}} + \boldsymbol{u}' \tag{1-23}$$

$$T = \overline{T} + T' \tag{1-24}$$

Here, Eqs.(1-23 and 1-23) $\boldsymbol{u}'$ and T' represent the velocity and temperature fluctuations due to the chaotic motion of the nanoparticles and the average values are given by $\overline{\boldsymbol{u}} = \frac{1}{\forall_f}\int_{\forall_f} \boldsymbol{u}\, d\forall$ and $\overline{T} = \frac{1}{\forall_f}\int_{\forall_f} T\, d\forall$ where $\forall$ is the volume of the working fluid. By ignoring the interface between the liquid and the nanoparticles, the energy equation is written:

$$\nabla \cdot (\rho_{n_f} c_{p_{nf}})\overline{\boldsymbol{u}T} = \nabla \cdot (\kappa_{n_f} \nabla \overline{T}) - \nabla \cdot (\rho_{n_f} c_{p_{nf}})\overline{\boldsymbol{u}' T'} \tag{1-25}$$

The last term on the right hand side of the Eq.(1-25) can be thought of as a term for the additional heat flux caused by temperature and velocity fluctuations. The heat flux generated by heat dissipation in the nanofluid is calculated as follows:

$$q_d = -\kappa_d \nabla \overline{T} = (\rho_{n_f} c_{p_{nf}})\overline{\boldsymbol{u}' T'}, \tag{1-26}$$

Where κ_d is the dispersed thermal conductivity (showing, the contribution of thermal dispersion in the improvement of thermal conductivity). Putting Eq. (1-26) into Eq.(1-25), the energy equation can be written in the following form:

$$\nabla \cdot (\rho_{n_f} c_{p_{nf}})\overline{\boldsymbol{u}T} = \nabla \cdot \left[(\kappa_{n_f} + \kappa_d)\right] \nabla \overline{T} \tag{1-27}$$

Compare Eq.(1-27) for nanofluids with the traditional single phase energy equation, an additional parameter κ_d appears, which denote the thermal dispersion effect of the nanoparticles in the nanofluid. The most important problem is determining the correlation for the parameter κ_d. The approach to get κ_d is not presented here, but readers can refer to Refs. [34, 44–49].

Several researchers have used single phase thermal dispersion model to simulate the flow and heat transfer of nanofluids. Yang et al. [50] performed direct numerical simulations (DNS) of turbulent flows of nanofluids to investigate the mechanism of improved convection-induced heat transfer upon addition of nanoparticles

into the conventional fluid. Taking into account the thermal dispersion effect of nanoparticles, a new thermal dispersion term is introduced in the energy equation for turbulent nanofluid flows, making the DNS of nanofluid turbulent flow with heat transfer available. The newly established thermal dispersion correlation is validated by comparing DNS results for heat transfer in turbulent nanoflud flow with experimental data. single phase homogeneous model is considered with the assumption of variable (temperature dependent) thermal conductivity by Özerinç and co-workers [45] to simulate water based Al2O3 nanofluid inside a tube with different boundary conditions. They found that the numerical estimates of the heat transfer rate (HTR) with this approach were lower than the experimental ones. Therefore, the thermal dispersion model was also tested and got a good agreement with the experimental data. Ameri et al.[51] used thermal dispersion model in their modeling to investigated the ability of nanofluids to improve heat transfer in a metal foam tube, where in this paper, the nanoparticles distribution is assumed to be non-uniform. In another study, Bahiraei and Vasefi [52] simulated laminar flows of various nanofluids in a horizontal tube geometry using both thermal dispersion and homogenous correlations in which the non-uniformity distribution of the nanoparticles were included in the thermal dispersion model. They found that with the increase of Re and the particle loading, the thermal dispersion technique is more suitable than the homogeneous to predict the experimental results. Akbaridoust et al.[53] investigated the flow of nanofluids in helically coiled tubes type geometry using both thermal dispersion and homogeneous models. The results show that the homogeneous model has a lower accuracy than the thermal dispersion model. Kumar et al.[54] performed an analysis of flow and thermal field in water-based/Cu nanofluids in a two-dimensional thermally driven cavity using single phase homogenous and thermal dispersion model. Bahiraei and Hosseinalipour [55] used a thermal dispersion model to simulate the convective heat transfer of water-based/TiO2 nanofluid in a circular tube using unequal concentration distribution. In another research, Bahiraei and Hosseinalipour [49] compared the effectiveness of the thermal dispersion technique (using unequal nanoparticles distribution) and the Euler-Lagrange technique to predict the internal heat transfer rate (HTR) in a circular tube with water based/alumina nanofluid. The results show that in terms of computational accuracy and calculation time, the use of thermal dispersion approach is reasonable.

1.2.5.3 Buongiorno model

In 2006, Buongiorno [33] proposed an improved model of thermal dispersion (where the thermal conductivity and dispersion of the nanoparticles are considered to be the main factors contributing to the improved heat transfer) and single-phase homogenous (where only an increase in thermal conductivity was thought to be responsible for improving heat transfer) [9]. Buongiorno studied the effects of seven slip mechanisms, including: (1) inertia (2) thermophoresis (3) Brownian diffusion (4) Magnus effect (5) diffusiophoresis (7) gravity and (6) fluid drainage and deduce that thermophoresis and Brownian diffusion are the most important slip mechanisms in nanofluids [13]. In, Buongiorno model, the relative velocity of the nanoparticle and the influence of the regular fluid are described in a mechanical manner rather than in the thermal dispersion model.

In, Buongiorno model, the relative velocity of the nanoparticle and the influence of the regular fluid are described in a mechanical manner rather than in the thermal dispersion model. Considering the thermophoresis and Brownian effects, and to avoid repetition, we discuss only the energy, we discuss only the energy and concentration equations. the energy equation in the homogeneous model are converted to [13],

$$\nabla \cdot (\rho_{n_f} c_{p_{nf}}) \boldsymbol{u} T = \nabla \cdot (\kappa_{n_f} \nabla T) + (\rho c_p)_s \left[D_B \nabla C \cdot \nabla T + D_T \frac{\nabla T \cdot \nabla T}{T} \right] \tag{1-28}$$

Concertation equation for the nanoparticles:

$$\boldsymbol{u} \cdot \nabla C = \nabla \cdot \left[D_B \nabla C + D_T \frac{\nabla T}{T} \right] \tag{1-29}$$

In Eq. (1-28 and 1-29) thermophoresis (or thermal diffusion coefficient) and Brownian diffusion can be manifest respectively as [33],

$$D_B = 0.26 \frac{\kappa_{n_f}}{2\kappa_{n_f} + \kappa_s} C \frac{\eta_{n_f}}{\rho_{n_f}}, \tag{1-30}$$

$$D_B = \frac{C_b T}{3\pi \eta_{n_f} d_s}, \tag{1-31}$$

where C_b denote Boltzmann constant and d_s diameter of the nanoparticles [13].

many investigations have been carried out regarding the analysis of convection heat transfer of nanofluids on the basis of Buongiorno model. Garoosi et al. [56] performed numerical simulations of natural convection of water based nanofluids of

Al2O3, Cu, and TiO2 in a 2D cavity consisting of several pairs of heaters and coolers according to the Buongiorno method. In other studies, Garoosi et al.[56, 57] analysed mixed convection and natural convection of water based Al2O3 nanofluids in a square cavity using the Buongiorno model. Sheremet and Pop [58] studied natural convection in a square porous enclure filled with nanofluids using a Buongiorno model taking into account the effects of thermophoresis Brownian diffusion. Shehzad et al. [59] addresses in his article the effect of convective heat transfer of nanofluids using the Buongiorno model in a wavy channel with constant pressure gradient. The simultaneous effects of thermophoresis and Brownian motion have been discussed. [60] carried out a comparative analysis of the oscillatory stagnation point flow of nanofluids. by discussing both the Buongiorno and phase flow models for oscillatory stagnation point flows and presenting a comparison between the theoretical and experimental models.

1.2.6 Two phase

Nanofluids have the characteristics of a two-phase fluid. In the two phase, behaviour of nanofluids, the nanoparticles and base liquid are projected as separate individual phases with different features such as velocity difference and temperature difference. In such environments the particles move in relation to base fluids. This velocity of particles in relation to base fluids is termed as slip velocity as it is in no way associated to the no-slip boundary condition. Assessing and trailing the movement in between nanoparticles and base fluids, the two phase phenomenon may give more detailed and realistic outcomes and hence used for several theoretical studies [61, 62]. Such trails needs much computer space and computation time and the relevant models are complex compare to single phase approach. Two different groups in general are assigned to the two phase approaches. These are Eulerian-Eulerian and Eulerian-Lagrangian models. Eulerian-Eulerian models state that base fluids and nanoparticles phase are taken as continuation of each other (and this approach is preferred for high solid volume fractions[32]), while Eulerian-Lagrangian (the most suitable approach in case of low solid volume fractions, is the Lagrangian-Eulerian which analyzes the based liquid according to the Eulerian hypothesis and particle phase according to the Lagrangian hypothesis [32]) state that the base fluid is continuum and nanoparticles are discrete phase. Eulerian-Lagrangian is also known as discrete phase approach [13]. In this phase model nanoparticles is assessed and its path calculated and determined [63] and references their in. Singh et al. [64] suggests that for micro-channels, the Eulerian-Lagrangian approach is

suitable for high Re conditions and the single phase techniques is suitable for low Re conditions. Sato et al.[65] investigate through this approach the mechanism of turbulent transport and two phase heat by solid particles suspended in a gas flow. While assuming the temperature field is not affected by enthalpy. Fig1-5 explain the phenomenon of Eulerian-Eulerian and Eulerian-Lagrangian models with blue arrows pointing fluid path and red arrows pointing the particle path. Eulerian-Lagrangian need more time for its assessment and calculation as compared to Eulerian-Eulerian. In fact, there are different Eulerian-Eulerian models see Fig 1-3. The Eulerian-Lagrangian gives more solid results and its model can be implied for a variety of problems.

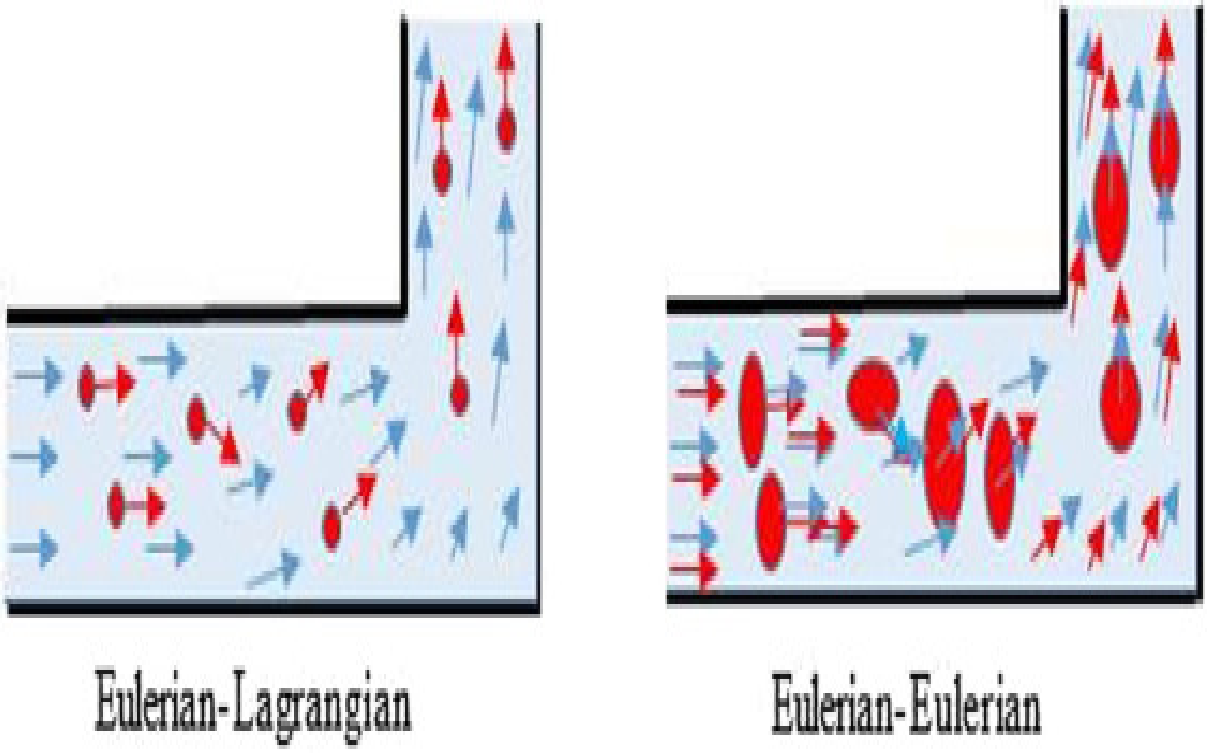

Fig. 1-5 A schematic of the concept of Eulerian–Eulerian and Eulerian–Lagrangian approaches [13].

1.3 Methods of heat flows

Heat flows from higher to lower temperature materials when two object have distinct temperature (T). Transfer of internal energy of one substance to the other is termed heat transfer. Heat transfer generally consists of three mechanisms, including conduction, convection and radiation, and seldom occurs by its own. heat transfer. Each of these mechanisms can become sub-branches [66].

1.3.1 Conduction

The direct heat transfer from one substance to other due to the collision of atoms and molecules is known as conduction. This type of heat transfer occurs in solids.

1.3.2 Convection

Energy transferred due to particles motions in relation to each other is called conviction. Fig1-6 shows some convection mechanisms and their sub-types.

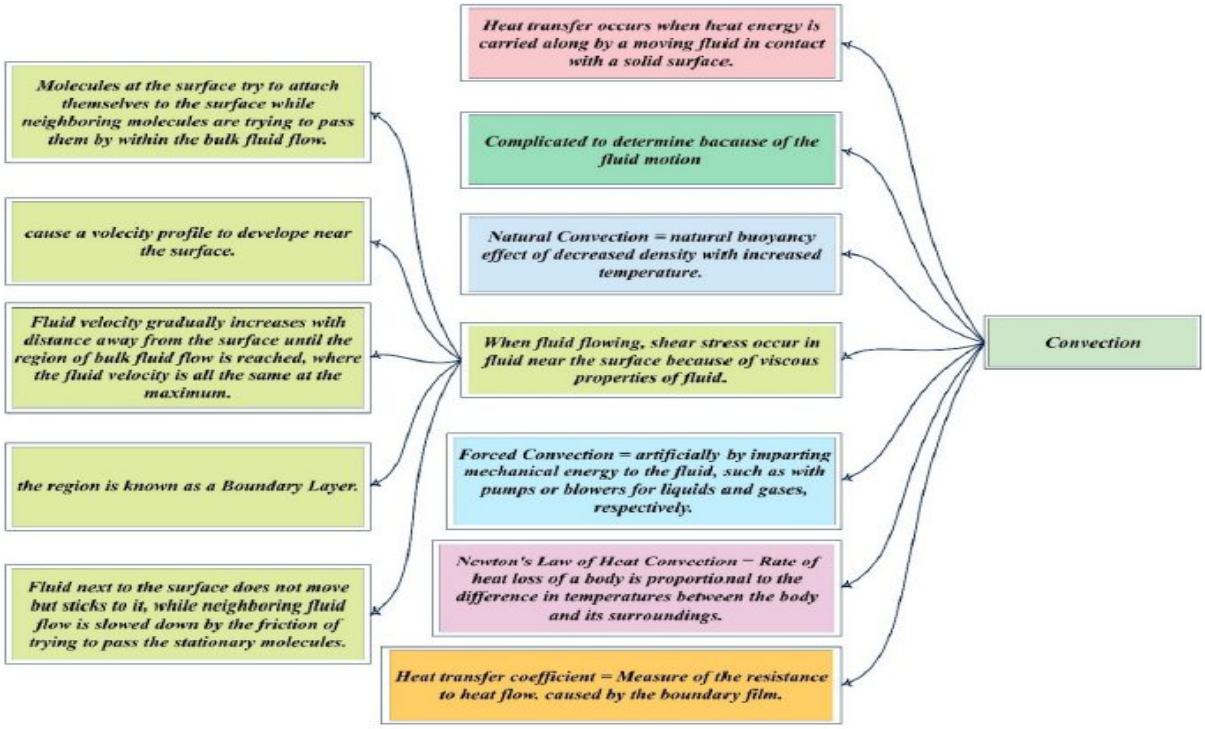

Fig. 1-6 A schematic of the Concept of Types of heat transfer mechanisms and their sub-types [67].

1.3.2.1 Force convection

In force convection, fluid motion is created by an external source like a fan or pump. This is one of the main forms of heat transfer in electronics cooling, air conditioning systems, in numerous other technologies and heat exchangers.

1.3.2.2 Natural or free convection

Free or natural convection occurs in various industries such as solar cells, air and space, food industry, solar and nuclear collectors, etc [67]. Natural or free convection phenomenon is generated by density variation in a fluid due to temperature (T) variation and exemplified by smoking out of fire or flow of blast wave moving across vacuum gradient.

1.3.2.3 Mixed convection

When forced and natural convictions are combined, a phenomena known as mixed conviction occurs. It also results from coupling of buoyant and pressure forces. This is the combination of natural convection and forced convection phenomenon's or it takes place when both buoyant forces and pressure forces interrelate.

1.3.3 Radiation

Emission of electric or electromagnetic energy needing no mode of transfer is radiation energy. Liquids and gases depend on radiation and conviction for energy transfer while solid only do it via conduction.

1.4 Rheology and compelx fluids

Rheology, a term first coined by Professor Eugene Bingham with the suggestions of his colleague, Markus Reiner, in nineteen twenties at Lafayette College Indiana USA. "ta panta rhei" encouraged this concept saying that in a given time scales everything will flow [68]. Due to overlapping properties materials cannot be easily graded as solid or liquids. Trial time observation or experiment and material time scale to relax, affect this classification. Deformation or time needed beyond stress yielding point is the time scale of the material.
Silicone material known as "Silly putty" exemplifies it i.e. it flows slowly in longer time scale, thus acts like a liquid but acts as solid for shorter time scales deformation process. The dimensionless number "Deborah" is used to denote the ratio of time of relaxation to that of observation. For low value of Deborah number viscous fluids like behaviour dominates and at high Deborah number the material act as a solid. For in between values the material is characterized as complex fluids.
Rheology holds a key importance in industrial and academic world especially for Complex fluids since a comprehensive study is needed to confer material status, standard of the complete material and studying their varied properties when different parameters are applied. The historical study of rheology can be found in [69], [70] and the references there in. Newton's Law of viscosity hold for the deformation properties of all classical Newtonian fluids and their flow is modelled using the Navier Stokes Equations. The mechanical properties of non-Newtonian fluids are unrelated to the pattern of classical Newtonian fluids and cannot be defined by a single set of equations. This then establish base of the field of rheology; i.e. to account for mechanical characteristic (the deformation and flow behaviour) of non-Newtonian fluids which is also term as complex fluids. Existence and value of

such fluids in daily life has made rheology an inevitable chapter of physics. Most of the industrial physiobiological events make use of the rheological principles. In these industrial and biological processes rheology has been subdivided into a diverse field to deal with each different entity. Examples are bio-rheology (dealing with blood, soft tissues and its derivatives). Other examples rheology of food and food products, polymer rheology, chemo-rheology and rheology dealing with suspension and its related substances.

Resistance to flow in practical applications is the intrinsic behaviour of the fluids response to stress or deformation. This behaviour is term as viscosity η of the fluids. Newtonian fluids exhibits constant viscosity at a given temperature, pressure and concentration despite deformation rates put on the fluids. All fluids however show variation in viscosity with changes in these variables i.e. temperature, pressure and concentration. There are different empirically proven non isothermal viscosity models in the literature [71] as given in Table:1-2 where B_1, B_2, C_1, C_2 are empirical constants. In general, temperature, pressure, time, shear rate, polymerization

Vogel's model	$\eta(T) = \eta_0 \exp\left(\frac{B_1}{T-T_0}\right)$
Arrhenius model	$\eta(T) = \eta_0 \exp\left(\frac{E}{RT}\right)$
Reynold's model	$\eta(T) = \eta_0 \exp\left(B_1 T\right)$
Nahme model	$\eta(T) = \eta_0 \exp\left(\frac{T-T_0}{T_0}\right)$
William-Landel-Ferry (WLF) model	$\eta(T) = \eta_0 \exp\left(\frac{C_1(T-T_0)}{C_2+T-T_0}\right)$
Fulcher model	$\log_{10}(\eta(T)) = -B_2 + \frac{B_1 10^3}{T-T_0}$

Table 1-2 Different Non-isothermal viscosity models [71].

rate (polymeric foams) [72] and volume fraction [73] all variables affect viscosity of the fluid. Non-Newtonian fluids exhibit unique characteristics of shear rate dependency. The only known Boger fluids are exempted from this phenomenon. These fluids exhibit no shear rate dependency. So the Newtonian viscosity model has put limitations on Newtonian fluids in majority of rheological implications. Apart from respective constitutive models for viscosity of Newtonian and Non Newtonian fluids this behaviour can also be described and explained by mathematically drawn empirical constitutive equations of the fluid stresses. The total stress for a fluid is denoted by σ, as,

$$\boldsymbol{\sigma} = -\nabla \boldsymbol{p} + \boldsymbol{\tau}, \tag{1-32}$$

Where p is the fluid pressure and τ is the extra stresses. So, the fluid dynamical system of equations under this framework is derived from the well-known laws of physics i.e. conservation of mass, momentum, and heat energy respectively define as:

$$\frac{\partial \rho}{\partial t} + \nabla \cdot (\rho \boldsymbol{u}) = 0, \tag{1-33}$$

$$\rho \frac{D\boldsymbol{u}}{Dt} = \boldsymbol{\sigma} + \rho F, \tag{1-34}$$

$$(\rho c_p) \frac{DT}{Dt} = -p\nabla \cdot \boldsymbol{u} + \nabla \cdot (\kappa \nabla T) + Q + \Psi_s \tag{1-35}$$

where $D/Dt = \partial/\partial t + \boldsymbol{u} \cdot \nabla$ is the material derivative and ∇ is the standard gradient operator and F is the body forces (say due to magnetic effects, gravity, buoyancy etc). Other notations are standard with fluid dynamics. Eqs.(1-33 –1-35) where derived for Newtonian fluids by two famous scientist Navier and Stokes in the 1900 century [74].

1.4.1 Newtonian Fluids

Newtonian fluids are the one obeying Newton's law of viscosity (given by a great scientist sir Isaac Newton) that is in simple shear flow,the shearing force per unit area, F/A, symbolize in tensor notation by τ need to produce the motion is directly proportional to the shear rate (velocity gradient, "$\frac{\partial u}{\partial y}$" (in case of one dimensional)) $\dot{\gamma}$ symbolize in tensor notation by S, Mathematically it can be written as:

$$\boldsymbol{\tau} = 2\eta \boldsymbol{S} \tag{1-36}$$

Where the deformation tensor S is defines as

$$\boldsymbol{S} = (\nabla \boldsymbol{u} + (\nabla \boldsymbol{u})^T)/2. \tag{1-37}$$

The constant of proportionate η is called dynamic viscosity or absolute [75, 76]. Viscosity in case of Newtonian fluid is independent on shear rate, polymerization rates (in case of reacting polymer foams) or time while it depends on temperature, concentration and pressure. The superscript ^{T} show transpose of the matrix. On the other hand, it can be stated as those fluids in which the graph of shear stress vs deformation rate (strain) is a linear curve passes through the origin as shown in Fig 1-7. But some experiments results indicates that this simple linear relationship between the shear stress and deformation rate is insufficient in practical application for the flow and deformation behaviour of a large class of fluids [69]. Moreover, no elastic properties are present in these fluids. Water, oil, all gases, glycerine, gasoline, alcohol, simple organic liquids, thin motor oils and low molecular weight inorganic solutions, are the typical examples of Newtonian fluids.

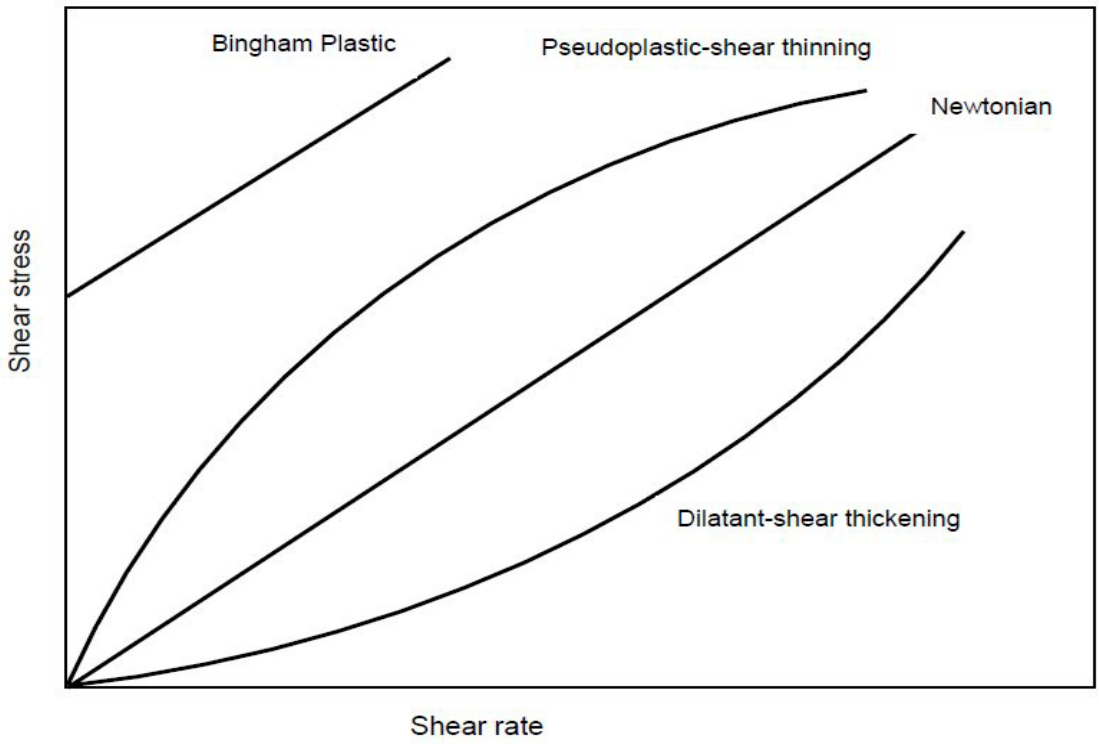

Fig. 1-7 Graphical representation(taken from [77]) of various types of non-Newtonian fluids,rheological behaviour.

1.4.2 Non-Newtonian Fluids

The fluids in which shear forces are not proportional to the rate of change of strain (deformation force) are non-Newtonian fluids and are broadly classified as complex fluids. It can also be stated as "fluids deviating from Newton's law of viscosity are non-Newtonian fluids". Thus it is explained that viscosity is not only affected by temperature, pressure and concentration but also a function of shear stress and shear rate. The relation of these two variables is:

$$\eta(\dot{\gamma}) = \tau/\dot{\gamma} \tag{1-38}$$

Complex fluids behaviour such as those acquired from high molecular weight liquids like polymers solution or polymer melts (polymers are long chain molecules build up from macromolecules called monomers which is combined together chemically). The macromolecular structure has the tendency to form clusters and significantly lead to non-linear behaviour between the applied stresses and the resulting strains (deformation rates). This non-linear behaviour between stress and strain makes these fluids non-Newtonian. This is a very major group of fluids with extensive industrial implementations in chemical engineering and biophysics.

Generally, non-Newtonian fluids further sub-divided as having three behaviours [75–

77] shown in Fig 1-8.

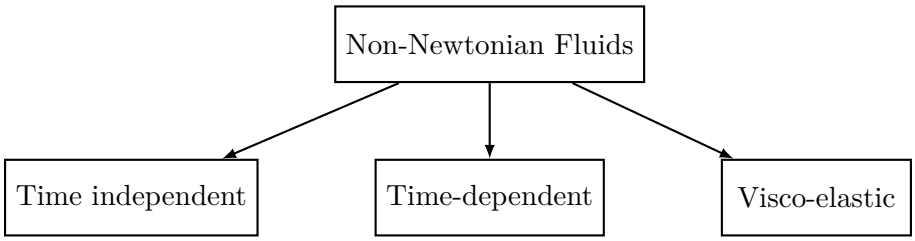

Fig. 1-8 Different types of non-Newtonian fluids

1.4.3 Time independent

Sub set of fluids for which at a given point the shear-rate is only dependent on the instantaneous shear stress at that point. Many empirical equations are present ([76] and the references their in) to model the observed relations between "τ_{xy}" and "$\frac{\partial u}{\partial y}$" (in case of one dimensional) for time independent fluids. They may be appropriately constituted for many engineering applications by the power law model, which for one-dimensional flow becomes [76].

$$\tau_{xy} = k\left(\frac{\partial u}{\partial y}\right)^{n} \quad \text{or} \quad \tau_{xy} = \eta\left(\frac{\partial u}{\partial y}\right) \qquad n \neq 1 \tag{1-39}$$

where $\eta = k\left(\frac{\partial u}{\partial y}\right)^{n-1}$ is term as apparent viscosity. Where n is index of flow behaviour and k is index of consistency. Eq.(1-39) reduce to "Newton law of viscosity" for $n = 1$.

Time independent fluids have three subclasses [75–77] shown in Fig 1-9.

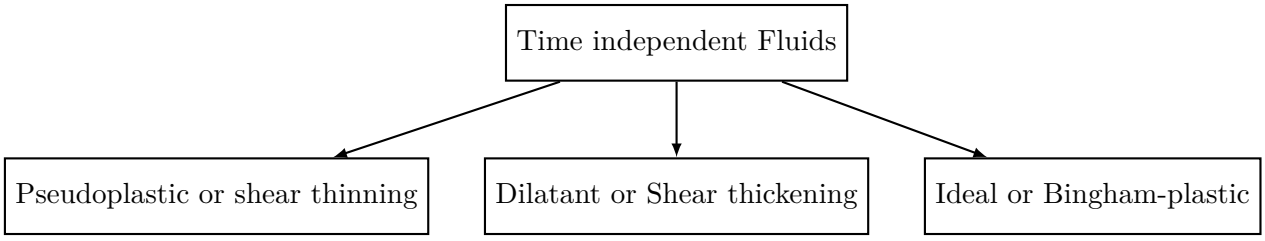

Fig. 1-9 Different types of time independent behaviours

1.4.3.1 Shear thickening

A group of fluids showing an obvious increase in apparent viscosity with the rise of deformation rate (i.e. $n > 1$ [76], as shown in Fig 1-7). It is also named as "Dilatant fluids" and exemplified by suspension of sands and corn starch, water and maize meal etc. Majority of such fluids acts as shear thinning in environments with low and very low shear rates [75].

1.4.3.2 Shear thinning

As against shear thickening these fluids exhibits to reduce their apparent viscosity as the shear rates is increased (i.e. $n < 1$ [76], as shown in Fig 1-7). Exemplified by paints and its related substances. These characteristics make these substances useful to be used over the walls and other smooth surfaces using brushes and applicators. These fluids apply evenly and flow smoothly when force is removed that is when the brushing element is removed and these do not trickle down [75]. Other examples are polymer solutions, paper pulp in water and colloidal suspensions [76].

1.4.3.3 Bingham plastics

The phenomena of threshold shear stress required to start flowing in a bunch of fluids. This threshold stress can also be named as yield stress. These fluids acts like solids below the yield stress exemplified by toothpaste and tooth lozenges. After the yield stress point these fluids start flowing like ordinary fluids see Fig 1-7. Visco-plastic fluids also fall under this subclass. These subclass fluids showing a proportional relationship to shear stress and shear rate but graph do not touch baseline and do not pass through the origin. Drilling muds, mayonnaise and clay suspension [75, 76] are few more examples exhibiting this behaviour.

1.4.4 Time dependent

A fluid whose viscosity depends on the flow duration is called time dependent non-Newtonian fluids. Which is further divided into two sub classes shown in Fig 1-10.

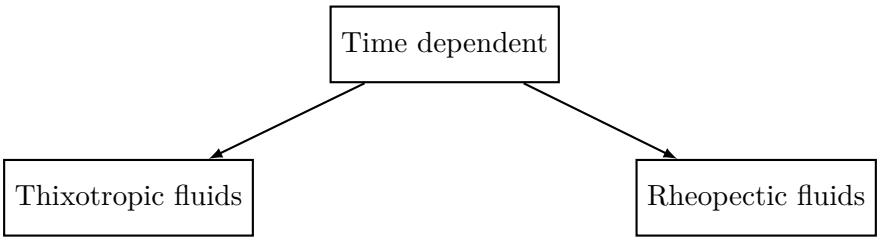

Fig. 1-10 Different types of time dependent behaviours

1.4.4.1 Rheopectic fluids:

Application of strain over a longer time (shearing time) increases the apparent viscosity (η as given in 1-39), this phenomena of time dependency of strain rate is "Rheopectic" characteristic of fluids. For these fluids shear stress is gradually increases to obtain constant shear rate. These can be exemplified by body synovial fluids [75], protein solutions and ink in the printing machines [76].

1.4.4.2 Thixotropic fluids:

Exactly to Rheopectic fluids or anti Rheopectic pertain to their opposing characteristics i.e. These fluids show a decrease in apparent viscosity (η) with time under a constant applied shear stress Such fluids become thinner with gradual increase in shear stress before reaching to a constant shear rate. These can be exemplified by many paints, Yoghurt, crude oil [75] and [76].

1.4.5 Viscoelastic Fluids

Hooke's law valid till the point proportionality reach. An ideal solid elasticity is the exhibition of this law. Viscoelastic fluids also known as memory fluids express characteristics of solid-like (elastic) and liquid-like (viscous) with deforming force [75]. Examples of these materials are dense colloidal suspensions (corn starch mixed in water), polymer solutions and melts, suspension of hard and deformable entities i.e. capsular or lipid bodies, biological cells. The prime flow pattern of viscoelastic fluids include rod climbing (when mixed and stirrup), extrudate swell and tubeless siphoning off. Other than the examples discussed above, there are also other cases such as, When stirring or jolting, egg white moves up the container [75].
Viscoelastic fluids are modelled through linear viscoelastic models at low deformation rate while having non-linear viscoelastic behaviour for higher time scale deformation process. Polymeric fluids are viscoelastic substances with their particles depending on the deformation force for its received stress and strain. Deborah number, a dimensionless number measure this characteristic denoted by De. At low Deborah number liquid-like characteristics dominate and at high Deborah number solid like characteristics dominate. When De = 0 shows a purely viscous characteristics [78]. For complete history and explanation of viscoelastic fluids, we refer the reader to the excellent literature in [69, 79].
Viscoelastic fluids manifest complicated characteristics pertaining to their complex response due to fluid stresses when deformation force is applied. They behave inversely to stresses applied than the inelastic fluids responding proportionally under applied stresses as per Newton's law of viscosity. Supportive constitutive stress models are added to the Eqs. (1-17 –1-18) to completely explain their mechanical response. Different viscoelastic fluids have different constitutive stress equations. A list of constitutive model equations is given in Table1-3. These equations remain same (objective) in term of work and energy produced when any possible arbitrary motion occur. Stress constitutive models rely on micro chemistry of the fluids shown by algebraic, differential, integral and integro differential forms [74]. The Giesekus

Table 1-3 List of different constitutive models [74].

Model Name	Equation
Oldroyd-B	$\boldsymbol{\tau} + \lambda \overset{\nabla}{\boldsymbol{\tau}} = 2\eta \boldsymbol{S}$
John-Segalman	$\boldsymbol{\tau} + \lambda \overset{\square}{\boldsymbol{\tau}} = 2\eta \boldsymbol{S}$
Leonov	$\boldsymbol{\tau} + \lambda \overset{\nabla}{\boldsymbol{\tau}} + \frac{1}{2}\boldsymbol{\tau}^2 = 2\eta \boldsymbol{S}$
Phan-Thien-Tanner	$\exp\left(\frac{\epsilon\lambda}{\eta}\right)\boldsymbol{\tau} + \lambda \overset{\square}{\boldsymbol{\tau}} = 2\eta \boldsymbol{S}$
FENE-P	$\left(1 + \frac{\frac{(3)}{(1-\frac{(3)}{(L_k)^2})} + \frac{\lambda}{\eta Tr(\boldsymbol{\tau})}}{(L_k)^2}\right)\boldsymbol{\tau} + \lambda \overset{\nabla}{\boldsymbol{\tau}} = \frac{2\eta \boldsymbol{S}}{(1-\frac{3}{(L_k)^2})}$
FENE-CR	$\left(\frac{(L_k)^2 + \frac{\lambda}{\eta Tr(\boldsymbol{\tau})}}{((L_k)^2-3)}\right)\boldsymbol{\tau} + \lambda \overset{\nabla}{\boldsymbol{\tau}} = 2\left(\frac{(L_k)^2 + (\lambda/(\eta)Tr(\boldsymbol{\tau}))}{((L_k)^2)-3}\right)\boldsymbol{S}$
EPTT	$\exp\left(\frac{\epsilon\lambda Tr(\boldsymbol{\tau})}{\eta}\right)\boldsymbol{\tau} + \lambda \overset{\square}{\boldsymbol{\tau}} = 2\eta \boldsymbol{S}$
Rolie-Poly	$\frac{D\boldsymbol{\tau}}{Dt} = -\frac{1}{\lambda}(\boldsymbol{\tau} - I) - 2\frac{\left(1-\sqrt{\frac{3}{Tr(\boldsymbol{\tau})}}\right)}{\lambda_R}\left[\boldsymbol{\tau} + \hat{B}(\frac{Tr(\boldsymbol{\tau})}{3})(\boldsymbol{\tau} - I)\right]$

constitutive equation (with suitable adjustment to incorporate the volume fraction of nanoparticles which will be discus in the coming chapters) will be focus in this thesis. The equation is presented as,

$$\boldsymbol{\tau} + \lambda \overset{\nabla}{\boldsymbol{\tau}} + \varepsilon \boldsymbol{\tau}^2 = 2\,\eta \boldsymbol{S}, \tag{1-40}$$

where ε is the Giesekus non-linear parameter (taking $\varepsilon = 0$ reduces to the Oldroyd-B model), λ is the reptation relaxation time and $\overset{\nabla}{\boldsymbol{\tau}}$ denote the upper convective derivative and given as,

$$\overset{\nabla}{\boldsymbol{\tau}} = \frac{D\boldsymbol{\tau}}{Dt} - \nabla \boldsymbol{u} \cdot \boldsymbol{\tau} - \boldsymbol{\tau} \cdot (\nabla \boldsymbol{u})^T . \tag{1-41}$$

1.5 Thermal runway

In inflammable substances thermal runway is a challenge, producing blasts and accidents. Such accidents increases in the form of moving fluids in pipes, industrial set ups, machinery and automobile sector. This is correlated with extraordinary exothermic reactions and chemical kinetics that are aggravated with temperature (T) increase. This phenomenon can be mitigated by using heat reduction techniques shown by [80]. This will be a marvellous job, to mathematically build up a condition to recognize the point of ignition at its earliest time. It could be of great importance if ways and means are sorted out to prevent and prolong this thermal runaway time. Various studies have been conducted to understand the role of liquid visco-elasticity in lowering the temperature of liquids [81], [82], [83]. At the end, it is also important to recognise the importance of temperature at "blow up point" (critical point).

1.6 Shear banding

Shear banding also called shear localization is known to happen not only in rocks. Apart from rocks, this phenomenon can also be observed in viscoelastic substances. This band (shear band) is a narrow rim of high strain produced shear stress manifested by Fig 1-11 two hypotheses clarify the occurrence and formation of these bands. Both of these theories make use of the mechanism of shear and strain produced when a material is subjected to any type of shear force.
The first theory involves the mechanism of melting of molecules secondary to plastic material heating in response to excessive shear forces. The second mechanism of shear banding is explained by the compressive shear stress leading to the hardening of the materials. Fig 1-11 shows opposite shear forces working on the fluid between two moving walls. The adjacent fluid layer to the lower plate moves in the shear force direction. Likewise, the lower fluid layer moves in the opposite direction with the lower plate. Because of plastic deformation and compressive shear forces at the middle region, establish three shear bands. Different shear-rates created by different fluid layers varying velocities lead to these shear bands [84].

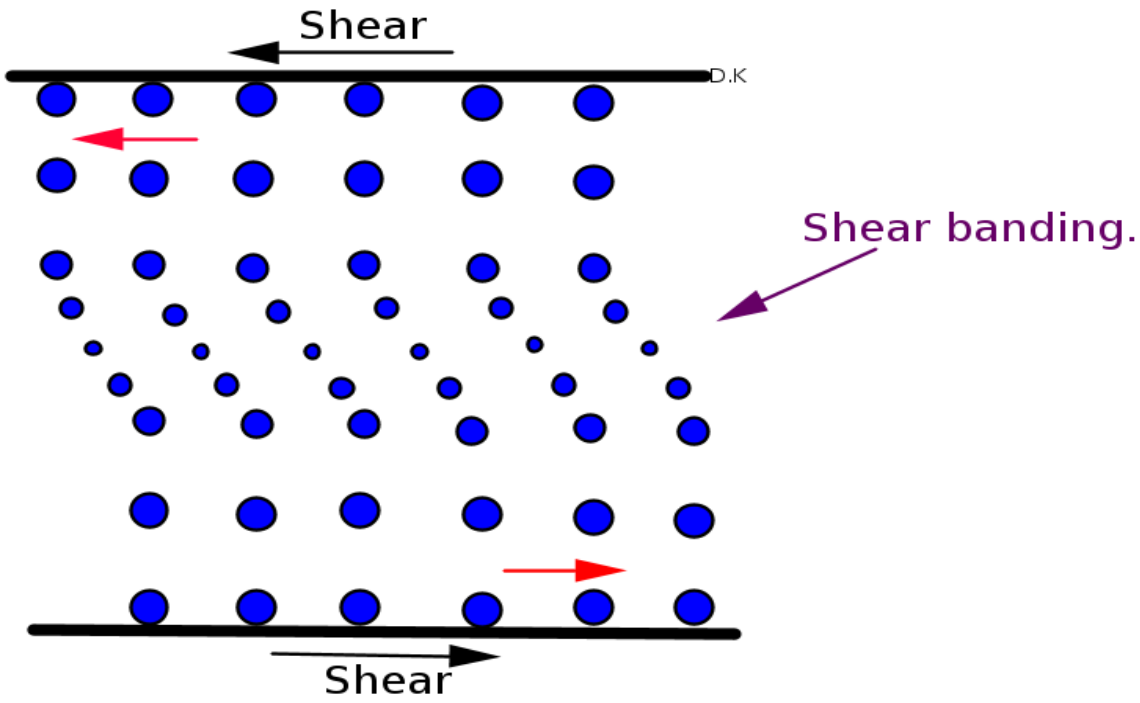

Fig. 1-11 Schematic of Shear banding phenomenon in viscoelastic fluids(taken from [84]).

Two distinct shear bands being relevant to high shear-rate as well as low shear-rate created along the velocity profile were obviously noted by [85]. Particles in

the shear belt are highly strained opposed to other regions by cause of high heat as well as high shear-rate. That discontinuity in shear-rate make a bend in the fluent substances. Moreover, certain viscoelastic fluids, for some values of parameters, submit a non-monotonic relationship between shear stress and the shear rate. In addition, there are many constitutive models (like Johnson-Segalman [86, 87]), (ROly-Poly, [88]) that exhibition shear banding. We use, as in [88], the Giesekus model. The choice of that latter model is possibly like it has completely developed heat equation. Extreme shear banding phenomenon can cause deformation and harm to tractable substances which attracts mathematical concern as scientists make an attempt to get the sort of harm created.

1.7 The Finite Difference Method (FDM)

As mentioned earlier the complex rheology of the Newtonian and non-Newtonian fluids is quite challenging task for numerical simulations. They are modelled mathematically using Partial Differential Equations (PDEs) which are then solved by using different (i.e. FDM, FEM and FVM etc.) numerical techniques. Among these the finite difference techniques is extensively used and will discuss here to carry out all the simulation in this thesis. Similar to other numerical schemes while assessing and solving Differential Equations (DEs), finite difference method and it's functional principle is based to approximate a differential operator using a differential quotients obtained from the Taylor series, instead of derivatives in computations and equations. These are discussed as the Partial Differential Equations are converted into a more usable and solvable system of algebraic differential equations [89]. The solution of the system of equation is calculated on the grid point by discretising the domain as shown below. Each grid point(or node see Fig 1-12) denotes the unknown value of the field variables. We assume the uniform grid (i.e the distance between two nodes both in time and space are equal). Taking as one-dimensional case to make it simple we can derive the approximation to first derivative. Let us consider a function $u(y)$ which is minimum three times differentiable in the neighbourhood of y, then by the Taylor theorem expansion:

$$u(y + \Delta y) = u(y) + \Delta y \frac{\partial u}{\partial y} + O((\Delta y))^2 \tag{1-42}$$

By setting $\Delta y = h$, truncating the series to first order and rearranging gives

$$\frac{\partial u}{\partial y} \approx \frac{u(y + h) - u(y)}{h} \tag{1-43}$$

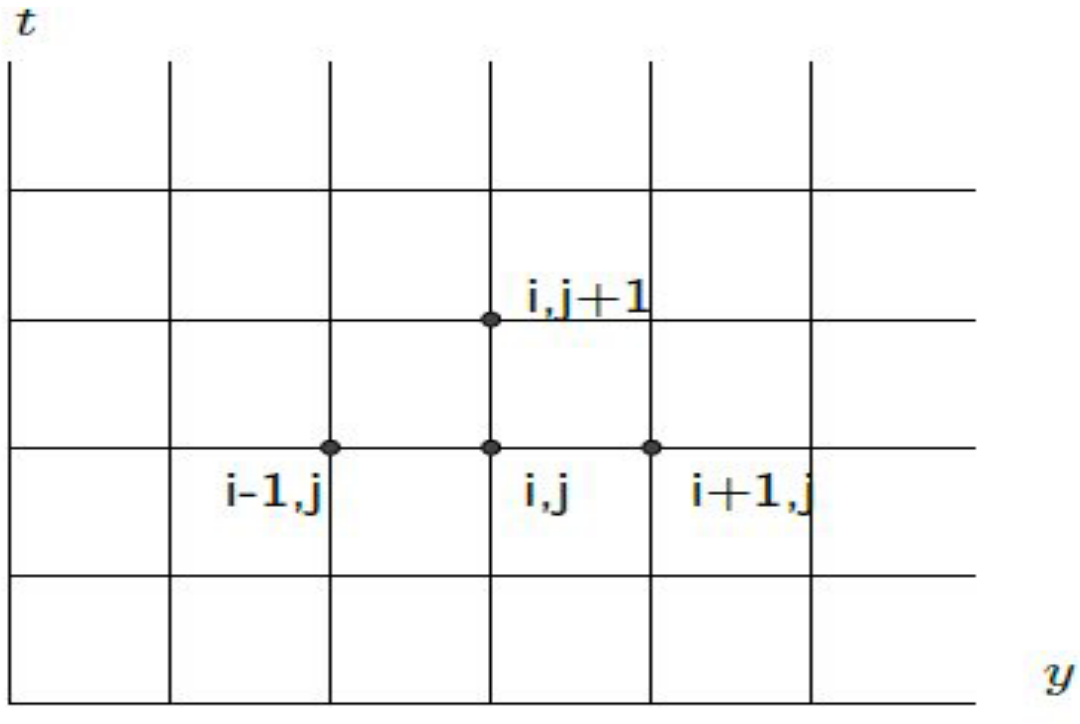

Fig. 1-12 Solution mesh [84]).

This is called forward difference. The truncation error is of order $O(h)$. In a similar way, we can expand the $u(y-\Delta y)$ to first order term as we did for $u(y+\Delta y)$, to get

$$\frac{\partial u}{\partial y} \approx \frac{u(y)-u(y+h)}{h} \tag{1-44}$$

This is known as backward difference with the same truncation error of approximation. To improve the accuracy we take the difference of two resulting truncated Taylor's expansion of $u(y+\Delta y)$ and $u(y-\Delta y)$ we obtain

$$\frac{\partial u}{\partial y} \approx \frac{u(y+h)-u(y-h)}{2h} \tag{1-45}$$

The Eq (1-45) known as central difference with error of order $O(h^2)$, which is better than other two. The central difference are used in an analogous way to approach second order derivative as

$$\frac{\partial u}{\partial y} \approx \frac{u(y+h)-2u(y)+u(y-h)}{h} \tag{1-46}$$

Now let us suppose $u(t,y)$ is a regular and smooth function of time t and space y. suppose the step size be $\Delta y = h$ and the time step to be set as $\Delta t = k$. We use a grid or mesh with point at equal distance with nodes defined as $(t_n, x_i) = (nk, ih)$ with n, i are non- negative integers. At the grid point (t_n, x_i) the approximation of solution is shown as u_i^n. The space derivatives of order first and second are approximated by

central difference while the time derivative can be approximated with three probable schemes i.e. implicit, explicit and Crank-Nicolson [90].

Implicit Scheme: when $\frac{\partial u}{\partial t}$ is approximated making use of backward difference method at time step t_{n+1} and approximating the spatial derivative via implication of central difference method at the point x_i. Implicit method is numerically convergent, accurate and stable for large time step Δt but difficult to implement [91].
Explicit scheme: when $\frac{\partial u}{\partial t}$ is approximated while using the forward difference technique at time step t_n and approximating the spatial derivative while making use of the central method at the point x_i. This technique is easy to implement but less accurate and work for small values of time step size.

Crank-Nicolson Scheme: This scheme is the midpoint and average of the two techniques discussed earlier in the above. This scheme make use of central difference method at time $t_{n+1/2}$ and repeat central difference at space point x_i. In comparison the Crank-Nicolson scheme is numerically stable, convergent and accurate for small time step but quite extensive to implement [90].

1.8 Outline of the thesis

This dissertation consists of five chapters, which is organised as followed: In chapter 2 the investigations are based on the "Computational analysis of the dynamics of generalized- viscoelastic-fluid-based nanofluids (GVFBNs) subject to exothermic reaction in shear flow" whereas, those in chapter 3 are based on the "Non-isothermal pressure-driven flow of generalized viscoelastic-fluid-based-nanofluids in a channel". In the subsequent chapter 4 is the "Computational analysis of shear-banding in simple-shear-flow of viscoelastic-fluid-based nanofluids subject to exothermic reactions". Followed by chapter 5 which provides "Computational analysis of non-isothermal dynamics of gravity driven flow of viscoelastic-fluid-based nanofluids down an inclined plane". Each chapter for the numerical scheme used has a brief graphical presentation of the spatial and temporal convergence. Furthermore, each of the thesis chapters has a detailed introduction and conclusion which addresses research questions along with corresponding findings that are relevant to understanding nanofluids. Finally, chapter 6 ends the thesis with the "Conclusion", which synthesizes findings of the empirical research chapters in relation to the overarching research question and study objectives as well as the future work.

Chapter 2 Computational analysis of the dynamics of generalized- viscoelastic-fluid-based-nanofluids subject to exothermic reaction in shear flow[1]

ABSTRACT

In this chapter we focuses on a novel problem that describes laminar simple shear-flow of generalized-viscoelastic-fluid-based nanofluids (GVFBN) containing spherical shaped nano-particles under non-isothermal conditions but with isothermal wall-temperature boundary-conditions is investigated. The GVFBN model is an extension of the VFBN to include shear-rate dependent viscosity effects. The Generalized non-isothermal Giesekus constitutive model (which is reducible to generalized Oldroyd-B model) with essential modifications for thermodynamics is used to account for the viscoelastic effects. Spherical shaped nano-particles are homogeneously mixed to the viscoelastic base fluid. To characterize the shear-thinning-viscosity, a viscosity-constitutive-model of the Carreau-type is employed. A temperature-dependent thermal conductivity is also considered. Additionally, empirical models are employed to account for to the nano-particle effects on the thermal conductivity. We use an efficient, semi-implicit, numerical scheme, based on finite difference methods (FDM), to obtain the numerical solutions of the model equations. The numerical scheme is computationally implemented in MATLAB. Results are graphically presented in both a qualitative and quantitative sense with regards to the various embedded parameters. Specifically, the thermodynamic and fluid-dynamical impacts of variations in the volume fraction of nano-particles are explored. In summary, we notice enhanced thermal conductivity and hence also increased temperature with increasing nano-particle volume fraction. The GVFBN model accounts for all four nanofluid types, Generalized-Newtonian-fluid-based nanofluids (GNFBN), Newtonian-fluid-based nanofluids (NFBN), Generalized-viscoelastic-fluid-based nanofluids (GNFBN), and viscoelastic-fluid-based nanofluids (VFBN). The comparative thermal runaway susceptibility of the four nanofluid types is presented and we demonstrate that the order of susceptibility from the most to the least susceptible is GNFBN, NFBN, GVFBN, VFBN.

[1]The contents of this chapter are from khan et.al [92]

2.1 Introduction

The enhancement, reduction, or improvement of heat transfer characteristics in fluids is of fundamental practical importance many industrial applications. The heating and cooling operations in heat exchangers and microelectronics are obvious examples. In addition to heat transfer enhancement, nanofluids are used in many other industrial applications, transportation, electronics, biomedicine, and food production, [93, 94]

The addition of nano-sized particles (which are generally referred to as nano-particles) to an existing base-fluid will naturally change important thermodynamic properties and characteristics of the resultant particle-fluid mixture. Mixing of nano-particles with a base-fluid gives an emulsion or suspension that is generally termed a nanofluid, [2]. Two possibilities arise with regards the composition of a nanofluid- either the nanofluid resembles, a two-phase, concentrated suspension of nano-particles heterogeneously mixed in the base-fluid; alternatively the final nanofluid mixture is a single-phase homogeneous emulsion or solution.

The addition of nano-particles (via either the two-phase or single-phase processes) to a base-fluid is essentially aimed at improving the thermodynamic properties of the original base-fluid. Nanofluids dynamics generally, therefore, finds wide application in the design of Heat-Transfer-Fluids (HTFs). As an example, [95] designed a nanofluid from a mixture of copper (Cu) nano-particles with deionized distilled water. They experimentally demonstrated that the comparative ratios of the effective-thermal-conductivities of the resultant nanofluid as compared to those of the original (particle free) fluid (deionized distilled water in this case) increases from a low of 1.24% to a high of 1.78% in the case where the mixture volume-fraction of the copper nano-particles is raised from a low of 2.5% per volume to a high 7.5% per volume. Using an ethylene glycol (EG) base-fluid, the researchers in [96] studied the effective thermal conductivity of the resultant nanofluids, resulting from an addition of 0.3% volume fraction Cu nanoparticles. This suspension of Cu nanoparticles in an EG base fluid enhanced the thermal conductivity by 40% . The work in [97] reported a 20% enhancement in thermal conductivity of a suspension of 4% volume, 35 nm size copper-oxide (CuO) particles in an EG base fluid.

Many other nanofluids, formed from both metallic and non-metallic nano-particles

show considerable enhancement (increase) in the effective-thermal-conductivities when compared to the original (particle free) fluid, [98]. For example, investigations in [36, 99] on heat-transfer properties in laminar (nanofluid) flow of aluminium-oxide/ethylene-glycol and aluminium-oxide/water nanofluids and report noticeable improvement in the heat-transfer-rate (HTR). Given their documented HTR enhancement and increased thermal-condictivities, nanofluids are therefore, not surprisingly, now widely used as the standard with regards heat-transfer-improvement fluids. Effective-thermal-conductivities of industrial nanofluids are naturally dependent on such properties as the size, the shape, and the volume-fractions of the embedded nano-particles. Possible methods of improving the heat-transfer characteristics of nanofluids therefore include, among others, increasing the Brownian motion of nano-particles suspended within the base-fluid, increasing the contact surface-area of the nano-particles, and increasing the contact of liquid layers around the nano-particles[100, 101].

The mathematical modelling and numerical analysis of nanofluid dynamics depends on whether the single-(homogeneous mixing)-phase (P1) or two-(heterogeneous mixing)-phase (P2) approach is adopted. The heterogeneous-mixing approach requires, in addition to the usual fluid dynamical equations, a concentration equation for the suspended nano-particles. In the single-phase approach, as adopted in this paper, the fluid dynamical equations are modified to include a volume fraction function for the homogeneously mixed nano-particles. Indeed, empirical models have been developed to include the nano-particle volume fraction into the constitutive models for the fluid viscosity, thermal conductivity, etc..

In the P2 approach, differences in the velocities of nano-particles and base-fluid play significant roles in HTR enhancement characteristics of resultant nanofluids. For water-based 1% by volume Cu-nanofluids in a pipe, [102] employed the P2 model to investigate HTR enhancement. Results demonstrated that the P2 approach gave better HTR enhancement than the single-phase homogeneous mixture (P1) approach. The computational (Eulerian) based two-phase approach, adopted in [103] to simulate the HTR characteristics of copper-water nanofluid (micro-channel) flow compared very well with experimental data. An Eulerian-Lagrange two-phase approach, [104] was similarly employed to investigate the HTR characteristics for copper and aluminium-oxide nanofluid flow.

The results of [20, 36] demonstrate that, under certain conditions, the base-fluid and nano-particles can reach a state of thermal equilibrium and both move with uniform velocity. In such cases, the nanofluid system would be homogeneous and hence the single-phase approach would be more appropriate to simulate such flows. This is the approach adopted in this paper. Mixing (solid and metallic) nano-particles to a base-fluid would naturally raises the resultant nanofluid effective-viscosities as compared to the base-viscosities of the original (particle free) fluids [105, 106]. These viscosity-altering effects of the nano-particles must be factored into the viscosity-constitutive-modelling. Implications for the real physical systems and applications mean that the increased drag, that results from the increased viscosities, would necessitate corresponding increases in the fluid driving forces, such as pumping pressures, etc.

Rather than employing usually costly driving force enhancement techniques such as increasing the pumping pressures, an increasingly popular approach to drag reduction is the use of turbulent drag-reducing fluids, Toms [107]. Turbulent drag-reducing fluids are viscoelastic liquids made by adding tiny amounts of polymers or surfactants to a Newtonian liquid, see for example [108] who demonstrated that reduction of drag and HTR enhancement happen simultaneously. Qi et al. [109] similarly studied the correspondence between HTR enhancement and turbulent drag-reducing properties.

The turbulent drag-reducing-liquids, in combination with the HTR enhancing nano-particles, produce the unique (nano)fluid that we term VFBN [110]. The work in [111] experimentally demonstrated that both viscoelastic fluids and VFBNs significantly induce drag-reduction in turbulent-flows and additionally that use of VFBNs lead to HTR enhancement.

Thermal runaway (blowing up of temperature in a finite time) is an actual physical problem that can cause explosions in flammable materials. The flow of fluids which are subject to exothermic reactions can indeed lead to self-ignition and thermal runaway. This phenomenon, being closely linked with exothermic reactions and chemical kinetics can be mitigated by employing heat reduction techniques [80]. Various investigations have been conducted to understand the role of fluid viscoelasticity in fluid-temperature reduction [80], [112], [82], [113], [114], [115], [116], [83], [117], [118], [15], [119]. Magnetic effects and energy dissipation of viscoelastic fluids

and nanofluids are also investigated in [120–128].

Motivated by the above literature, the main aims of this paper are to explore the HTR characteristics of GVFBN, essentially, therefore, investigating the combined effects of nano-particles and viscoelasticity. Specifically, we investigate the characteristics of the nanofluids formed by adding nano-particles to each of the four most general fluid types; Newtonian, Generalized Newtonian, viscoelastic, and Generalized viscoelastic. The following sequence is adopted in the paper. Section 2.2 gives the development and details of the underlying mathematical equations and models. The FDM-based numerical-algorithms as well as the basic (graphical) tests and fundamental efficacy of the computational methodologies are given in Section 2.3. The main results are presented graphically in Section 2.4, including the parameter-sensitivity of solution variables. Concluding and related remarks are given in section 2.5.

2.2 Problem Formulation

Fig. 2-1 gives a schematic geometry of the physical flow model.

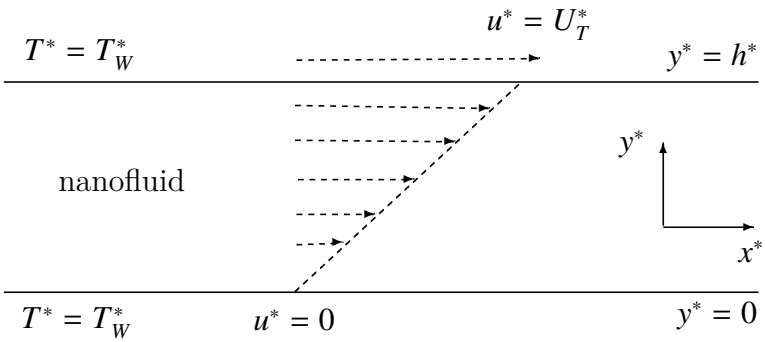

Fig. 2-1 Geometry of the model problem.

Underlying flow assumptions are otherwise summarized as follows:

- The physical setup of the model problem is a Couette-type shear-flow of GVFBN enclosed by two parallel walls of infinite (longitudinal) extent.
- The walls are located (apart) at a vertical parallel distance of h^*.
- We assume that the upper-wall is located at height $y^* = h^*$, and moves to the right at the constant speed of $u^* = U_T^*$.
- This results in a simple shear flow, driven by the moving upper plate and whose velocity is independent of the longitudinal direction, x^*.

- The lower-plate is fixed, with velocity $u^* = 0$, and located at height $y^* = 0$.
- Given that we are only interested in simple shear flow, the pressure will be considered constant.
- Both the lower and plates are maintained at the isothermal temperature $T^* = T_W^*$.

The governing (nano) fluid-dynamics equations (i.e. continuity, momentum, energy, etc.) for the GVFBN are defined in Eqs. (2-1 - 2-10) below.

$$\nabla^* \cdot \boldsymbol{u}^* = 0, \tag{2-1}$$

$$\rho_{nf}^* \frac{D\boldsymbol{u}^*}{Dt^*} = -\nabla^* p^* + \nabla^* \cdot (\boldsymbol{\sigma}^*), \tag{2-2}$$

$$(\rho\, c_p)_{nf}^* \frac{DT^*}{Dt^*} = -\nabla^* \cdot \boldsymbol{\phi}_q^* + Q_D^* + Q^*\, A^*\, C^*\, \exp\left(\frac{E^*}{R^*\, T^*}\right), \tag{2-3}$$

Here $\boldsymbol{u}^*$ represents the GVBNF velocity, ρ_{nf}^* the GVBNF density, T^* the GVBNF temperature-field, $c_{p_n f}^*$ the GVBNF specific heat capacity, p^* the GVBNF pressure-field, $\boldsymbol{\sigma}^*$ the total stress-tensor. E^* the activation-energy, C^* the residue-concentration, A^* the Arrhenius-prefactor, Q^* the energy-released due to exothermic-reaction, see [80], and R^* is the gas constant.
The total stress tensor is defines as,

$$\boldsymbol{\sigma}^* = \boldsymbol{\tau}^* + \frac{\eta_s^*}{(\sqrt{1-\varphi})^5}\, \boldsymbol{S}^*,$$

where the polymeric tensor, $\boldsymbol{\tau}^*$, is described by the non-isothermal Giesekus model, the nano-particle volume-fraction is φ, and the deformation-rate-tensor is,

$$\boldsymbol{S}^* = \nabla^* \boldsymbol{u}^* + (\nabla^* \boldsymbol{u}^*)^T .$$

The operators, $D/(Dt^* = \partial/\partial t^* + \boldsymbol{u}^* \cdot \nabla^*$ and ∇^* are respectively the substantive derivative and the gradient. The heat-flux vector follows Fourier's law,

$$\boldsymbol{\phi}_q^* = -\nabla^* (\kappa_{nf}^* T^*),$$

with κ_{nf}^* the temperature-dependent nanofluid thermal-conductivity [113]. For visco-elastic materials, (mechanical) energy is partially saved and partially dissipated [114] and the dissipation function is therefore defined as,

$$Q_D^* = \frac{\eta_s^*}{(\sqrt{1-\varphi})^5}\boldsymbol{S}^* : \nabla^*\boldsymbol{u}^* + \gamma\boldsymbol{S}^* : \boldsymbol{\tau}^* + (1-\gamma)\frac{\hat{G}^*}{2\lambda^*}\left(I_1 + \mathrm{Tr}(\boldsymbol{b}^{-1}) - 6\right), \tag{2-4}$$

where the irreversibility component $\frac{\eta_s^*}{(\sqrt{1-\varphi})^5}\boldsymbol{S}^* : \nabla^*\boldsymbol{u}^*$ represents mechanical dissipation and the component, $\gamma\boldsymbol{S}^* : \boldsymbol{\tau}^*$, is the reversibility part.

In Eq. (2-4), $\hat{G}^*$ is the shear Modulus, λ^* is the relaxation time, γ is a constant with range, $0 \le \gamma \le 1$. The constant γ is incorporated to model the energy reversibility due to the elastic behaviour of viscoelastic (nano) fluids. The choice $\gamma = 1$ corresponds to the case of pure entropy elasticity [114] in which the material behaves as purely viscous and the mechanical energy is released as work done. On the other hand, the choice $\gamma = 0$ corresponds to the case in which mechanical energy is stored as elastic energy, and the material behaves as purely elastic [114, 115]. The intermediate values $0 < \gamma < 1$ correspond to a linear combination of the stress work and dissipation. The notation (:) represents the double dot product between two tensors. The conformation tensor, $\boldsymbol{b}^*$, is linked to the polymer stress tensor, $\boldsymbol{\tau}^*$, via Eq.(2-5),

$$\boldsymbol{\tau}^* = \hat{G}^*(B^*\boldsymbol{b}^* - \boldsymbol{I}), \tag{2-5}$$

where $\boldsymbol{B}^*$ is a material constant. The polymer stress tensor $\boldsymbol{\tau}^*$ is described by the non-isothermal Gisekus constitutive model, [116],

$$\boldsymbol{\tau}^* + \varepsilon^*\boldsymbol{\tau}^{*2} + \lambda^*\left[\overset{\nabla^*}{\boldsymbol{\tau}} - \boldsymbol{\tau}^*\frac{D}{Dt^*}\left(\ln\left(\frac{T^* - T_W^*}{T_W^*}\right)\right)\right] = \frac{\eta_p^*}{(\sqrt{1-\varphi})^5}\boldsymbol{S}^*, \tag{2-6}$$

where the upper convective time derivative, $\overset{\nabla^*}{\boldsymbol{\tau}}$, is define as,

$$\overset{\nabla^*}{\boldsymbol{\tau}} = \frac{D\boldsymbol{\tau}^*}{Dt^*} - \nabla^*\boldsymbol{u}^*\cdot\boldsymbol{\tau}^* - \boldsymbol{\tau}^*\cdot(\nabla^*\boldsymbol{u}^*)^T. \tag{2-7}$$

In Eq. (2-6), η_p^* is the polymer viscosity and η_s^* is the solvent viscosity, so that the total viscosity, η^* is,

$$\eta^*(T^*) = \eta_p^*(T^*) + \eta_p^*(T^*). \tag{2-8}$$

We assume that the temperature dependence of both the relaxation time and the solvent viscosity follow Nahme-type laws,

$$\lambda^* = \lambda_0^*\frac{T_W^*}{T^*}\exp\left(-\frac{T^* - T_W^*}{T_W^*}\right), \qquad \eta_s^* = \eta_{s0}^*\exp\left(-\frac{T^* - T_W^*}{T_W^*}\right), \tag{2-9}$$

where λ_0^* and η_{s0}^* respectively denote constant relaxation time and solvent viscosity under isothermal conditions.

Addition to temperature dependence, the polymer viscosity is also assumed to be shear rate dependent, following a Carreau model, [112],

$$\eta_p^* = \left[\eta_{p\infty}^* + \left(\eta_{p0}^* - \eta_{p\infty}^*\right)\left(1 + (\lambda^*\,\dot{\gamma}^*)^2\right)^{\frac{n-1}{2}}\right]\exp\left(-\frac{T^* - T_W^*}{T_W^*}\right), \tag{2-10}$$

where $\dot{\gamma}^*$ represents the shear rate,

$$\dot{\gamma}^* = \sqrt{\boldsymbol{S} : \boldsymbol{S}/2}.$$

The reference viscosities, $\eta_{p\infty}^*$ and η_{p0}^* respectively represent polymer viscosity at infinite shear rate and polymer viscosity at zero shear rate. The power, n, models shear-thinning and shear-thickening properties.

2.2.1 Dimensionless equations

We introduce the following non-dimensional variables,
Non-dimensional variables

$$\boldsymbol{x} = \frac{\boldsymbol{x}^*}{h^*},\ t = \frac{U_T^*}{h^*}\,t^*,\ \nabla = h^*\,\nabla^*,\ \boldsymbol{u} = \frac{\boldsymbol{u}^*}{U_T^*},\ T = \frac{T^* - T_W^*}{\alpha\,T_W^*},$$

$$p = \frac{p^*}{\rho_f^*\,U_T^{*2}},\ \eta_s = \frac{\eta_s^*}{\eta^*},\ \eta_p = \frac{\eta_p^*}{\eta^*},\ \lambda = \frac{\lambda^*}{\lambda_0^*},\ \varepsilon = \frac{\eta^*\,U_T^*}{h^*}\,\varepsilon^*,$$

$$\boldsymbol{\tau} = \frac{h^*}{\eta^*\,U_T^*}\,\boldsymbol{\eta}^*,\ \boldsymbol{S} = \frac{h^*}{\eta^*}\,\boldsymbol{S}^*,\ \hat{G} = \frac{h^*}{\eta^*\,U_T^*}\,\hat{G}^*. \tag{2-11}$$

Dimensionless parameters

The dimensionless parameters of interest are the; Reynolds number (Re), Brinkman number (Br), Deborah number (De), activation energy parameter (α), Prandtl number (Pr), Peclet number (Pe = Re · Pr, Frank-Kamenetskii parameter (δ_1), and the ratio of the polymer to the total viscosity (β). These are defined as follows,

$$\beta = \frac{\eta_p^*}{\eta^*},\ \mathrm{De} = \frac{\lambda_0^*\,U_T^*}{h^*},\ \mathrm{Re} = \frac{\rho_f^*\,U_T^*h^*}{\eta^*},\ \mathrm{Pr} = \frac{c_{p_f}^*\,\eta^*}{\kappa_f^*},\ \mathrm{Br} = \frac{\eta^*\,U_T^{*2}}{\kappa_f^*\,\alpha\,T_W^*},$$

$$\mathrm{Re}_{nf} = \frac{\rho_{nf}}{\rho_f}\,\mathrm{Re},\ \mathrm{Pe}_{nf} = \frac{(\rho\,c_p)_{nf}}{(\rho\,c_p)_f}\,\mathrm{Pe},\ \alpha = \frac{R^*\,T_W^*}{E^*},\ \delta_1 = \frac{Q^*\,A^*\,C^*\,h^{*2}}{\kappa_f^*\,R^*\,T_W^{*2}}\exp\left(-\frac{1}{\alpha}\right). \tag{2-12}$$

The nanofluid quantities $(_{nf})$ are obtained from a combination of the volume fractions (φ) of the base fluid $(_f)$ and the nanoparticles $(_s)$,

$$\rho_{nf} = \varphi\,\rho_s + (1-\varphi)\,\rho_f, \qquad (\rho\,c_p)_{nf} = \varphi\,(\rho\,c_p)_s + (1-\varphi)\,(\rho\,c_p)_f.$$

Introducing the non-dimensional variables and dimensionless parameters into the governing equations yields the dimensionless equations listed below.

$$\nabla\cdot\boldsymbol{u} = 0, \tag{2-13}$$

$$\mathrm{Re}_{nf}\,\frac{D\boldsymbol{u}}{Dt} = -\mathrm{Re}_{nf}\,\nabla p + \nabla\cdot(\boldsymbol{\sigma}), \tag{2-14}$$

$$\mathrm{Pe}_{nf}\,\frac{DT}{Dt} = -\nabla\cdot\left(\kappa_{nf}\,\nabla T\right) + \mathrm{Br}\,Q_D + \delta_1\,\exp\left(\frac{T}{1+\alpha T}\right), \tag{2-15}$$

$$\boldsymbol{\tau} + \varepsilon\,\boldsymbol{\tau}^2 + \mathrm{De}\,\bar{\lambda}(T)\left[\overset{\nabla}{\boldsymbol{\tau}} - \boldsymbol{\tau}\,\frac{D}{Dt}\left(\ln(1+\alpha T)\right)\right] = \frac{\eta_p(T)}{(\sqrt{1-\varphi})^5}\,\boldsymbol{S}, \tag{2-16}$$

In Eqs. (2-13 - 2-16), ε is the dimensionless Giesekus non-linear parameter (taking $\varepsilon = 0$ reduces to the Oldroyd-B model), the dimensionless total stress tensor is,

$$\boldsymbol{\sigma} = \boldsymbol{\tau} + \frac{\eta_s(T)}{(\sqrt{1-\varphi})^5}\,\boldsymbol{S},$$

where the dimensionless deformation rate tensor is,

$$\boldsymbol{S} = \nabla\boldsymbol{u} + (\nabla\boldsymbol{u})^T.$$

The dimensionless upper convective time derivative is,

$$\overset{\nabla}{\boldsymbol{\tau}} = \frac{D\boldsymbol{\tau}}{Dt} - \nabla\boldsymbol{u}\cdot\boldsymbol{\tau} - \boldsymbol{\tau}\cdot(\nabla\boldsymbol{u})^T. \tag{2-17}$$

The dimensionless dissipation term for the single-mode non-isothermal Gieskus model is,

$$Q_D = \frac{\boldsymbol{\eta}_s(T)}{(\sqrt{1-\varphi})^5}\,\boldsymbol{S}:\nabla\boldsymbol{u} + \gamma\boldsymbol{S}:\boldsymbol{\tau} + (1-\gamma)\,\frac{\hat{G}}{2\mathrm{De}\,\bar{\lambda}(T)}\left(I_1 + \mathrm{Tr}(\boldsymbol{b}^{-1}) - 6\right), \tag{2-18}$$

where the polymeric stress tensor $(\boldsymbol{\tau})$ and conformation tensor $(\boldsymbol{b})$ are related by,

$$\boldsymbol{\tau} = \hat{G}\,(\boldsymbol{b} - \boldsymbol{I}). \tag{2-19}$$

The dimensionless temperature dependent viscosities, thermal conductivity, and relaxation times are,

$$\eta_s(T) = \left(1 - \frac{\beta}{m}\right) \exp(-\alpha T), \quad \text{so that} \quad (\eta_s)_{nf} = \frac{\eta_s(T)}{(\sqrt{1-\varphi})^5}, \tag{2-20}$$

$$\eta_p(\dot{\gamma}, T) = \frac{\beta}{m}\left[1 + (m-1)\left(1 + (\lambda\dot{\gamma})^2\right)^{\frac{n-1}{2}}\right] e^{(-\alpha T)}, \Rightarrow (\eta_p)_{nf} = \frac{\eta_p(\dot{\gamma}, T)}{(\sqrt{1-\varphi})^5}, \tag{2-21}$$

$$\eta = \eta_s(T) + \eta_p(\dot{\gamma}, T), \quad \text{with} \quad \eta_{nf} = \frac{\eta}{(\sqrt{1-\varphi})^5}, \tag{2-22}$$

$$\bar{\lambda}(T) = \frac{1}{1+\alpha T} \exp(-\alpha T), \tag{2-23}$$

$$\kappa_{nf} = \frac{\kappa_s + (1-\aleph)\kappa_f - (\aleph - 1)\phi(\kappa_f - \kappa_s)}{\kappa_s + (1-\aleph)\kappa_f + \phi(\kappa_f - \kappa_s)}(1 + \alpha A_2 T). \tag{2-24}$$

It is customary to recast Eq. (2-24) in terms of the thermal conductivity ratio, κ_f/κ_s. In Eqs. (2-21 - 2-24), $m \geq 1$ is the shear-rate viscosity parameter, $0 \leq n \leq 1$ is the shear-thinning parameter, A_2 is a thermal conductivity parameter, $\aleph$ is the empirical shape factor (for spherical shaped nanoparticles, $\aleph = 3$, [15]). The shear-rate viscosity parameter, m, gives the ratio of zero shear-rate to the infinite shear-rate viscosities. The value $m = 1$ indicates that the viscosity is independent of shear-rates, as would obtain for Newtonian fluids and for ordinary viscoelastic fluids. The Generalized Newtonian fluid model is obtained by taking $m = \beta$ and De = 0. The choice De $= \beta = 0$ represents a Newtonian fluid. For more details, we refer the reader to [82].

2.2.2 Initial and boundary conditions

The following initial and boundary conditions apply,

$$u(0, y) = 0, \quad T(0, y) = 0, \quad \boldsymbol{\tau}(0, y) = 0, \qquad 0 \leq y \leq 1, \tag{2-25}$$

$$u(t, 0) = 0, \quad u(t, 1) = 1, \quad T(t, 0) = 0, \quad T(t, 1) = 0, \qquad t \geq 0. \tag{2-26}$$

Given the hyperbolic nature of the polymer stress equations, the corresponding boundary conditions are reconstructed from the main flow, [112].

2.3 Numerical Solution

Computational solutions of the governing equations follow finite difference numerical methodologies with semi-implicit treatment, see for example [83, 117, 119, 129, 130]. The terms that will be considered implicit are computed at the $n+\xi$ (time level), with $0 \leq \xi \leq 1$. Except possibly at boundaries, central-difference approximations will be used to compute the space derivatives. For shear-flow, we have zero pressure-gradient, $\nabla p \equiv 0$. The numerical scheme for the fluid velocity is,

$$\mathrm{Re}_{nf}\frac{u^{(n+1)}-u^{(n)}}{\Delta t} = \frac{\partial}{\partial y}\tau_{12}^{(n)} + \left((\eta_s)_{nf}^{(n)}\,\frac{\partial^2}{\partial y^2}u^{(n+\xi)} + \frac{\partial}{\partial y}u^{(n)}\,\frac{\partial}{\partial y}(\eta_s)_{nf}^{(n)}\right), \tag{2-27}$$

where

$$u^{(n+\xi)} = \xi u^{(n+1)} + (1-\xi)u^{(n)}.$$

The velocity therefore updates in time to, $u^{(n+1)}$, via the equation,

$$\begin{aligned}-r_1 u_{j-1}^{(n+1)} + (\mathrm{Re}_{nf}+2r_1)u_j^{(n+1)} - r_1 u_{j+1}^{(n+1)} = \mathrm{Re}_{nf}\,u_j^{(n)} + (1-\xi)\,\Delta t\,(\eta_s)_{nf}^{(n)}\,\frac{\partial^2}{\partial y^2}u^{(n)} \\ +\Delta t\,\frac{\partial}{\partial y}\tau_{12}^{(n)} + (1-\beta)\,\Delta t\,\frac{\partial}{\partial y}u^{(n)}\,\frac{\partial}{\partial y}(\eta_s)_{nf}^{(n)},\end{aligned} \tag{2-28}$$

where

$$r_1 = \xi\,(\eta_s)_{nf}^{(n)}\,\frac{\Delta t}{\Delta y^2}.$$

The resultant system of algebraic equations represent a diagonally dominant tri-diagonal linear system. The discretized temperature equation reads,

$$\mathrm{Pe}_{nf}\frac{\partial T}{\partial t} = \kappa_{nf}\,\frac{\partial^2}{\partial y^2}T^{(n+\xi)} + \frac{\partial}{\partial y}T^{(n)}\,\frac{\partial}{\partial y}\kappa_{nf}^{(n)} + \mathrm{Br}\,Q_D^{(n)} + \delta_1\,\exp\left(\frac{T^{(n)}}{1+\alpha\,T^{(n)}}\right). \tag{2-29}$$

Rearranging the Eq. (2-29) similarly leads to a diagonally dominant tri-diagonal system,

$$\begin{aligned}-r_2 T_{j-1}^{(n+1)} + (\mathrm{Pe}_{nf}+2r_2)T_j^{(n+1)} - r_2 T_{j+1}^{(n+1)} = \mathrm{Pe}_{nf}\,T_j^{(n)} + (1-\xi)\,\Delta t\,\kappa_{nf}\,\frac{\partial^2}{\partial y^2}T^{(n)} \\ +\Delta t\,\frac{\partial}{\partial y}T^{(n)}\,\frac{\partial}{\partial y}\kappa_{nf}^{(n)} + \Delta t\,\mathrm{Br}\,(\eta_s)_{nf}^{(n)}\left(\frac{\partial}{\partial y}u^{(n)}\right)^2 + \delta_1\,\exp\left(\frac{T^{(n)}}{1+\alpha\,T^{(n)}}\right) \\ +\Delta t\,\mathrm{Br}\,\gamma\,\tau_{12}^{(n)}\frac{\partial}{\partial y}u^{(n)} + (1-\gamma)\Delta t\,\mathrm{Br}\,\frac{\hat{G}}{2\mathrm{De}\bar{\lambda}(T)}(I_1 + \mathrm{Tr}\,(\boldsymbol{b}^{-1}) - 6),\end{aligned} \tag{2-30}$$

where

$$r_2 = \xi\,\kappa_{nf}\,\frac{\Delta t}{\Delta y^2}.$$

The semi-implicit scheme for the extra stress tensor, $\boldsymbol{\tau}$ is,

$$\boldsymbol{\tau}^{(n+\xi)} + \varepsilon\,(\boldsymbol{\tau}^2)^{(n)} + \mathrm{De}\,\bar{\lambda}^{(n)}\frac{\boldsymbol{\tau}^{(n+1)} - \boldsymbol{\tau}^{(n)}}{\Delta t} = \text{explicit terms.}$$

The solutions for the tensor components, $\tau_{11}^{(n+1)}$, $\tau_{12}^{(n+1)}$, and $\tau_{22}^{(n+1)}$ therefore follow directly,

$$(\mathrm{De}\,\bar{\lambda}^{(n)} + \xi\,\Delta t)\,\boldsymbol{\tau}^{(n+1)} = \text{explicit terms.} \tag{2-31}$$

The 'right hand side' expressions for τ_{11}, τ_{12} and τ_{22} are,

$$[\mathrm{De}\,\bar{\lambda}^{(n)} - (1-\xi)\Delta t]\,\tau_{11}^{(n)} + \Delta t\,\mathrm{De}\,\bar{\lambda}^{(n)}\left[\tau_{12}^{(n)}\frac{\partial}{\partial y}u^{(n)} + \tau_{11}^{(n)}\frac{\partial}{\partial y}\log\left(1+\alpha T^{(n)}\right)\right] - \varepsilon\,\Delta t\,(\tau_{11}^2 + \tau_{12}^2), \tag{2-32}$$

$$[\mathrm{De}\,\bar{\lambda}^{(n)} - (1-\xi)\Delta t]\,\tau_{12}^{(n)} + \Delta t\,\mathrm{De}\,\bar{\lambda}^{(n)}\left[\tau_{22}^{(n)}\frac{\partial}{\partial y}u^{(n)} + \tau_{12}^{(n)}\frac{\partial}{\partial y}\log\left(1+\alpha T^{(n)}\right)\right] + \Delta t\,(\eta_p)_{nf}\,\frac{\partial}{\partial y}u^{(n)} - \varepsilon\,\Delta t\,(\tau_{11}\tau_{12} + \tau_{22}^2), \tag{2-33}$$

$$[\mathrm{De}\,\bar{\lambda}^{(n)} - (1-\xi)\Delta t]\,\tau_{22}^{(n)} + \Delta t\,\mathrm{De}\,\bar{\lambda}^{(n)}\,\tau_{22}^{(n)}\frac{\partial}{\partial y}\log\left(1+\alpha T^{(n)}\right) - \varepsilon\,\Delta t\,(\tau_{12}^2 + \tau_{22}^2). \tag{2-34}$$

2.4 Results

Graphical results are presented for the velocity (u), temperature (T), polymeric-stress components $(\tau_{11}, \tau_{12}, \tau_{22})$, and the normal stress difference, N_1,

$$N_1 = \tau_{11} - \tau_{22}.$$

Unless otherwise indicated, the following list of values, for the embedded parameters, will be assumed,

$$\begin{aligned}&\alpha = 0.1,\ \mathrm{Br} = 1,\ \mathrm{Re} = 1,\ \mathrm{Pr} = 1,\ \mathrm{De} = 3,\ \gamma = 0.5,\ \beta = 0.6,\ \Delta y = 0.01,\\ &\Delta t = 0.01,\ t = 50,\ \hat{G} = 10^{-3},\ m = 2,\ \delta_1 = 0.1,\ \lambda = 0.01,\ n = 0.5,\ \zeta = 1,\\ &\varphi = 0.04,\ \varepsilon = 0,\ A_2 = 0.2,\ \aleph = 3.\end{aligned} \tag{2-35}$$

2.4.1 Devolvement of steady solutions

Figs. (2-2 - 2-8) show the development (in time) of solutions until steady-states are reached. Figs. (2-6) and (2-7) show that, $\tau_{22} \equiv 0$, and hence that $N_1 = \tau_{11} - \tau_{22} \equiv \tau_{11}$. This is the case in all our computations and hence the graphs of both N_1 and

τ_{22} are omitted thereafter. Likewise, steady-state solutions for velocity reproduce the same linear graph and will be omitted in the subsequent analysis. Fig. (2-5) is designed to show the maximum values of all fluid variables at steady state, $t = 50$.

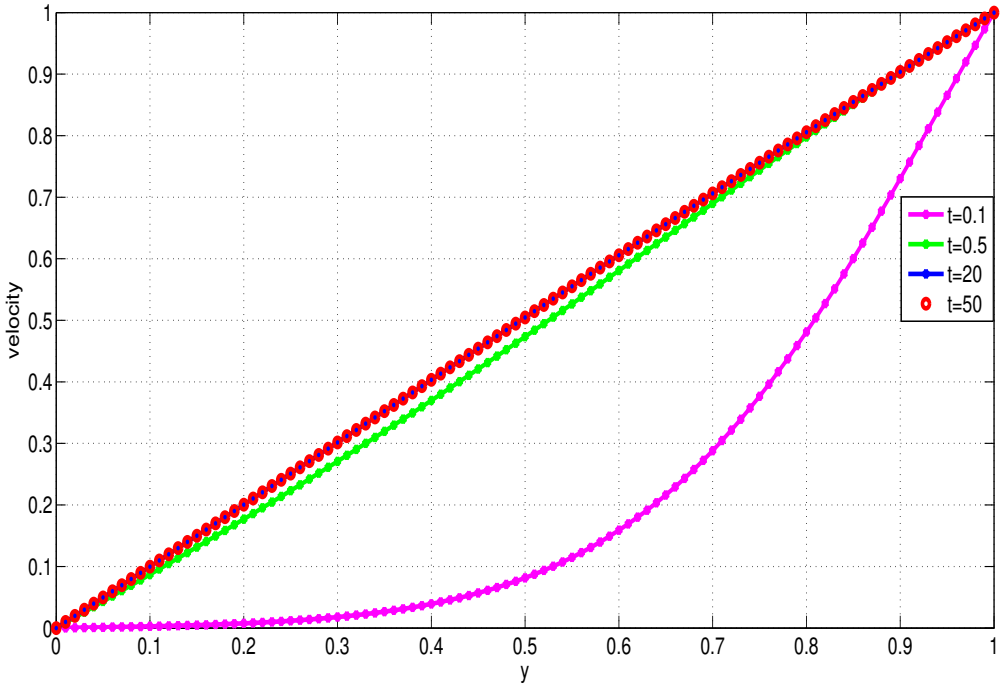

Fig. 2-2 Transient development of velocity profiles to steady state.

2.4.2 Temporal and spatial convergence

We now demonstrate the temporal and spatial convergence of our numerical algorithms using different time step and mesh sizes. Figs. (2-9) and (2-10) show that the solutions are independent of time step and mesh sizes.

2.4.3 Parameter dependence of solutions

We turn our attention to investigating the parameter-dependence of solutions. Figs. (2-11 - 2-14) illustrate the effects of varying values of φ on the GVFBN temperature, thermal-conductivity and polymeric-stresses respectively. As expected and in line with the behaviour of heat transfer fluids (HTFs), the nanofluid temperature and the thermal conductivity both increase with increasing nano-particles volume fraction, see Figs. (2-11) and (2-14). This is physically acceptable, since the higher the concentration of heat-conducting nanoparticles, higher the corresponding thermal-conductivity of the resultant nanofluid, and hence, the higher the temper-

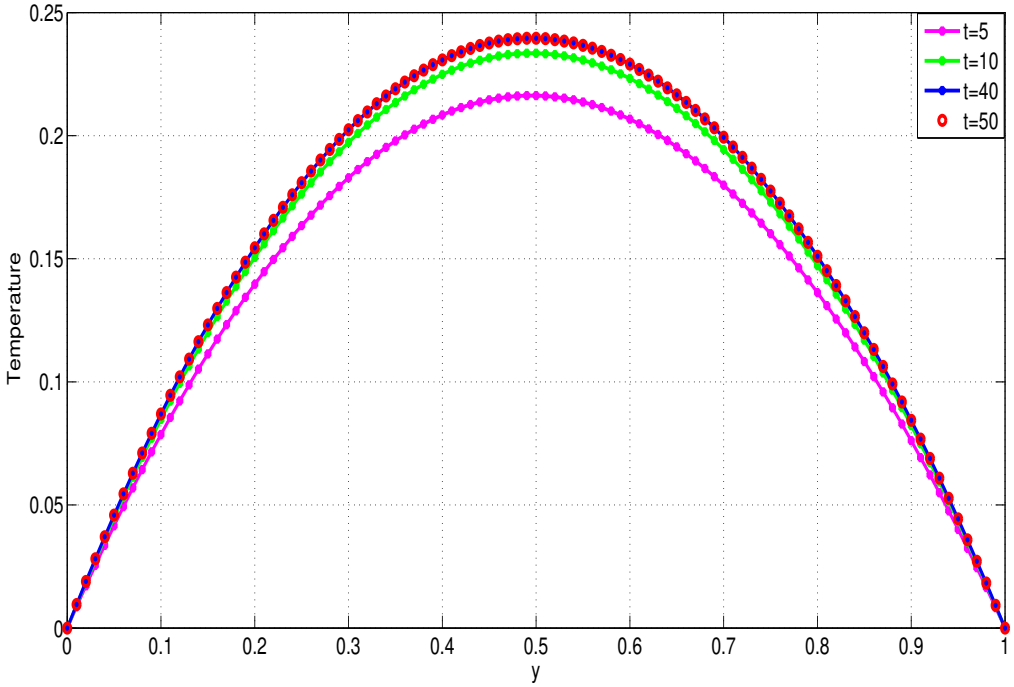

Fig. 2-3 Transient development of temperature profiles to steady state.

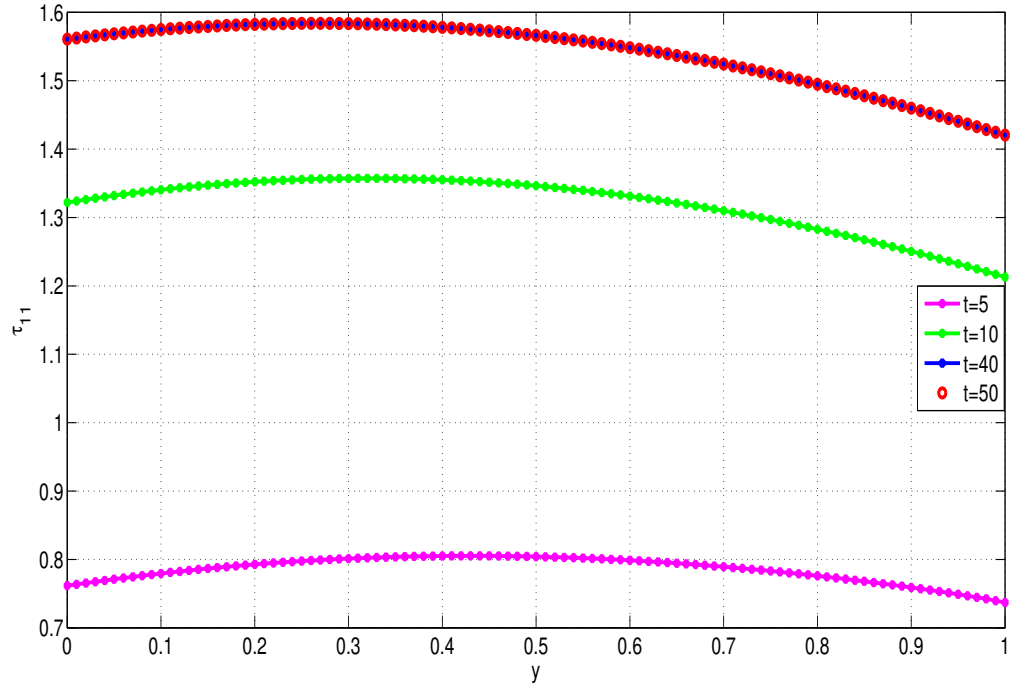

Fig. 2-4 Transient development of τ_{11} stress profiles to steady state.

atures in the nanofluid. The polymer-stress components exhibit opposite behaviour to temperature and thermal conductivity and decrease with increasing nano-particle volume fraction, see Figs. (2-12) and (2-13).

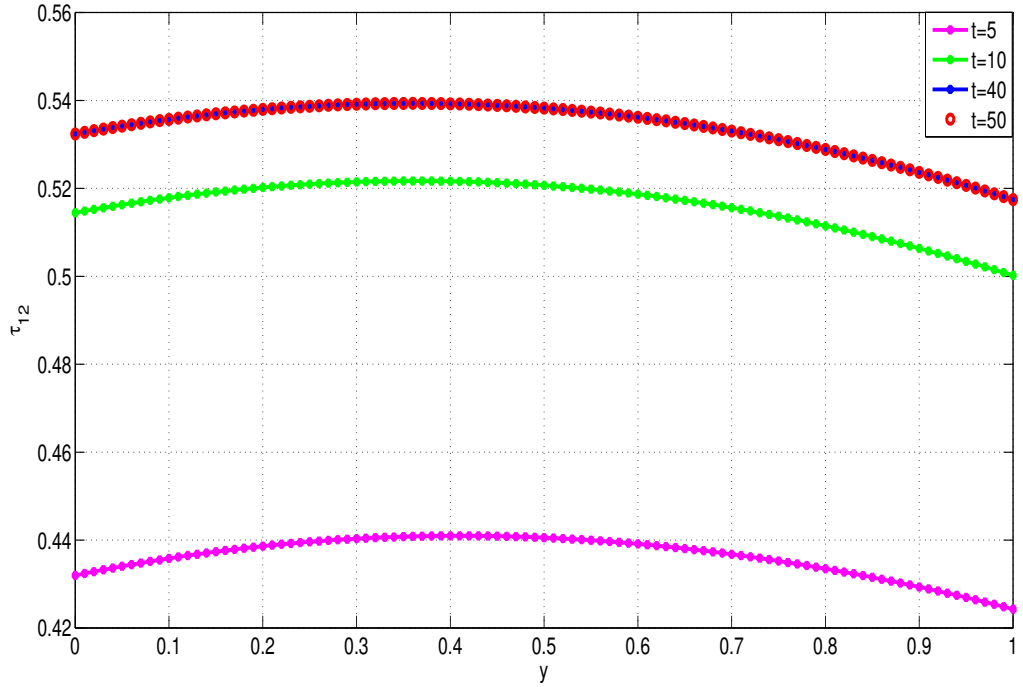

Fig. 2-5 Transient development of τ_{12} stress profiles to steady state.

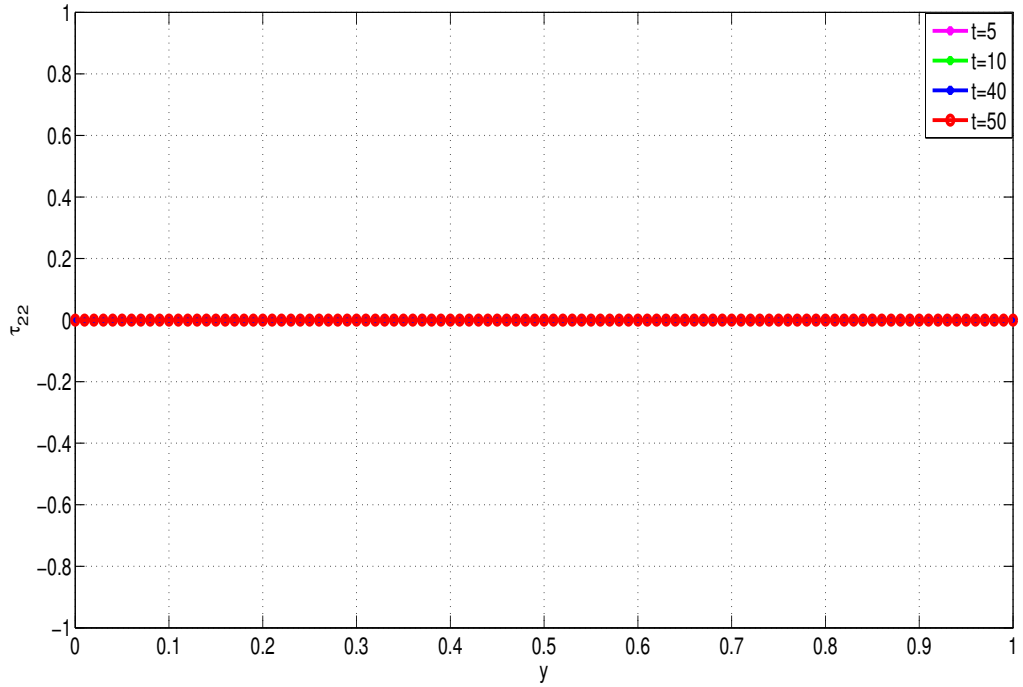

Fig. 2-6 Transient development of τ_{22} stress profiles to steady state.

Fig. (2-15) shows, as expected, an increase in GVFBN temperature with increasing strength of exothermic-reactions, i.e. increasing δ_1. The polymeric stresses, on the other hand, decrease with increasing Frank-Kamenetskii parameter (δ_1) see

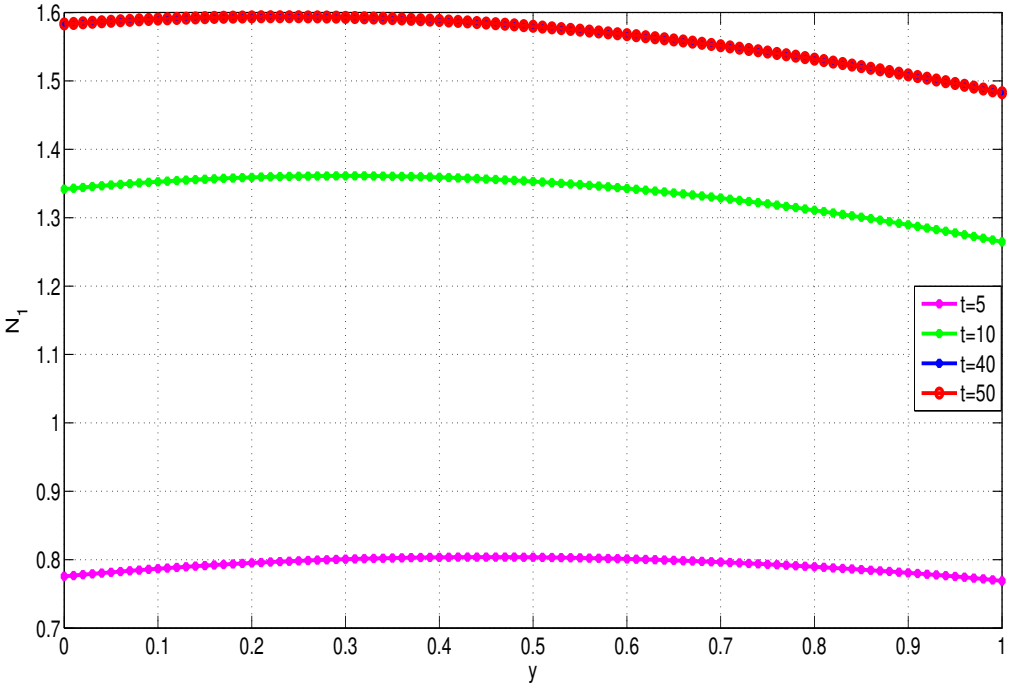

Fig. 2-7 Transient development of first normal stress difference, N_1, profiles to steady state.

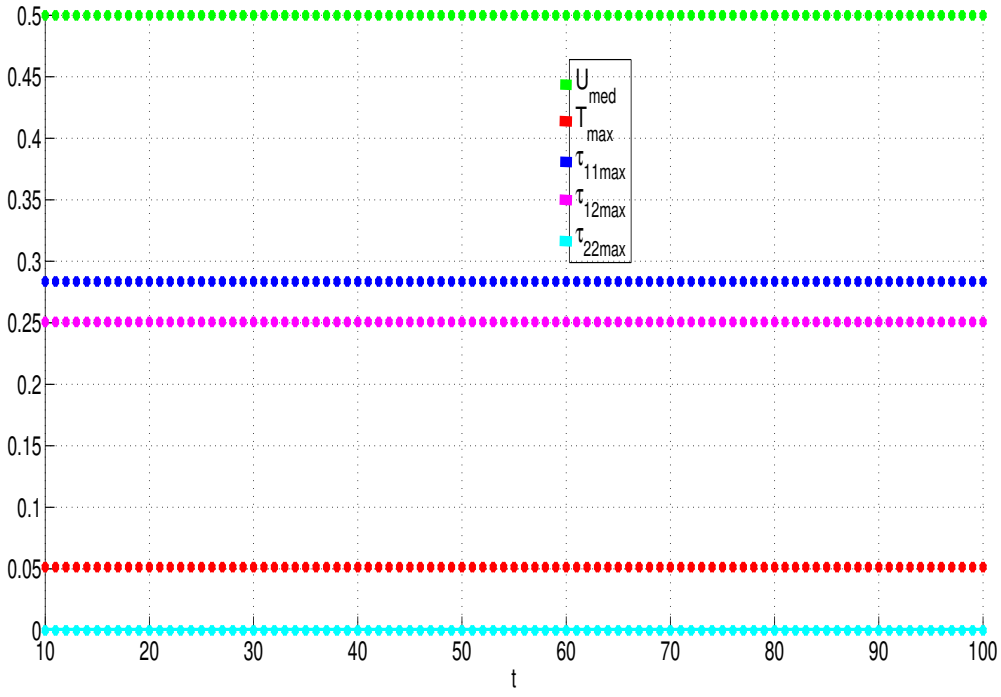

Fig. 2-8 Time development of maximum and median flow quantities.

Figs. (2-17) and (2-18). The exothermic-reaction parameter (δ_1) should be carefully controlled to mitigate against thermal runaway. Fig. (2-16) gives an illustration of thermal-runway for the different fluid types. Evidently, the GNFBN have greatest

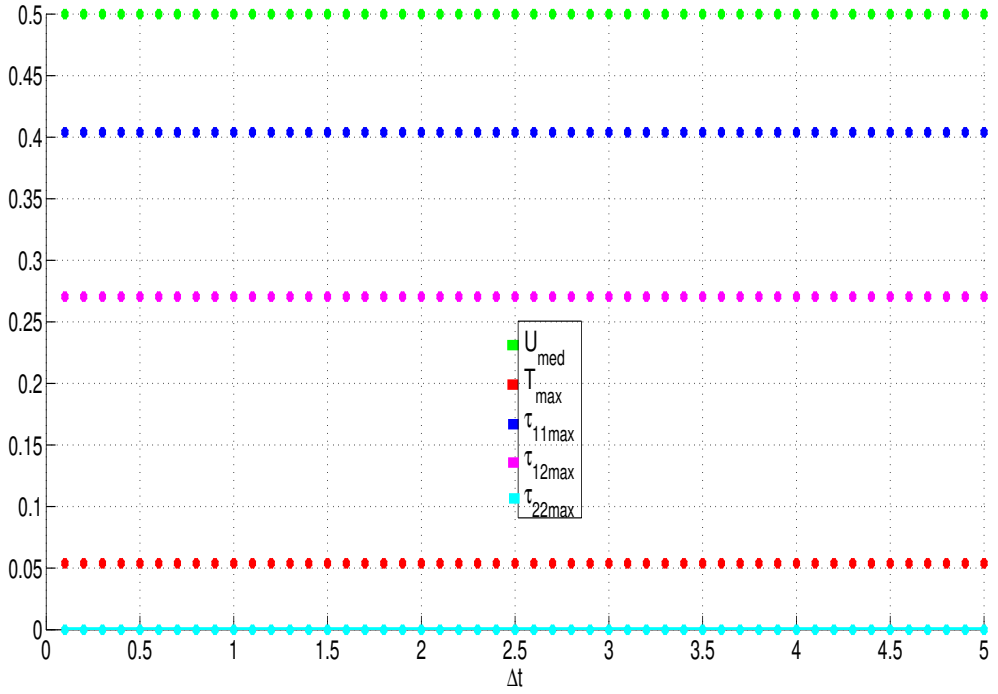

Fig. 2-9 Dependence of solutions on time step size.

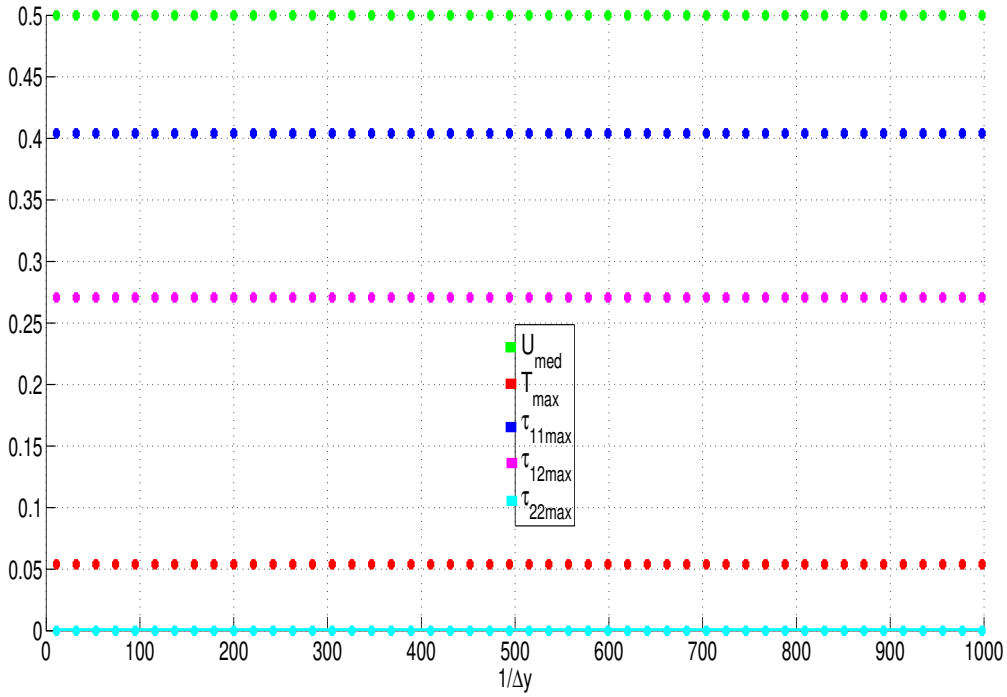

Fig. 2-10 Dependence of solutions on mesh size.

susceptibility to thermal blow-up and runaway, followed by NFBN, and then by the GVFBN and lastly the VFBN (m = 1). These results are consistent with the result of [82, 117]. Figs. (2-19) and (2-22) illustrate the variation of solutions for

different values of the viscosity ratio, β. A rise in β, increases in polymer viscosity and expectedly increases the polymeric-stresses (τ_{11}, τ_{12} as well as the first-normal-stress-difference, N_1). Given the energy storage capabilities of viscoelastic (polymeric) fluids, the elastic liquids will always therefore attain lower temperatures as compared with corresponding in-elastic (i.e. Newtonian and generalized Newtonian liquids). This explains the results in Figs. (2-17) and (2-20). Generalized viscoelastic fluid based nanofluids (GVFBN) have comparatively higher temperatures than normal viscoelastic fluid based nanofluids (VFBN) with $m = 1$, see Fig. (2-20).

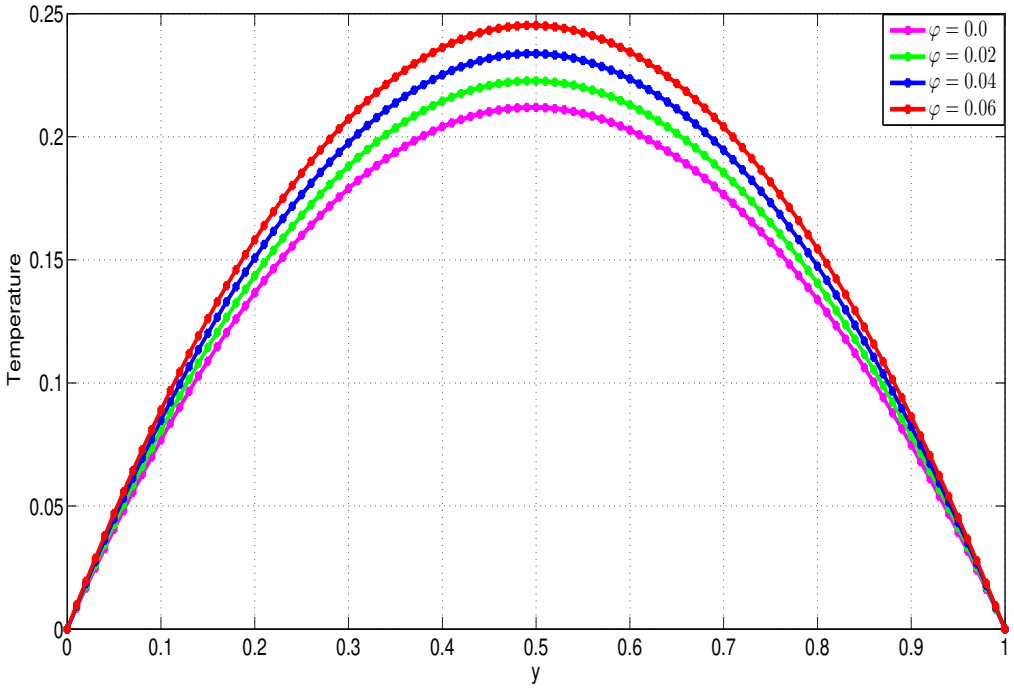

Fig. 2-11 Effects of nanoparticles volume fraction, φ, on temperature.

Figs. (2-23 - 2-26) show the effects of variations in the Brinkman-number, Br. The solutions behave similarly to variations in δ_1. The only difference here is the absence of the thermal runaway phenomenon given that the temperature growth is linear rather than exponential, see [82]. Fig. (2-23) shows that temperature increases with increasing Br, This is physically realistic because viscous heating of the fluid particles within the flow channel causes temperature to rise with increasing Br, while fluid viscoelasticity shows an opposite behaviour, see Figs. (2-25) and (2-26). Similarly to the behaviour with respect to the exothermic reaction parameter, Fig. (2-24) shows that the Generalized-Newtonian-fluid-based nanofluids (GNFBN) show the least resistance to fluid temperature increases, followed by Newtonian-fluid-based nanofluids (NFBN), and then by generalized-viscoelastic-fluid-based nanoflu-

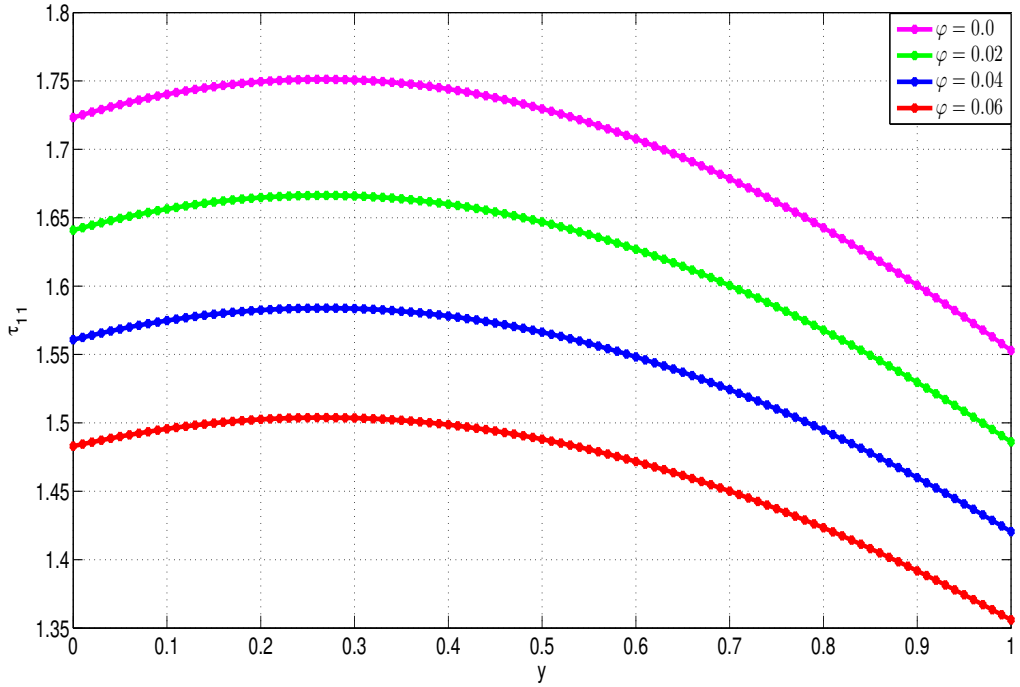

Fig. 2-12 Effects of nanoparticles volume fraction, φ, on τ_{11}.

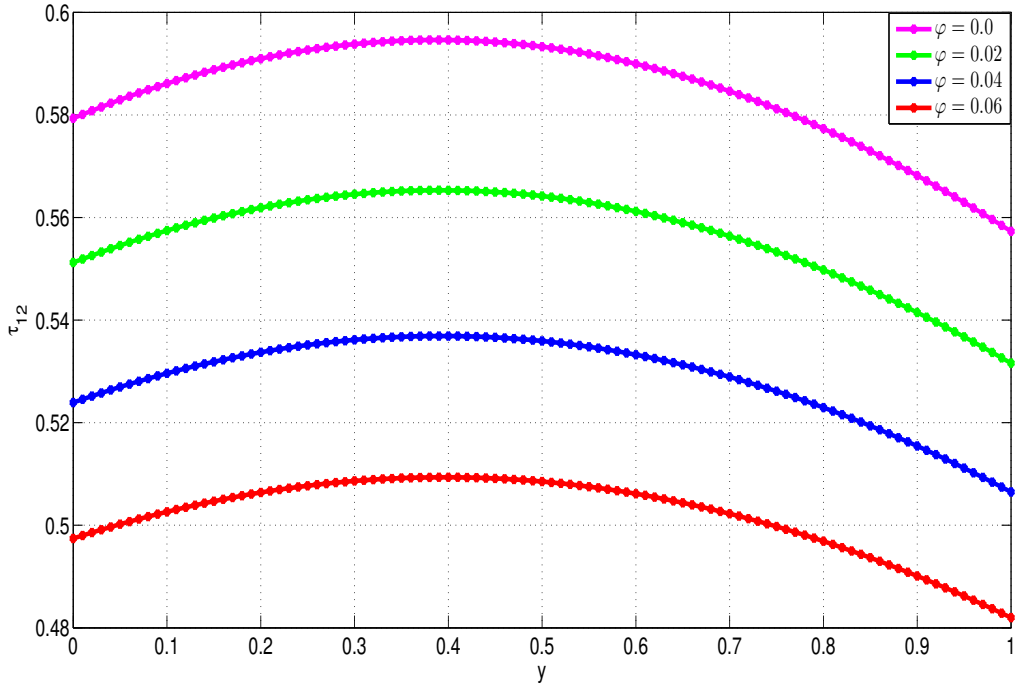

Fig. 2-13 Effects of nanoparticles volume fraction, φ, on τ_{12}.

ids (GVFBN) (with $m \neq 1$ *and* $\beta \neq 0$), and finally the normal viscoelastic-fluid-based nanofluids (VFBN) with $m = 1$ being the most resistant to temperature increase.

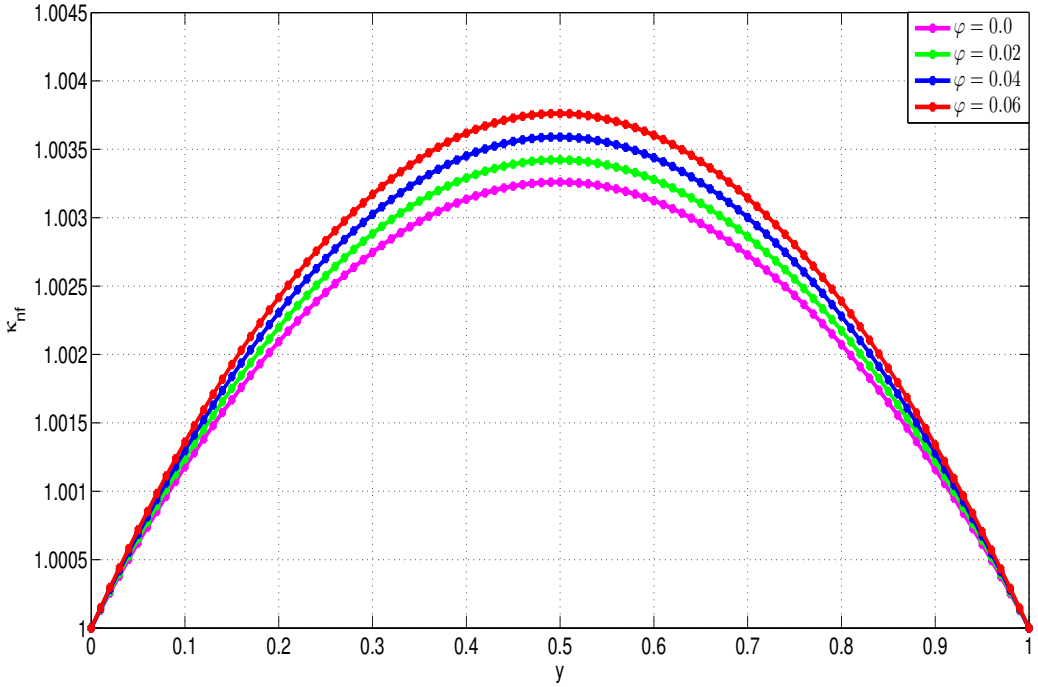

Fig. 2-14 Effects of nanoparticles volume fraction, φ, on thermal conductivity.

The temperature behaviour in response to variations in m is similar to that with respect to either Br or δ_1, see Fig. (2-27). As before, the polymer stresses behave oppositely to the fluid temperature. Specifically, the polymer stress components, τ_{11} and τ_{12} decrease with increasing m, see Figs. (2-29), and (2-30). The variations of solutions with varying shear-thinning parameter, n, are illustrated in Figs. (2-31) - (2-34). The behaviour of solutions with varying values of n is similar to the behaviour for m, with differences only in the magnitude of the increase/decrease of quantities. Negligible effects are however noticed in the nanofluid temperature.

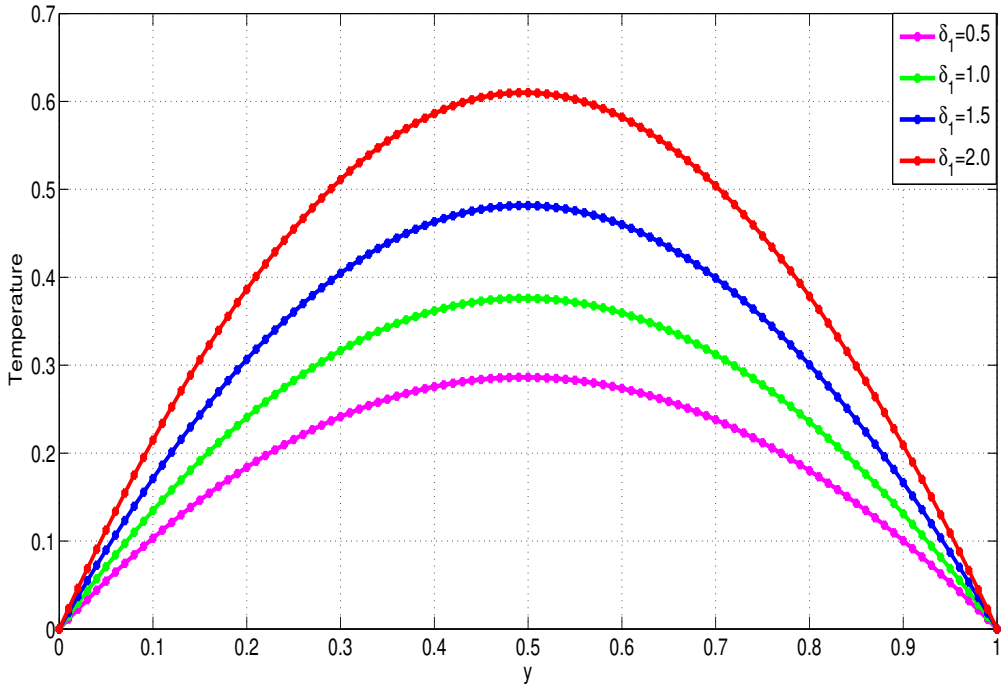

Fig. 2-15 Effects of the exothermic reaction parameter, δ_1, on nanofluid Temperature.

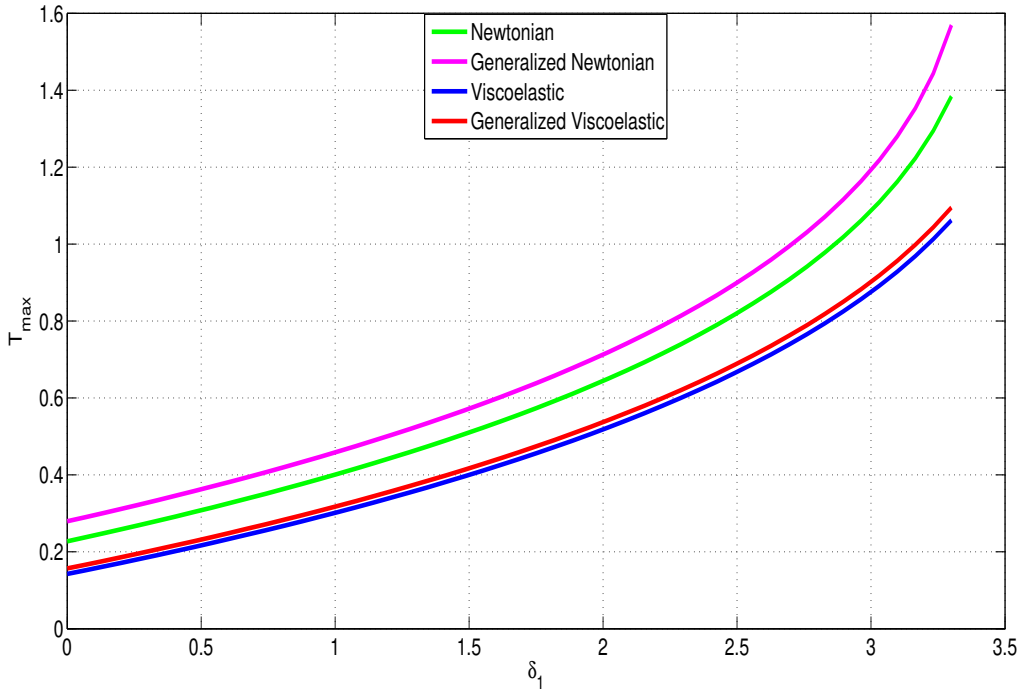

Fig. 2-16 Thermal runaway, with increasing δ_1, for different nanofluid types.

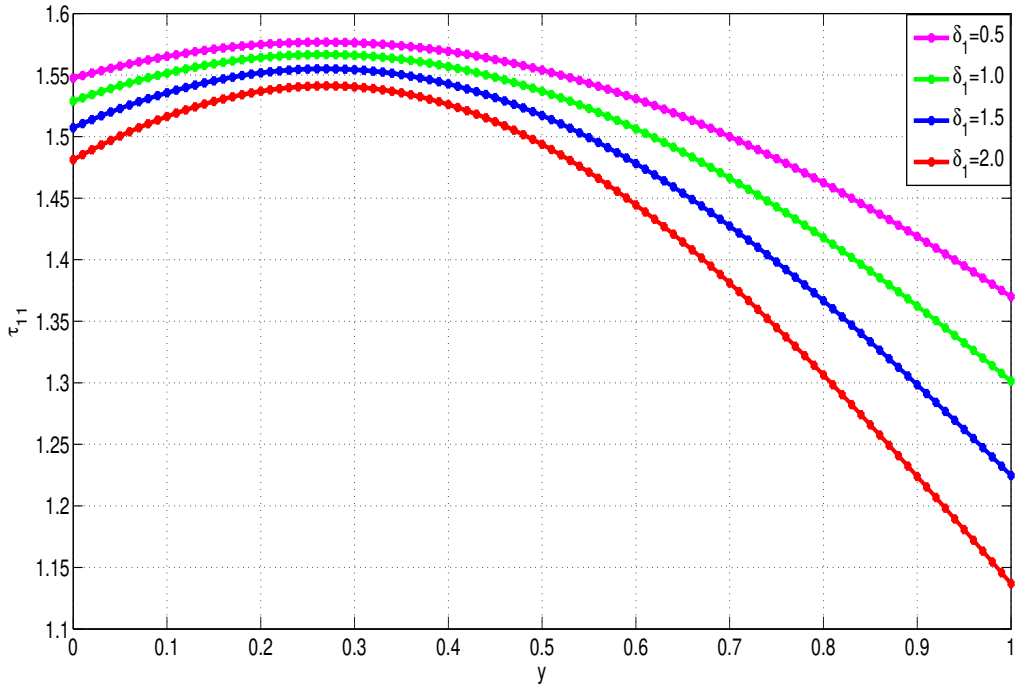

Fig. 2-17 Effects of exothermic reaction parameter, δ_1, on τ_{11}.

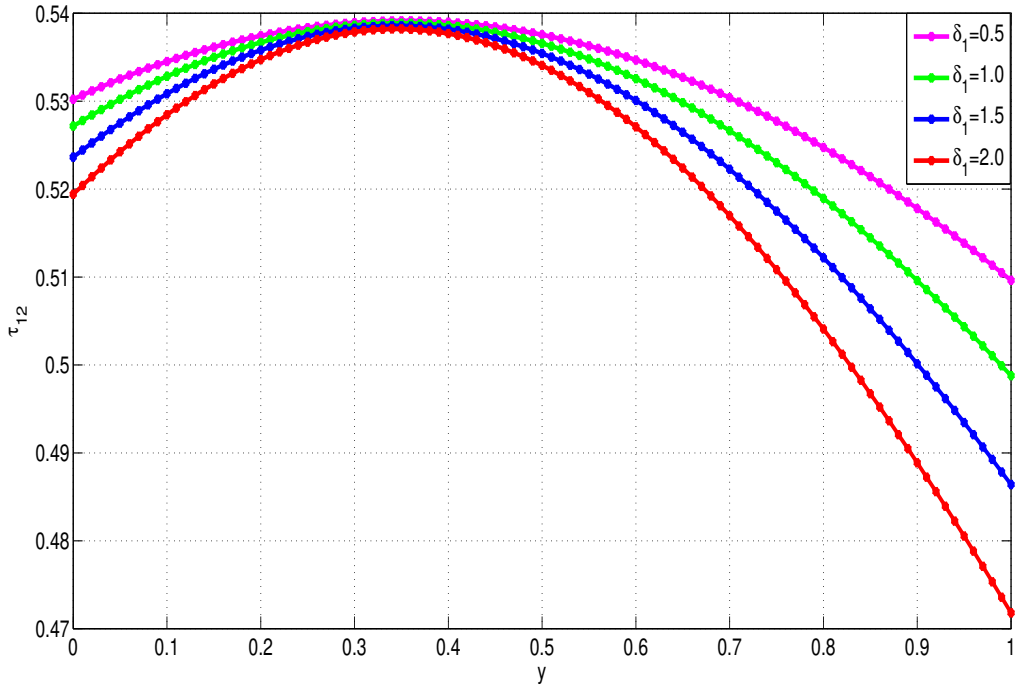

Fig. 2-18 Effects of exothermic reaction parameter, δ_1, on τ_{12}.

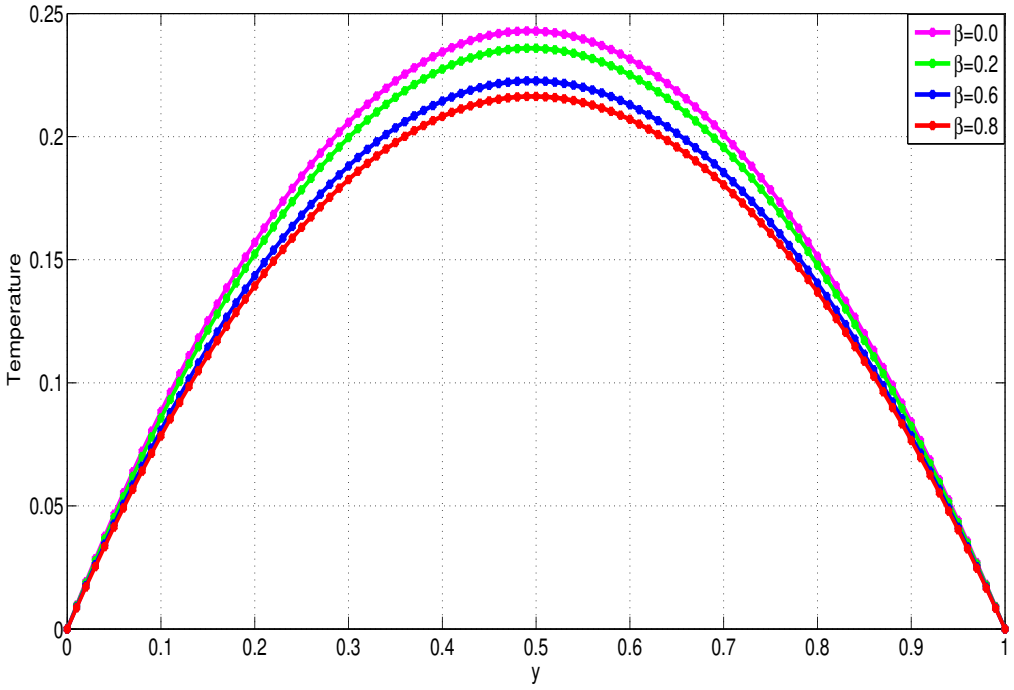

Fig. 2-19 Effects of viscosity ratio, β, on fluid temperature.

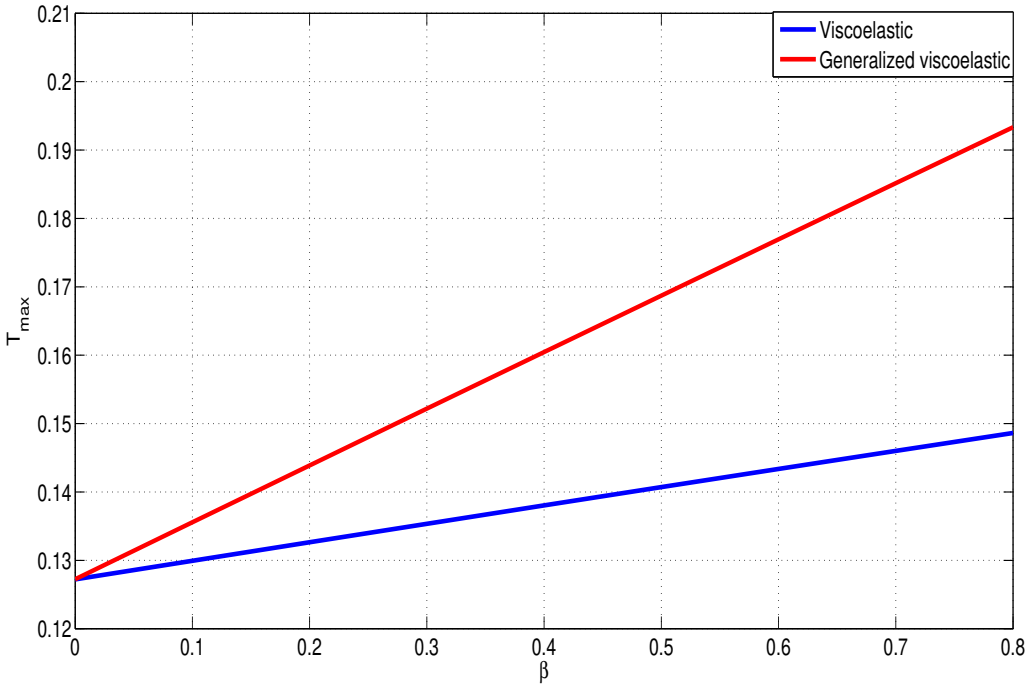

Fig. 2-20 Variation of maximum fluid Temperature with viscosity ratio, β.

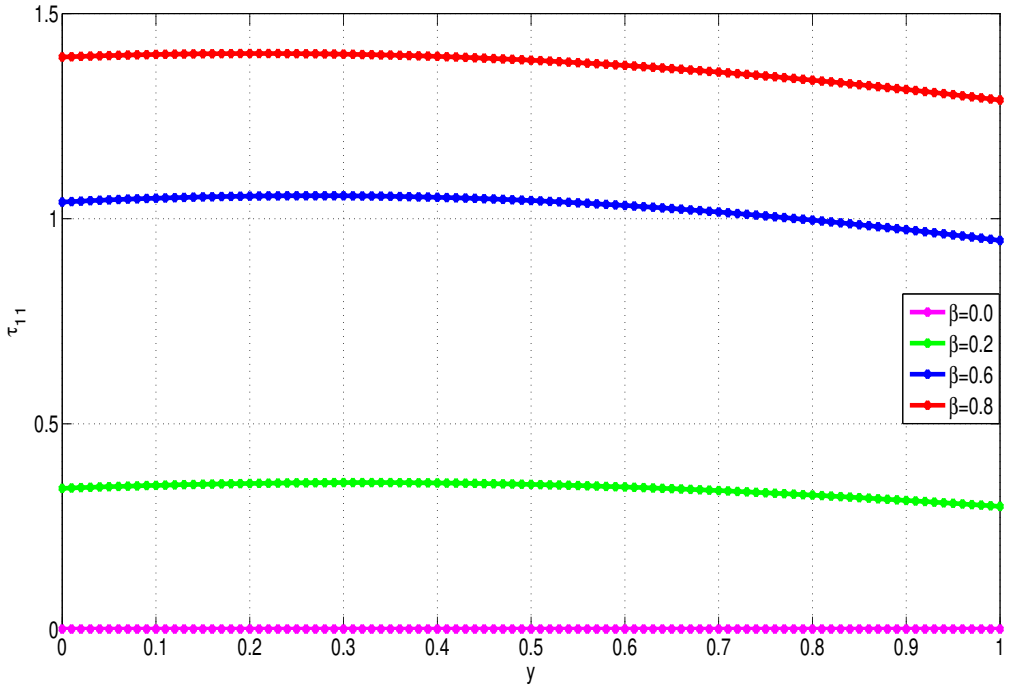

Fig. 2-21 Effects of viscosity ratio, β, on τ_{11}.

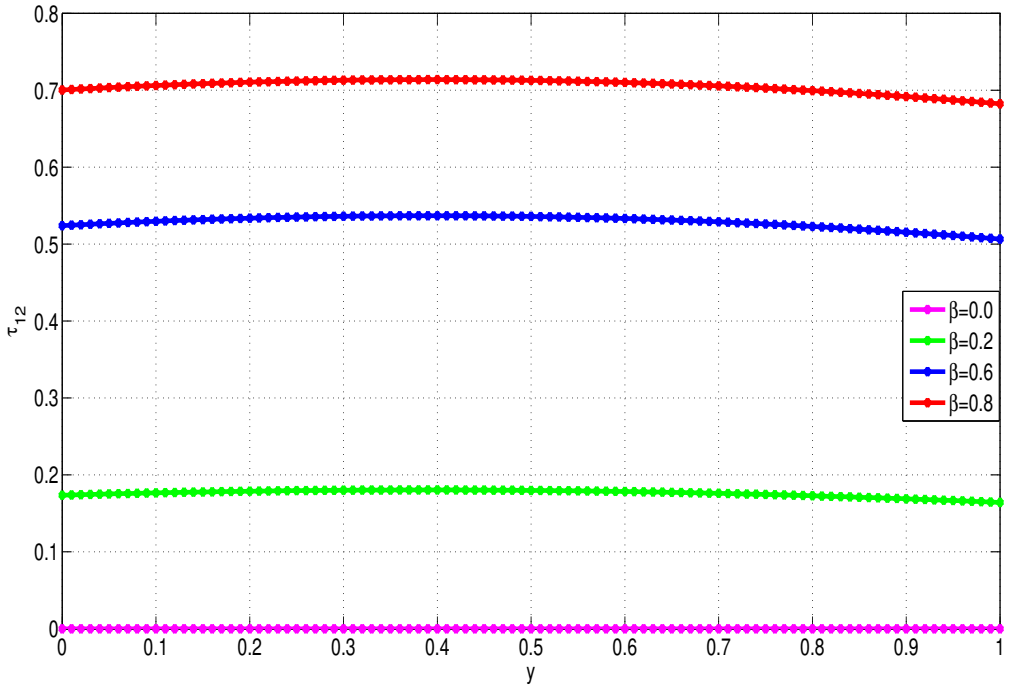

Fig. 2-22 Effects of viscosity ratio, β, on τ_{12}.

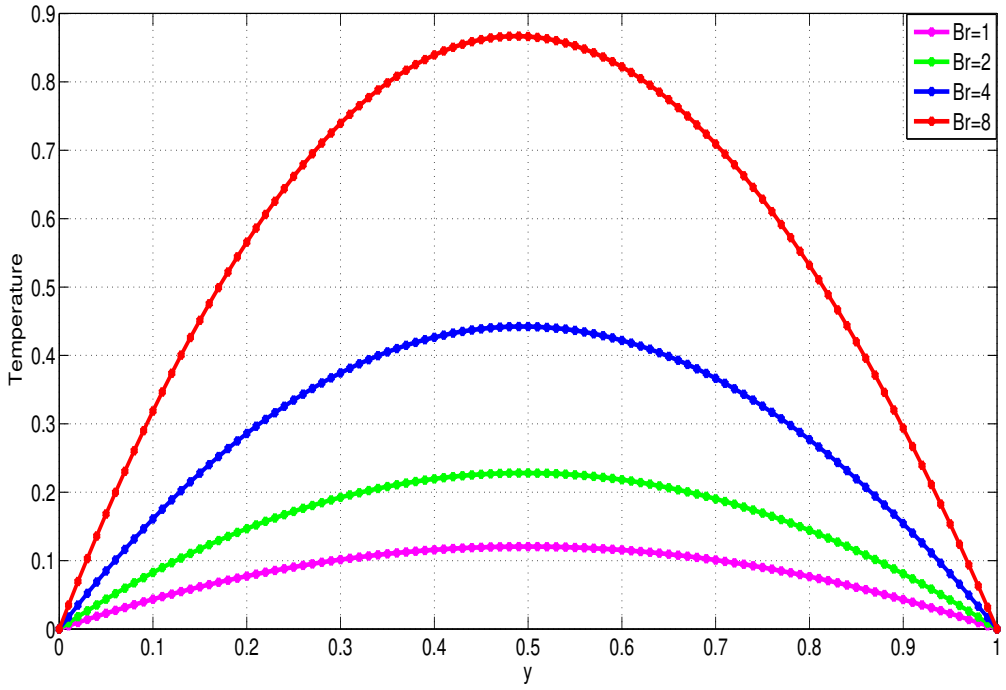

Fig. 2-23 Effects of Brinkman number, Br, on fluid temperature.

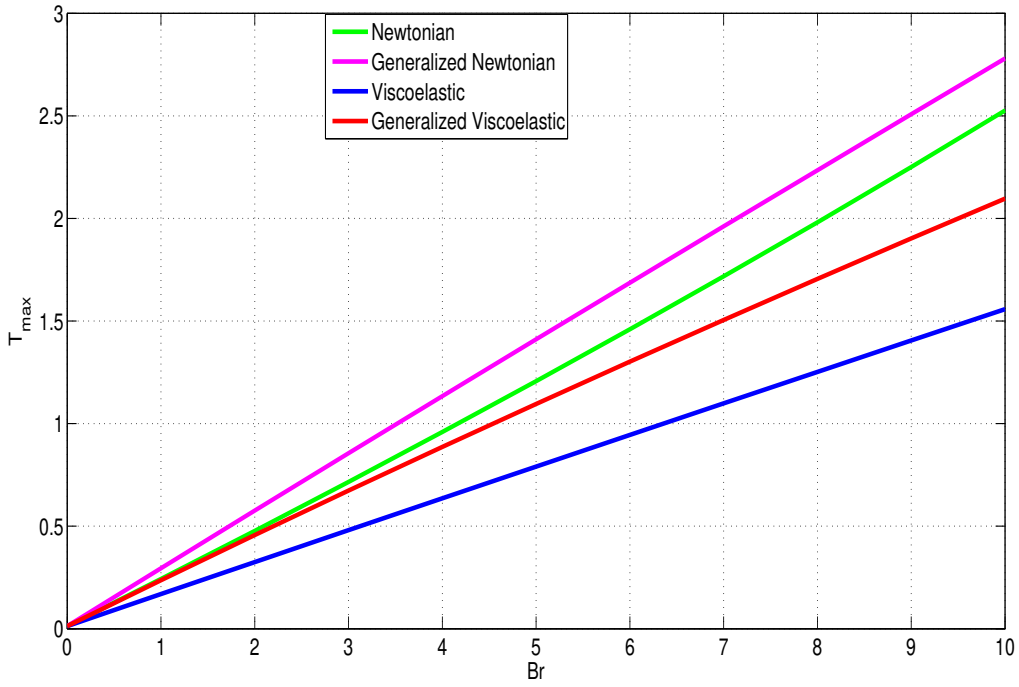

Fig. 2-24 Variation of maximum fluid Temperature with Brinkman number, Br.

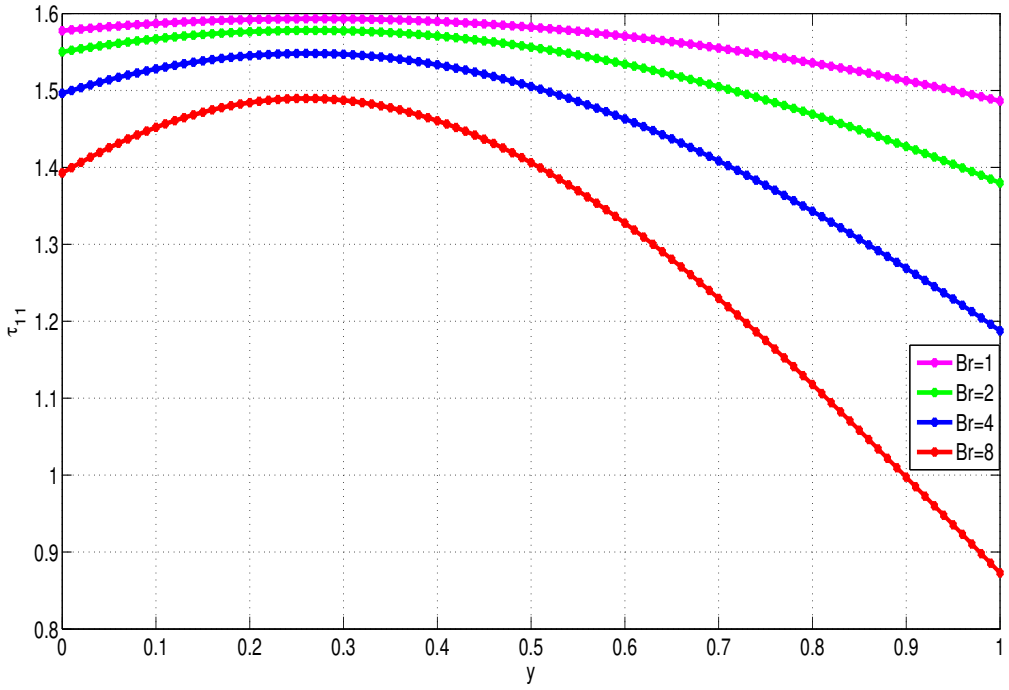

Fig. 2-25 Effects of Brinkman number, Br, on τ_{11}.

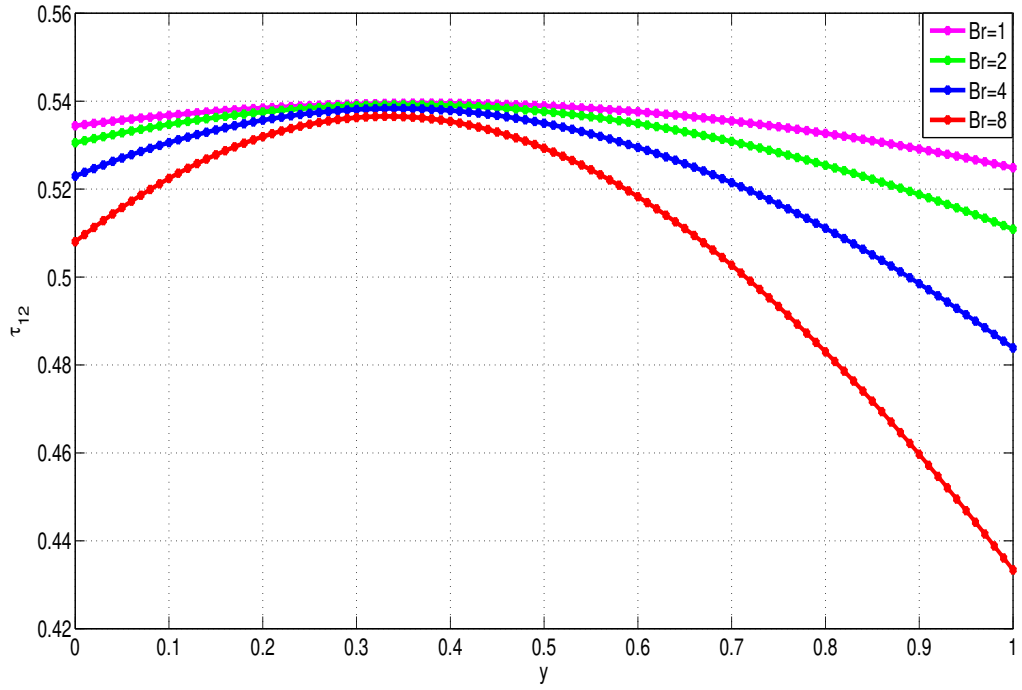

Fig. 2-26 Effects of Brinkman number, Br, on τ_{12}.

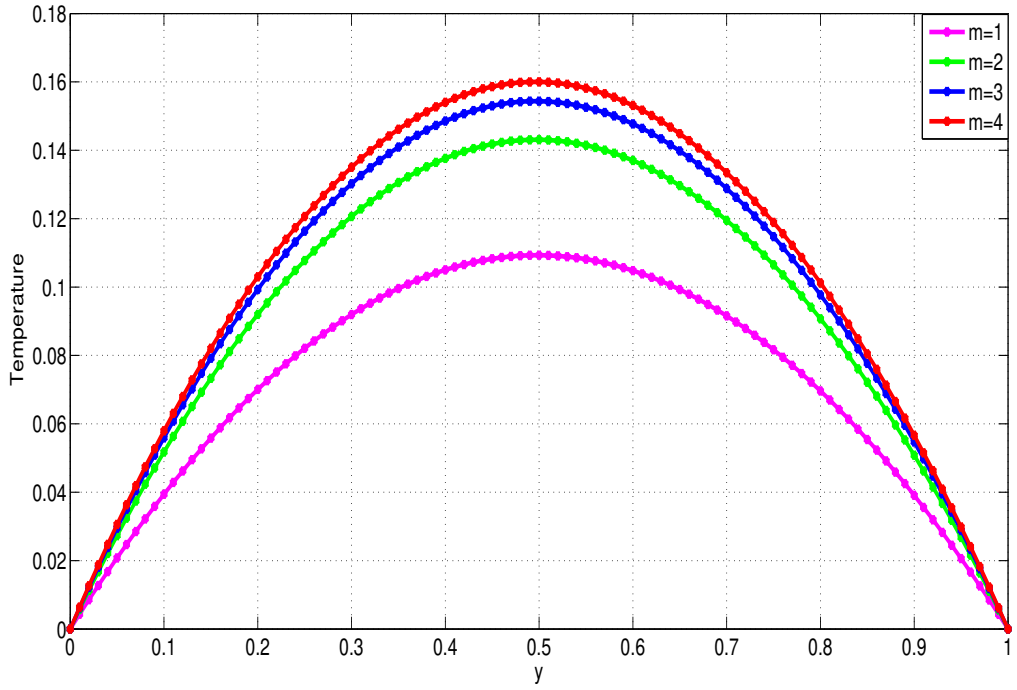

Fig. 2-27 Effects of shear-rate viscosity parameter, m, on fluid Temperature.

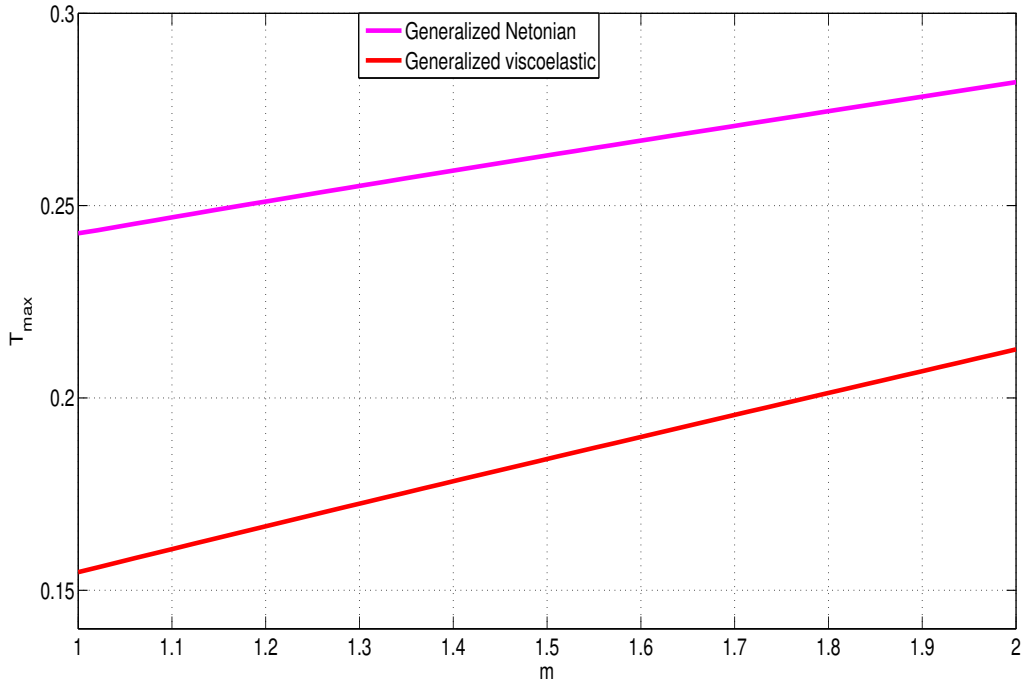

Fig. 2-28 Variation of maximum fluid temperature with shear-rate viscosity parameter, m.

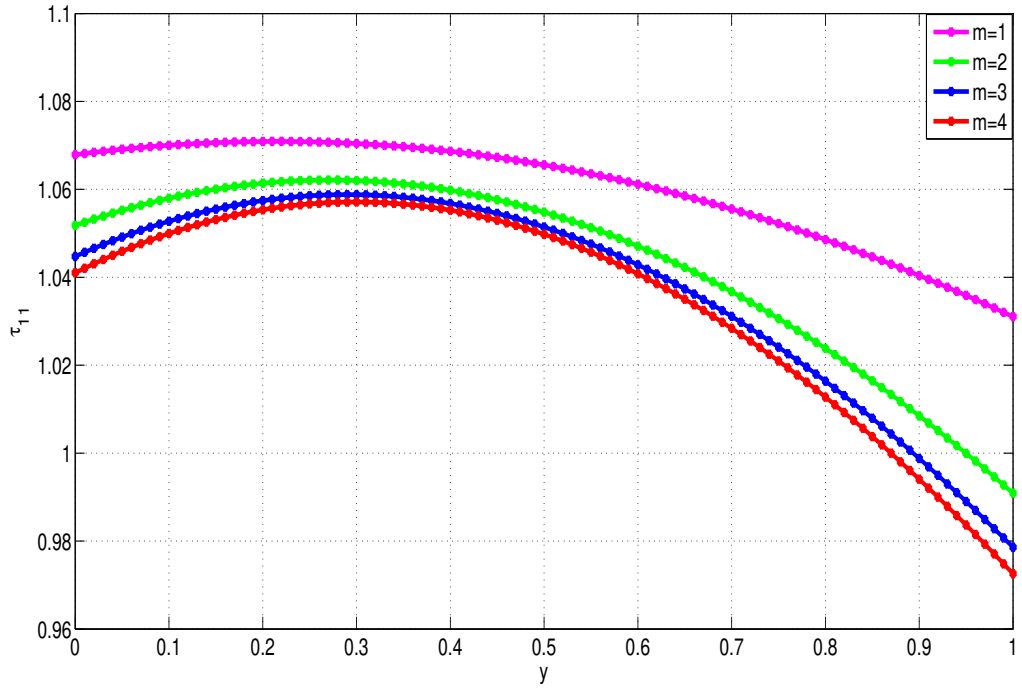

Fig. 2-29 Effects of shear-rate viscosity parameter, m, on τ_{11}.

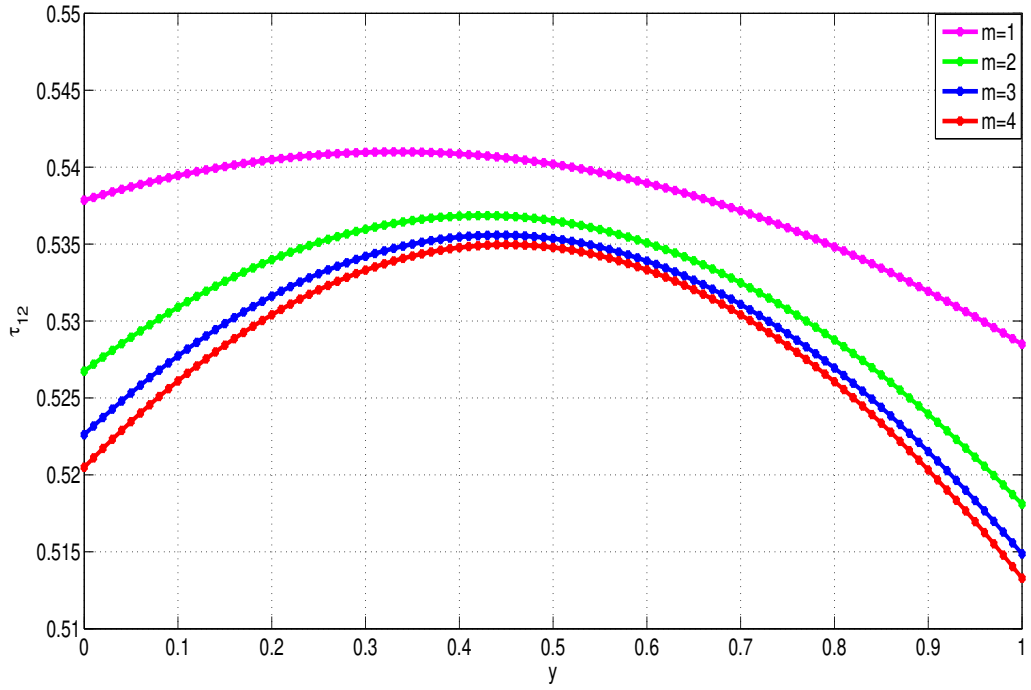

Fig. 2-30 Effects of shear-rate viscosity parameter, m, on τ_{12}.

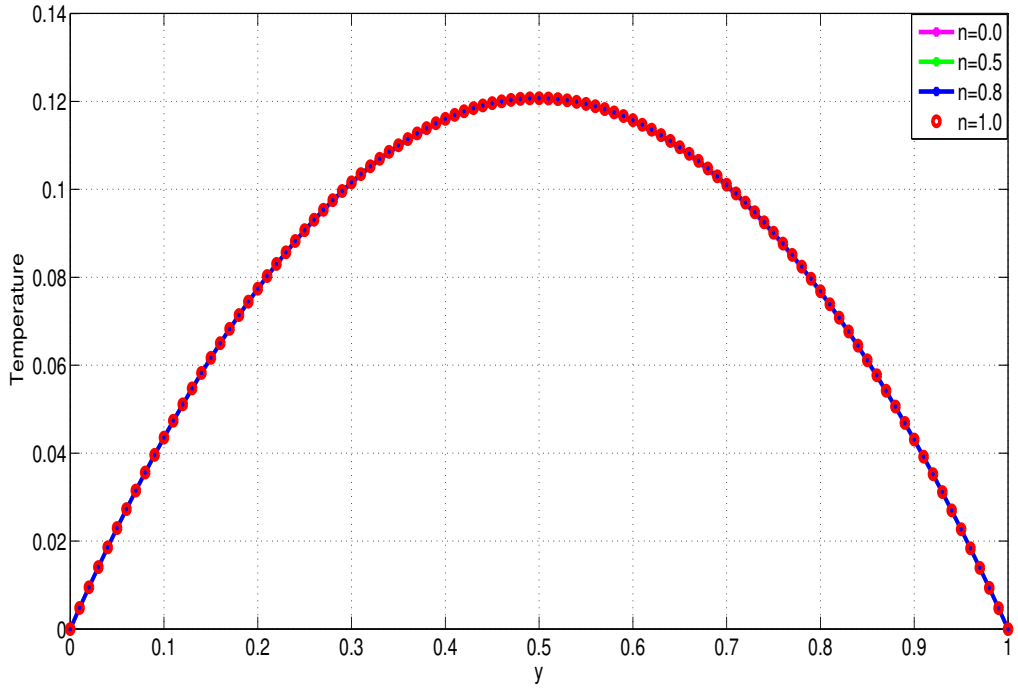

Fig. 2-31 Effect of shear-thinning parameter, n, on fluid temperature

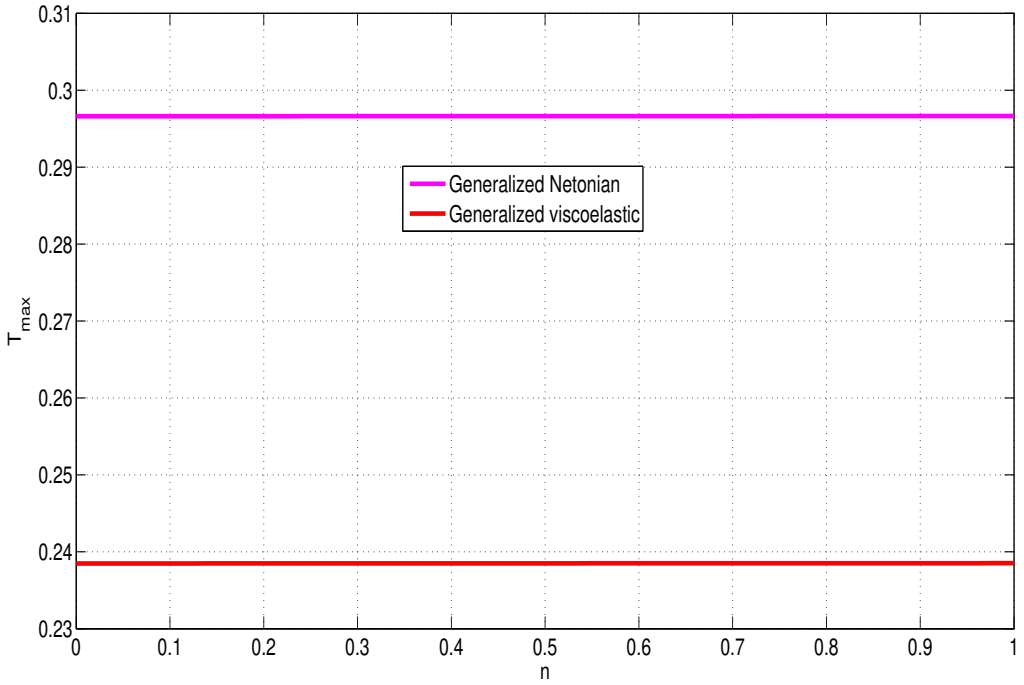

Fig. 2-32 Variation of maximum fluid Temperature with n.

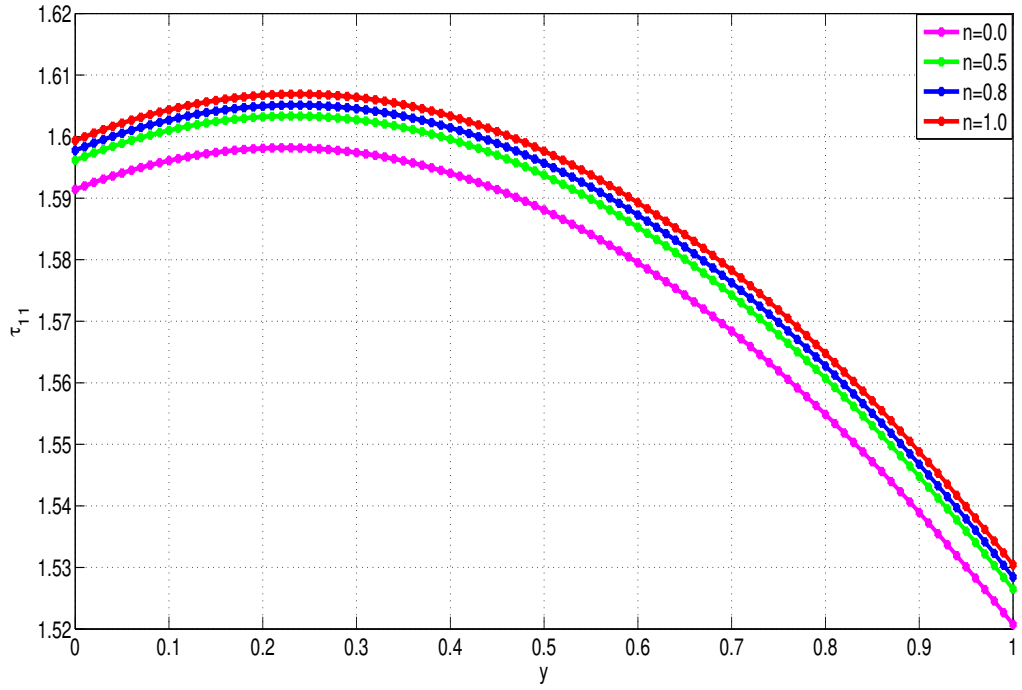

Fig. 2-33 Effects of shear-rate viscosity parameter, n, on τ_{11}.

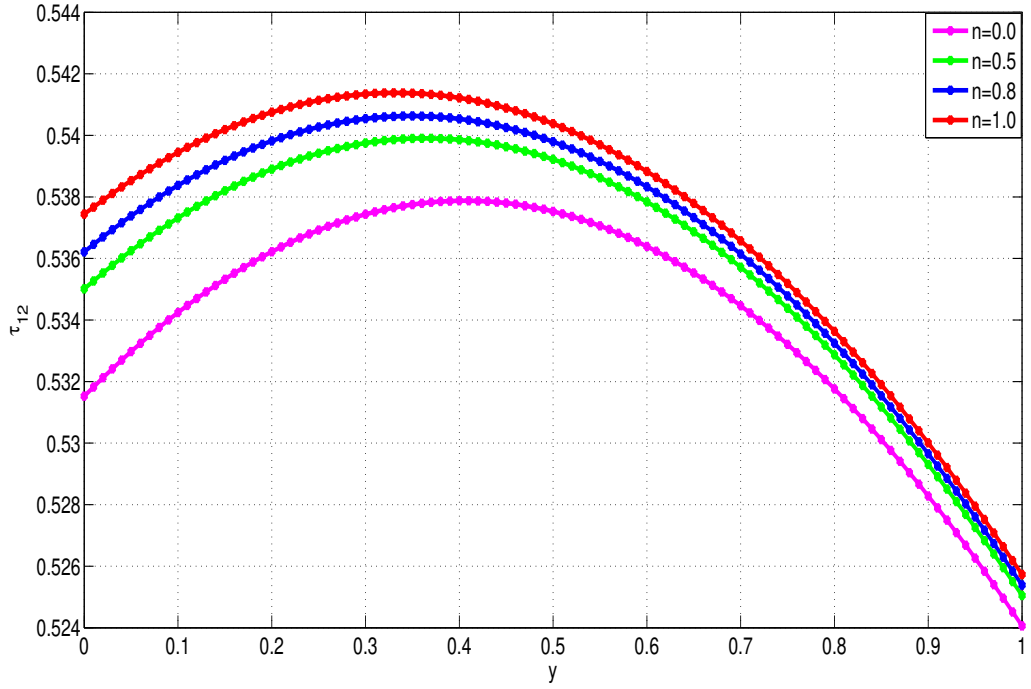

Fig. 2-34 Effects of shear-rate viscosity parameter, n, on τ_{11}.

2.5 Concluding Remarks

We numerically investigated the thermophysical characteristics of generalized-viscoelastic-fluid-based nanofluids (GVBNF) in shear flow subject to exothermic reactions. Our mathematical model was based on a single-phase nanofluid model in which the nano-particles are homogeneously mixed with the generalized viscoelastic fluid base-fluid. We demonstrated that the nano-particle volume-fractions play fundamental roles in the fluid-dynamical and thermo-dynamical properties of the resultant GVFBN. Specifically, the effective nanofluid thermal-conductivity and the nanofluid temperature both increase while the shear-viscosity decreases with increasing nano-particle volume-fraction. The GVFBN model accounts for all the four nanofluid types, Generalized-Newtonian-fluid-based nanofluids (GNFBN, De = $\beta = 0$), Newtonian-fluid-based nanofluids (NFBN, De = $\beta = \gamma = 0$), Generalized-Viscoelastic-fluid-based nanofluids (GNFBN), and Viscoelastic-fluid-based nanofluids (VFBN, $m = 1$). The comparative thermal runaway susceptibility of the four nanofluid types is presented and we demonstrated that the order of susceptibility from the most to the least susceptible is GNFBN, NFBN, GVFBN, VFBN. Similar susceptibility results are documented in the literature for ordinary base-fluids, without nano-particles [82]. The results are of important industrial significance, say in heat exchanger design and in other heating and cooling applications.

Acknowledgements

The authors would like to extend their sincere gratitude to National Research Foundation (NRF) for providing financial support to publish this work.

Chapter 3 Dynamics of Non-Isothermal Pressure-Driven Flow of Generalized Viscoelastic-Fluid-Based Nanofluids in a Channel[1]

abstract

The investigation considers numerical analysis and computational solution of unsteady, pressure driven channel flow of a generalized viscoelastic-fluid-based nanofluid (GVFBN) subject to exothermic reactions. Temperature dependent fluid thermal conductivity is considered and the flow is subject to convective cooling at the walls. The non-isothermal generalized Giesekus constitutive model is employed for the GVFBN. A Carreau model is used to describe the shear-rate dependence of fluid viscosity and exothermic reactions are assumed to follow Arrhenius kinetics. An efficient semi-implicit numerical technique based on the finite difference method is applied to obtain computational solutions to the model equations. The computational methodologies are built into the MATLAB software. The effects of the various fluid and flow parameters, specifically the nanoparticle volume-fraction are explored. The results demonstrate that those parameters which only directly couple to the energy equation (but are otherwise indirectly coupled to momentum and stress-constitutive equations, say via the temperature dependent viscosities and relaxation times) would only show prominent effects on fluid temperature but not on the fluid velocity or the polymer stresses. The results also demonstrate, as in the literature on exothermic flows, that the values of exothermic-reaction parameter must be carefully controlled as large values would lead to thermal runway phenomena. The illustrated results are consistent with the existing literature and additionally add novel new contributions to non-isothermal and pressure-driven channel flow of GVFBN under convective cooling conditions.

[1]The contents of this chapter are from khan et.al [131]

3.1 Introduction

A mixture of metallic (silver, copper, etc.) nanometre-sized particles suspended in a conventional base-fluid (water, oil, etc.) is referred to as a nanofluid. For a comprehensive description of nanofluids and their utility, in the heat-transfer-rate (HTR) characteristics, the reader is referred to, [92].

Optimal material conditions for, say, fluid viscosity and thermal conductivity may be enhanced by simultaneously using several types of nanoparticles (say three different types) of various shapes, sizes, density, etc. in the same nanofluid mixture, see for example [132, 133]. The present research focuses on the effects of shear-dependent viscosity and fluid elasticity and hence will use homogeneous nanoparticles of one kind for illustrative purposes.

Similar investigations, as in [92], on thermodynamic properties and effects of various types of nanofluids have been conducted, say in [20, 36, 93, 95–106, 110, 134–138]. The importance of such investigations cannot be overstated, especially considering the novel applications of nanofluids to thermal-conductivity and HTR improvement, micro-fluidics, fuel-cell development, chemotherapy, thermal storage, electronic cooling and heating, etc.

A vast majority of the research on nanofluid flow has been conducted with Newtonian base fluids. The recent developments in non-isothermal constitutive-models for viscoelastic fluid flow and their related applications, see for example [82, 92, 112, 116, 117, 119, 139] have made it possible for the extension of the Newtonian based-fluid models to more general non-Newtonian (and specifically viscoelastic) fluid based nanofluids. The current work represents such an extension to viscoelastic nanofluidics, specifically using GVFBN.

The extensions to more general non-Newtonian fluid based nanofluids is not simply a theoretical and mathematical nicety but is rather driven by the vast and contemporary relevance to industrial, technological, and medical applications of non-Newtonian fluids in general and viscoelastic fluids in particular, see [140]. The work in [92] focused on novel development and analysis of GVFBN in shear-driven isobaric flows. The current work extends this analysis to non-isobaric (pressure driven) channel flow of GVFBN. Additionally, instead of the isothermal wall boundary conditions employed in [92], the current work explores symmetrical convective cooling on the channel walls.

The chapter is organized in the following sequence. Section 3.2 summarizes the model and governing equations. Section 3.3 gives the numerical algorithms

and computational methodologies for the model problem as well as preliminary test results on temporal and spatial convergence. The exploration and discussion of the effects of the various embedded parameters is detailed in Section 3.4. Concluding remarks follow in section 3.5.

3.2 Problem Formulation

The schematic of the model problem is displayed in Fig. 3-1.

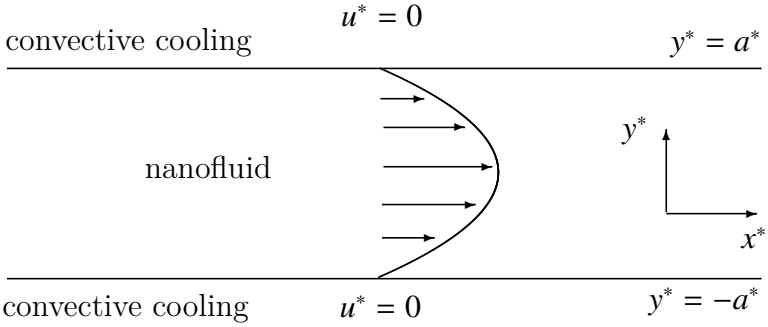

Fig. 3-1 Geometry of the model problem.

An incompressible GVFBN is subjected to unsteady, laminar, pressure-driven flow of in a channel formed by two infinitely long parallel walls. The GVFBN is assumed to have both variable shear-viscosity and variable thermal-conductivity and is susceptible to exothermic reactions following Arrhenius theory. The x^*-axis is considered parallel to the flow direction and the y^*-axis perpendicular to it.

Following the model developments in Chapter 2 (see Eq. (2-11)), the appropriate dimensionless parameters of current interest are the Reynolds number (Re), ambient-temperature parameter (θ_a), Brinkman number (Br), Deborah number (De), activation-energy parameter (α), Prandtl number (Pr), Peclet number (Pe = Re · Pr), Frank-Kamenetskii parameter (δ_1), Biot number (Bi) and the ratio of the polymer-to-the-total viscosity (β),

$$\beta = \frac{\eta_p^*}{\eta^*},\ \mathrm{De} = \frac{\lambda_0^* U_0^*}{h^*},\ \mathrm{Re} = \frac{\rho_f^* U_0^* a^*}{\eta^*},\ \mathrm{Pr} = \frac{c_{p_f}^* \eta^*}{\kappa_f^*},\ \theta_a = \frac{T^* - T_0^*}{\alpha T_0^*},\ \mathrm{Br} = \frac{\eta^* U_0^{*2}}{\kappa_f^* \alpha T_0^*},\ \mathrm{Bi} = \frac{h^* a^*}{k_0^*},$$

$$\mathrm{Re}_{nf} = \frac{\rho_{nf}}{\rho_f}\mathrm{Re},\ \mathrm{Pe}_{nf} = \frac{(\rho c_p)_{nf}}{(\rho c_p)_f}\mathrm{Pe},\ \alpha = \frac{R^* T_0^*}{E^*},\ \delta_1 = \frac{Q^* A^* C^* a^{*2}}{\kappa_f^* R^* T_W^{*\,2}} \exp\left(-\frac{1}{\alpha}\right). \qquad (3\text{-}1)$$

The nanofluid quantities ($_{nf}$) are obtained from linear combinations of the volume-fractions (φ) of the base fluid ($_f$) and of the solid nanoparticles ($_s$), e.g.

$$\rho_{nf} = \varphi \rho_s + (1-\varphi)\rho_f, \qquad (\rho c_p)_{nf} = \varphi (\rho c_p)_s + (1-\varphi)(\rho c_p)_f.$$

The appropriate dimensionless governing equations are,

$$\nabla \cdot \boldsymbol{u} = 0, \tag{3-2}$$

$$\mathrm{Re}_{nf} \frac{D\boldsymbol{u}}{Dt} = -\mathrm{Re}_{nf} \nabla p + \nabla \cdot (\boldsymbol{\sigma}), \tag{3-3}$$

$$\mathrm{Pe}_{nf} \frac{DT}{Dt} = -\nabla \cdot \left(\kappa_{nf} \nabla T\right) + \mathrm{Br}\, Q_D + \delta_1 \exp\left(\frac{T}{1+\alpha T}\right), \tag{3-4}$$

$$\boldsymbol{\tau} + \varepsilon \boldsymbol{\tau}^2 + \mathrm{De}\, \bar{\lambda}(T) \left[\overset{\nabla}{\boldsymbol{\tau}} - \boldsymbol{\tau} \frac{D}{Dt} (\ln(1+\alpha T))\right] = \frac{\eta_p(T)}{(\sqrt{1-\varphi})^5} \boldsymbol{S}, \tag{3-5}$$

with,

$$\boldsymbol{\sigma} = \boldsymbol{\tau} + \frac{\eta_s(T)}{(\sqrt{1-\varphi})^5} \boldsymbol{S}, \quad \boldsymbol{S} = \nabla \boldsymbol{u} + (\nabla \boldsymbol{u})^T, \quad \overset{\nabla}{\boldsymbol{\tau}} = \frac{D\boldsymbol{\tau}}{Dt} - \nabla \boldsymbol{u} \cdot \boldsymbol{\tau} - \boldsymbol{\tau} \cdot (\nabla \boldsymbol{u})^T. \tag{3-6}$$

The dimensionless dissipation term for the single-mode non-isothermal Giesekus model is,

$$Q_D = \frac{\boldsymbol{\eta}_s(T)}{(\sqrt{1-\varphi})^5} \boldsymbol{S} : \nabla \boldsymbol{u} + \gamma \boldsymbol{S} : \boldsymbol{\tau} + (1-\gamma) \frac{\hat{G}}{2\mathrm{De}\, \bar{\lambda}(T)} \left(I_1 + \mathrm{Tr}(\boldsymbol{b}^{-1}) - 6\right), \tag{3-7}$$

where the polymeric stress tensor ($\boldsymbol{\tau}$) and conformation tensor ($\boldsymbol{b}$) are related by,

$$\boldsymbol{\tau} = \hat{G} (\boldsymbol{b} - \boldsymbol{I}). \tag{3-8}$$

The dimensionless temperature dependent viscosities, thermal conductivity, and relaxation times are,

$$\eta_s(T) = (1-\beta) \exp(-\alpha T), \quad (\eta_s)_{nf} = \frac{\eta_s(T)}{(\sqrt{1-\varphi})^5}, \tag{3-9}$$

$$\eta_p(\dot{\gamma}, T) = \left[\beta + (m-1)\left(1 + (\lambda \dot{\gamma})^2\right)^{\frac{n-1}{2}}\right] e^{(-\alpha T)}, \quad (\eta_p)_{nf} = \frac{\eta_p(\dot{\gamma}, T)}{(\sqrt{1-\varphi})^5}, \tag{3-10}$$

with,

$$\eta = \eta_s(T) + \eta_p(\dot{\gamma}, T), \quad \eta_{nf} = \frac{\eta}{(\sqrt{1-\varphi})^5}, \tag{3-11}$$

$$\bar{\lambda}(T) = \frac{1}{1+\alpha T} \exp(-\alpha T), \tag{3-12}$$

$$\kappa_{nf} = \frac{\kappa_s + (1-\aleph)\kappa_f - (\aleph-1)\varphi(\kappa_f - \kappa_s)}{\kappa_s + (1-\aleph)\kappa_f + \varphi(\kappa_f - \kappa_s)}\,(1 + \alpha\, A_2\, T). \tag{3-13}$$

In Eqs. (3-2 - 3-13), $m \geq 1$ is the shear-rate-viscosity parameter, $0 \leq n \leq 1$ is the shear-thinning parameter, $\aleph$ is the empirical shape factor (where $\aleph = 3$ for nanoparticles of spherical shape), [?]. The shear-rate viscosity parameter, m, gives the ratio of zero shear-rate to the infinite shear-rate viscosities. The value $m = 1$ indicates that the viscosity is independent of shear-rates, as would obtain for Newtonian (nano) fluids and for ordinary viscoelastic (nano) fluids. The generalized-Newtonian-fluid-based nanofluid (GNFBN) model is obtained by taking $\beta = 0$ (and $m \neq 1$) and $\mathrm{De} = 0$. The choice $\mathrm{De} = \beta = 0$ and $m = 1$ represents a Newtonian nanofluid refer to [82, 92].

3.2.1 Initial and boundary conditions

Given the symmetric flow geometry for the pressure-driven flow, it is sufficient to consider only the upper half channel $y \in [0, 1]$ instead of the full channel $y \in [-1, 1]$. The following initial- and boundary- conditions therefore apply,

$$u(0, y) = 0, \quad T(0, y) = 0, \quad \boldsymbol{\tau}(0, y) = 0, \quad \text{for} \quad 0 \leq y \leq 1, \tag{3-14}$$

$$\frac{\partial}{\partial y}u(t, 0) = 0, \quad \frac{\partial}{\partial y}T(t, 0) = 0, \quad \text{for} \quad t > 0. \tag{3-15}$$

$$u(t, 1) = 0, \qquad \frac{\partial}{\partial y}T(t, 1) = -\mathrm{Bi}\,[T(t, 1) - \theta_a], \quad \text{for} \quad t > 0. \tag{3-16}$$

3.3 Numerical Solution

The semi-implicit finite-difference numerical and computational methodologies are based on the ideas described in [82, 92]. The velocity equation is descretized thus,

$$\mathrm{Re}_{nf}\frac{u^{(n+1)} - u^{(n)}}{\Delta t} = \mathrm{Re}_{nf}\, G + \frac{\partial}{\partial y}\tau_{12}^{(n)} + \left((\eta_s)_{nf}^{(n)}\,\frac{\partial^2}{\partial y^2}u^{(n+\xi)} + \frac{\partial}{\partial y}u^{(n)}\,\frac{\partial}{\partial y}(\eta_s)_{nf}^{(n)}\right), \tag{3-17}$$

where $G = \frac{\partial p}{\partial x} = 1$ denotes the constant pressure-gradient in the flow direction.The velocity updates in time via the scheme,

$$-r_1 u_{j-1}^{(n+1)} + (\mathrm{Re}_{nf} + 2r_1) u_j^{(n+1)} - r_1 u_{j+1}^{(n+1)} = \mathrm{Re}_{nf}\, u_j^{(n)} + \mathrm{Re}_{nf}\, G + (1-\xi)\,\Delta t\,(\eta_s)_{nf}^{(n)} \frac{\partial^2}{\partial y^2} u^{(n)} \quad +$$

$$\Delta t \frac{\partial}{\partial y} \tau_{12}^{(n)} + (1-\beta)\,\Delta t \frac{\partial}{\partial y} u^{(n)} \frac{\partial}{\partial y} (\eta_s)_{nf}^{(n)}, \tag{3-18}$$

where

$$r_1 = \xi\,(\eta_s)_{nf}^{(n)} \frac{\Delta t}{\Delta y^2}.$$

The resultant system of algebraic equations represent a diagonally dominant tri-diagonal linear system. The semi-implicit finite-difference method for temperature equation follows similarly,

$$\mathrm{Pe}_{nf} \frac{\partial T}{\partial t} = \kappa_{nf}^{(n)} \frac{\partial^2}{\partial y^2} T^{(n+\xi)} + \frac{\partial}{\partial y} T^{(n)} \frac{\partial}{\partial y} \kappa_{nf}^{(n)} + \mathrm{Br}\, Q_D^{(n)} + \delta_1 \exp\left(\frac{T^{(n)}}{1+\alpha\, T^{(n)}}\right). \tag{3-19}$$

Specifically, the temperature updates in time via the scheme,

$$\begin{aligned} -r_2 T_{j-1}^{(n+1)} + (\mathrm{Pe}_{nf} + 2r_2) T_j^{(n+1)} - r_2 T_{j+1}^{(n+1)} &= \mathrm{Pe}_{nf}\, T_j^{(n)} + (1-\xi)\,\Delta t\, \kappa_{nf} \frac{\partial^2}{\partial y^2} T^{(n)} \\ &+ \Delta t \frac{\partial}{\partial y} T^{(n)} \frac{\partial}{\partial y} \kappa_{nf}^{(n)} + \Delta t\, \mathrm{Br}\, (\eta_s)_{nf}^{(n)} \left(\frac{\partial}{\partial y} u^{(n)}\right)^2 + \delta_1 \exp\left(\frac{T^{(n)}}{1+\alpha\, T^{(n)}}\right) \\ &+ \Delta t\, \mathrm{Br}\, \gamma\, \tau_{12}^{(n)} \frac{\partial}{\partial y} u^{(n)} + (1-\gamma) \Delta t\, \mathrm{Br}\, \frac{\hat{G}}{2\mathrm{De}\bar{\lambda}(T)} (I_1 + \mathrm{Tr}\,(\boldsymbol{b}^{-1}) - 6), \end{aligned} \tag{3-20}$$

where

$$r_2 = \xi\, \kappa_{nf} \frac{\Delta t}{\Delta y^2}.$$

The equations for the extra stress tensor, $\boldsymbol{\tau}$ Eq. (3-5), are solved analogously,

$$\boldsymbol{\tau}^{(n+\xi)} + \varepsilon\,(\boldsymbol{\tau}^2)^{(n)} + \mathrm{De}\,\bar{\lambda}^{(n)} \frac{\boldsymbol{\tau}^{(n+1)} - \boldsymbol{\tau}^{(n)}}{\Delta t} = \text{explicit terms.}$$

The solutions for the various tensor components therefore follow directly,

$$(\mathrm{De}\,\bar{\lambda}^{(n)} + \xi\,\Delta t)\,\boldsymbol{\tau}^{(n+1)} = \text{explicit terms.} \tag{3-21}$$

The explicit terms for τ_{11}, τ_{12} and τ_{22} are respectively,

$$\begin{aligned} &[\mathrm{De}\,\bar{\lambda}^{(n)} - (1-\xi)\Delta t]\,\tau_{11}^{(n)} + \Delta t\,\mathrm{De}\,\bar{\lambda}^{(n)} \left[\tau_{12}^{(n)} \frac{\partial}{\partial y} u^{(n)} + \tau_{11}^{(n)} \frac{\partial}{\partial y} \log\left(1+\alpha T^{(n)}\right)\right] \\ &\qquad - \varepsilon\,\Delta t\,(\tau_{11}^2 + \tau_{12}^2), \end{aligned} \tag{3-22}$$

$$[\mathrm{De}\,\bar{\lambda}^{(n)} - (1-\xi)\Delta t]\,\tau_{12}^{(n)} + \Delta t\,\mathrm{De}\,\bar{\lambda}^{(n)} \left[\tau_{22}^{(n)} \frac{\partial}{\partial y} u^{(n)} + \tau_{12}^{(n)} \frac{\partial}{\partial y} \log\left(1+\alpha T^{(n)}\right)\right]$$

$$+ \Delta t\,(\eta_p)_{nf}\,\frac{\partial}{\partial y}u^{(n)} - \varepsilon\,\Delta t\,(\tau_{11}\tau_{12} + \tau_{22}^2), \tag{3-23}$$

$$[\mathrm{De}\,\bar{\lambda}^{(n)} - (1-\xi)\Delta t]\,\tau_{22}^{(n)} + \Delta t\,\mathrm{De}\,\bar{\lambda}^{(n)}\,\tau_{22}^{(n)}\frac{\partial}{\partial y}\log\left(1+\alpha T^{(n)}\right) - \varepsilon\,\Delta t\,(\tau_{12}^2 + \tau - 12\,\tau_{22}). \tag{3-24}$$

3.4 Results

Unless otherwise indicated, the following list of values, for the embedded variables and material parameters, will be assumed,

$$\begin{aligned}&\alpha = 0.1,\ \mathrm{Br} = 1,\ \mathrm{Re} = 1,\ \mathrm{Pr} = 1,\ \mathrm{De} = 2,\ \gamma = 0.5,\ \beta = 0.2,\ \Delta y = 0.01,\\ &\Delta t = 0.1,\ t = 50,\ \hat{G} = 10^{-3},\ m = 1.2,\ \delta_1 = 0.1,\ \lambda = 0.01,\ n = 0.5,\ \zeta = 1,\\ &\varphi = 0.04,\ \varepsilon = 0,\ A_2 = 0.2,\ \mathrm{Bi} = 1,\ \theta_a = 0.1,\ \aleph = 3.\end{aligned} \tag{3-25}$$

The above will constitute the default variable and parameter values in this study. In the subsequent graphical results, it will be assumed and understood that, where variable and parameter values are not explicitly stated, they will be given by the default values.

3.4.1 Convergence in time and space

It is important to validate the utility of a numerical and computational algorithm before deploying it to solving physical problems. Figs. 3-2, 3-3, 3-4, and 3-5 show, as required, that the computational algorithms are independent of both time-step and mesh size - specifically, the algorithms give the same results for a large range of time-steps and mesh sizes.

3.4.2 Transient development of solutions to steady state

Given the focus on unsteady flow, it is equally important (in addition to the demonstration of time-step and mesh size convergence) to demonstrate that the algorithms are capable of capturing the transient (time) development of steady solutions, including the capabilities to also illustrate the final steady-state solutions. Figs. 3-6 and 3-7 show, as required, the development of solutions in time until steady states are reached.

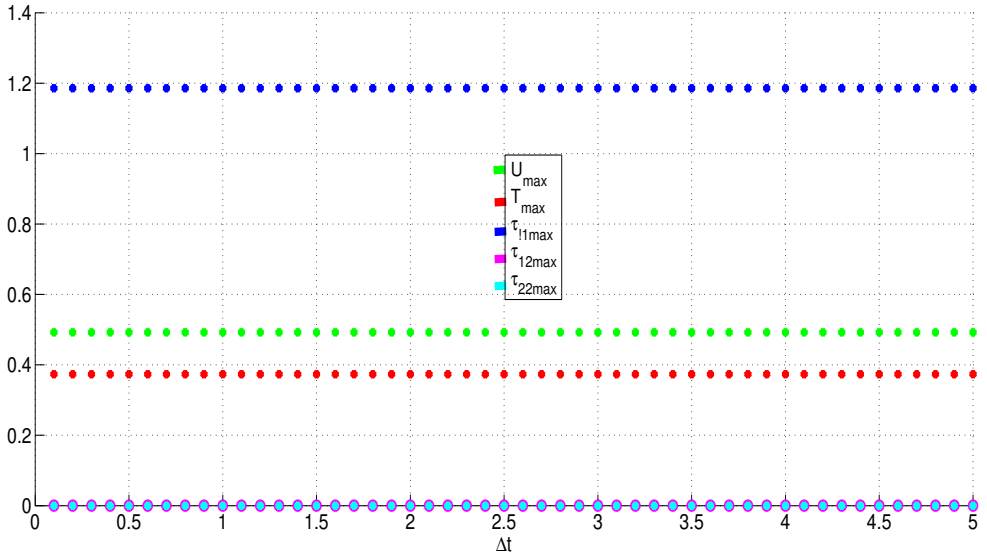

Fig. 3-2 Dependence of solutions on time step size.

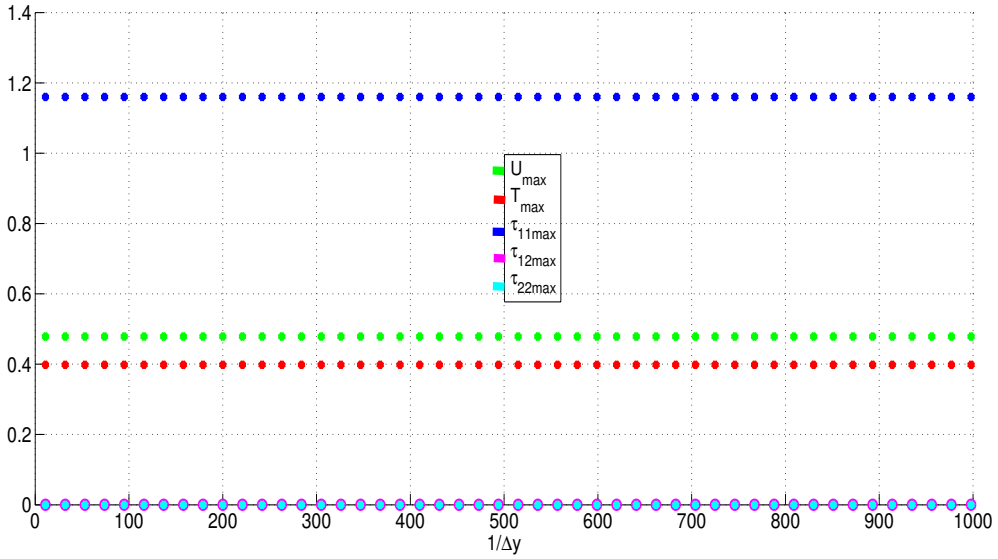

Fig. 3-3 Dependence of solutions on mesh size.

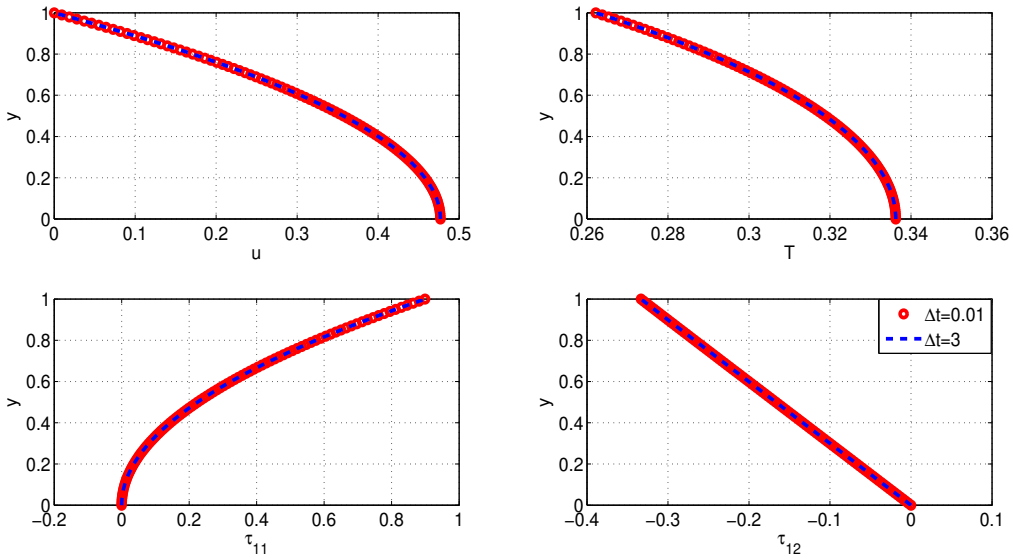

Fig. 3-4 Dependence of solutions on time step size.

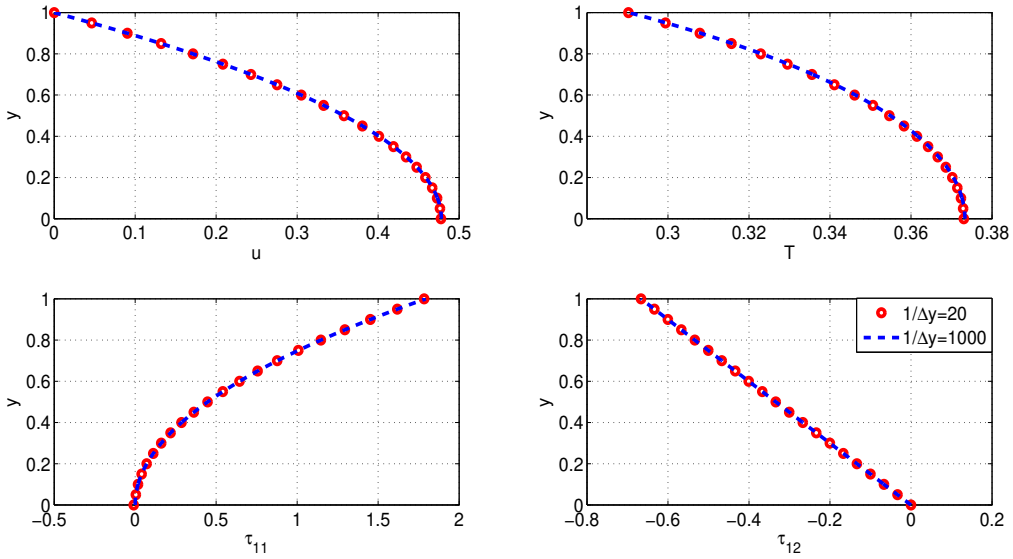

Fig. 3-5 Dependence of solutions on mesh size.

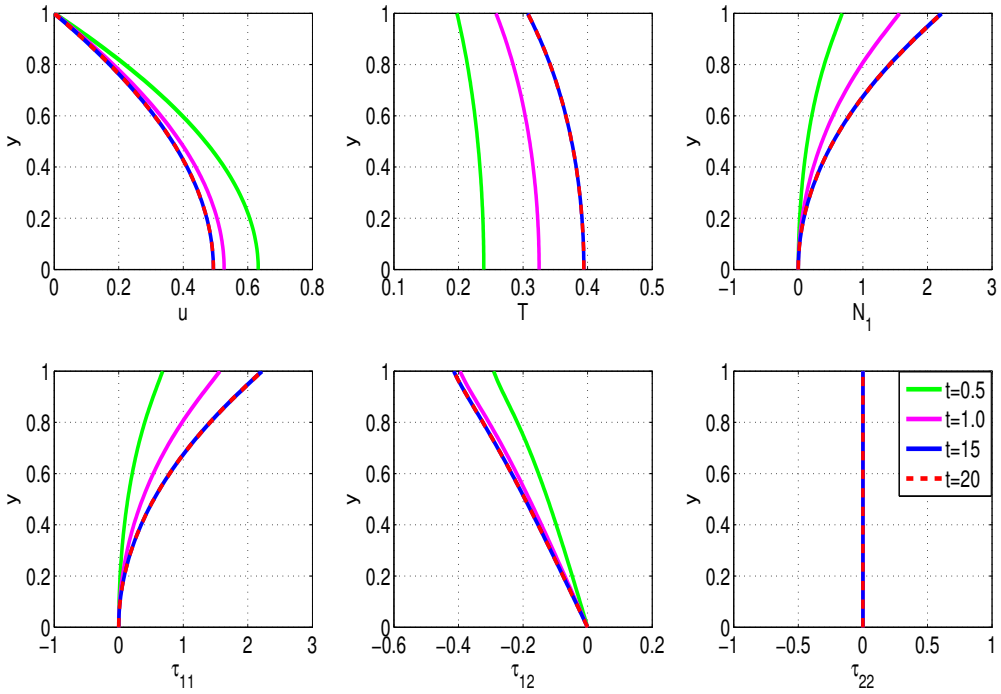

Fig. 3-6 Transient development to steady state profiles, $\Delta t = 0.05$

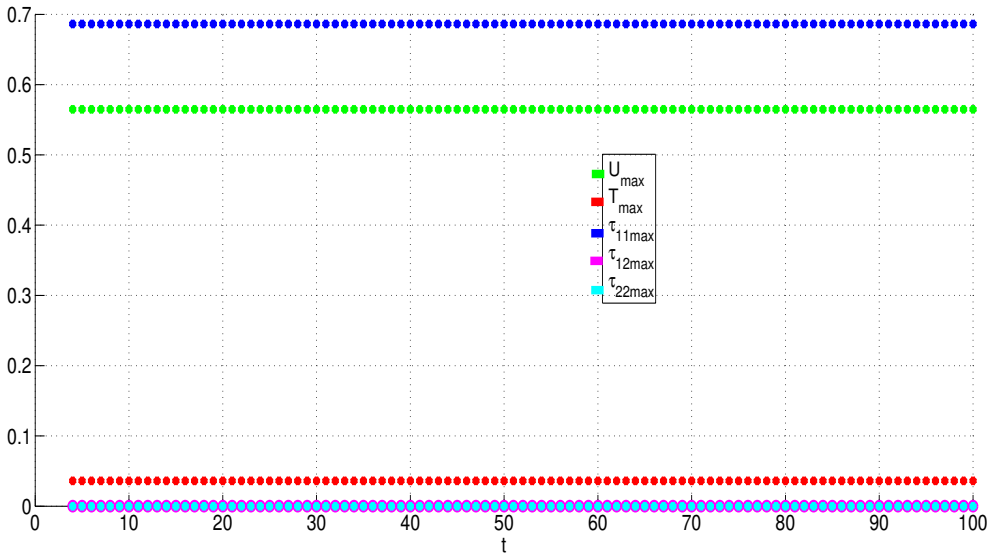

Fig. 3-7 Transient development of steady maximum flow quantities.

3.4.3 Parameter dependence of solutions

Fig. 3-8 gives an illustration of the variation of flow quantities with φ, the volume-fraction of the embedded nano-particles. The results show an increase in the flow quantities with increasing φ. The increase in fluid temperature with increasing φ is obvious, given that the increased volume of heat conducting nano-particles would directly also increase fluid thermal conductivity, see Fig. 3-9.

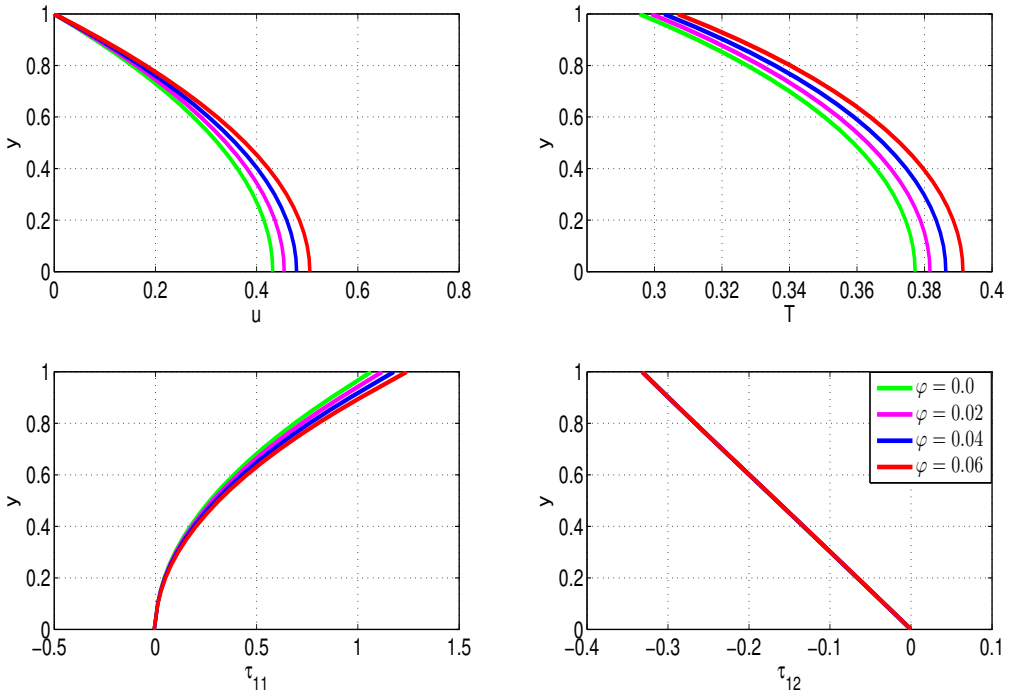

Fig. 3-8 Response of flow quantities to variations in φ.

The increase in fluid temperature naturally also decreases the fluid viscosity and hence also diminishes the viscous drag effects, hence the increase in fluid velocity with increasing φ as observed in Fig. 3-8.

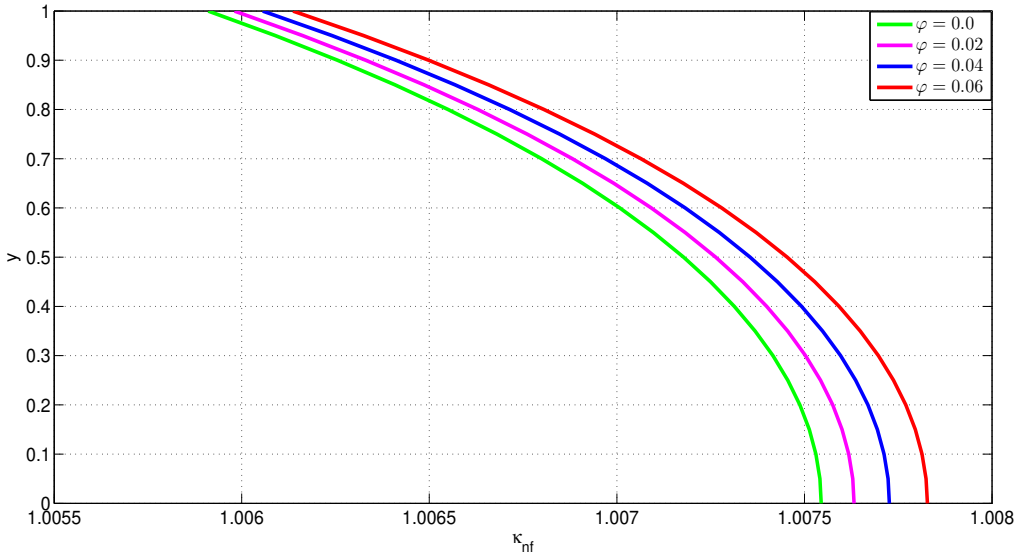

Fig. 3-9 Response of nanofluid thermal-conductivity to variations in φ

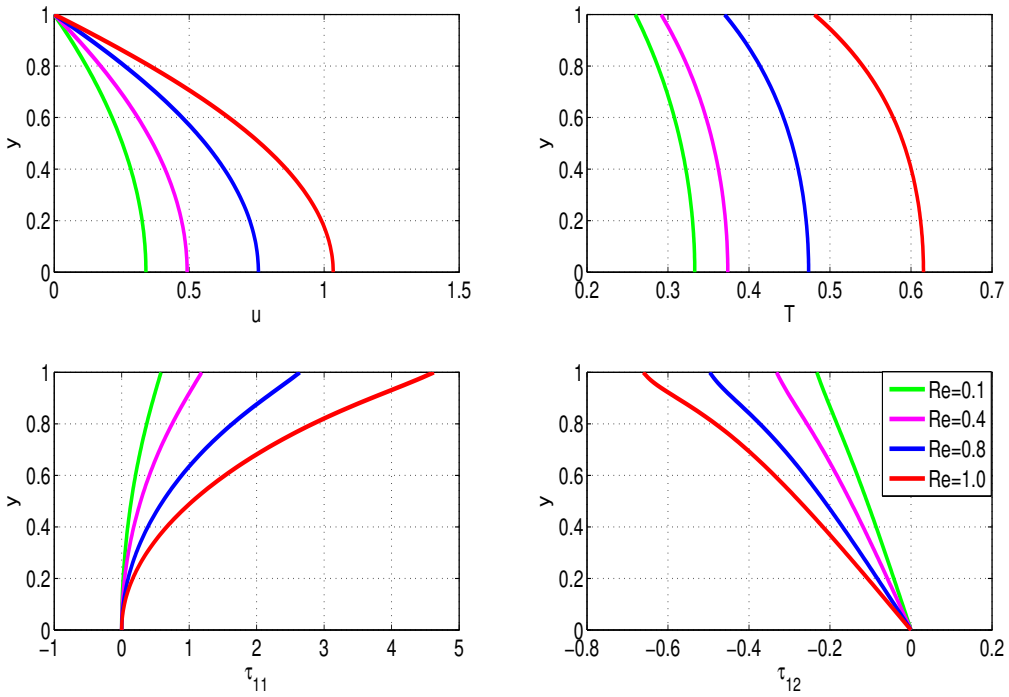

Fig. 3-10 Response of flow quantities to variations in Re.

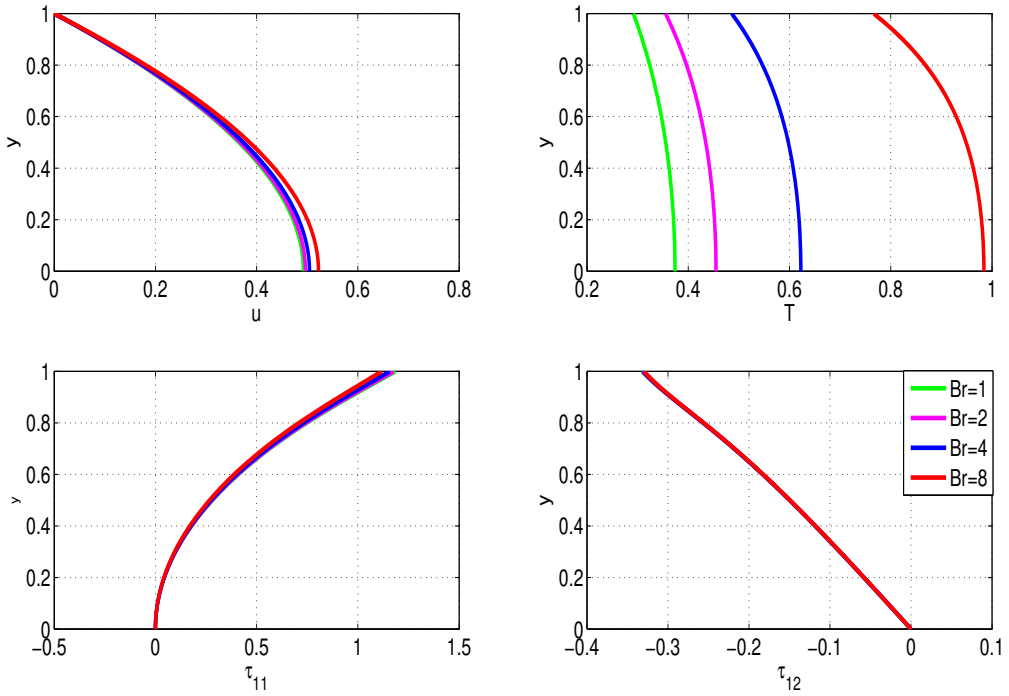

Fig. 3-11 Response of flow quantities to variations in Br.

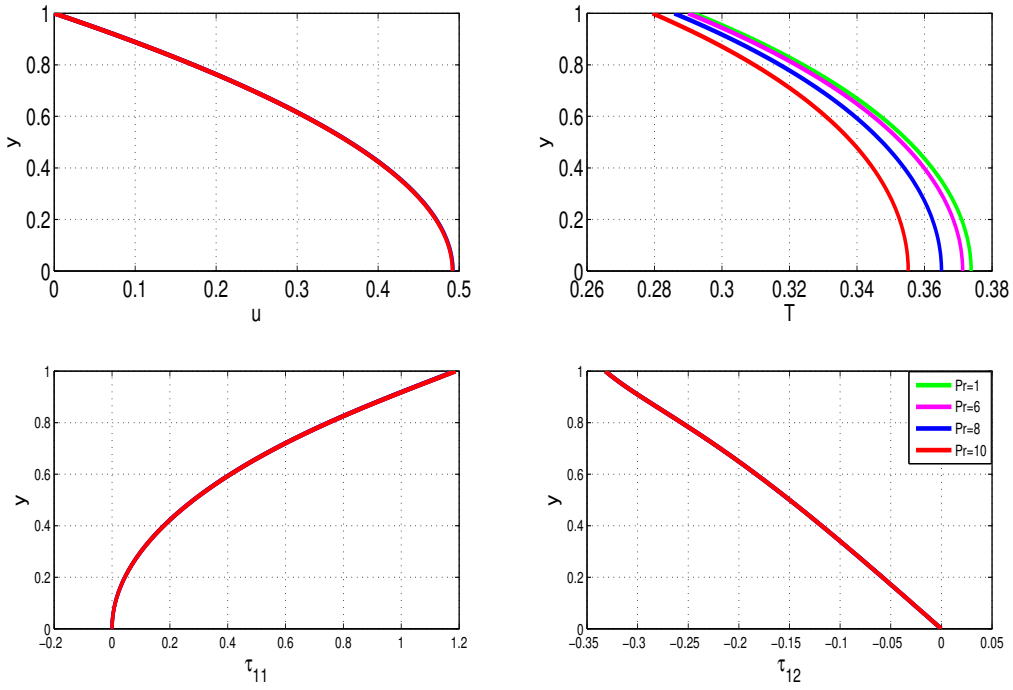

Fig. 3-12 Response of flow quantities to variations in Pr.

Viscous effects are inversely proportional to the Reynolds number, Re. Alternatively, high speed flows are synonymous with high Reynolds numbers. Fig. 3-10 therefore demonstrates, as expected, an increase in velocity with increasing Re. As a result of the higher velocities, temperature increses as shown in 3-10.

Fig. 3-11 shows the dependence of flow quantities with Brinkman number, Br. Since Br is directly connected to the strength of the heat sources, the fluid temperature (and hence also the fluid velocity) are expected to increase with increasing Br as illustrated in Fig. 3-11. The polymeric stress component τ_{11}, on the other hand, decreases with increasing Br.

The reaction of flow quantities to changes in the Prandtl number, Pr, is shown in Fig. 3-12. Both temperature dissemination and the thickness of the thermal boundary layer condense as the Prandtl number Pr increases. Physically, the Prandtl number Pr is inversely proportional to thermal diffusivity, an increase in the Prandtl number leads to worsening thermal diffusion. As a result, temperature decreases

The reaction of flow quantities to changes in the Prandtl number, Pr, is shown in Fig. 3-12. A high Prandtl number, Pr, implies a fluid with poor thermal conductivity, resulting in a smaller thermal boundary layer structure. Furthermore, when the amount of Pr rises, the rate of thermal diffusion reduces. With rising Pr, the VFBN temperature should drop. These expected outcomes are shown in Fig. 3-12 accordingly.

The Prandtl number indirectly enters the momentum and polymeric-stress equations via the temperature dependence of the viscosity. For these reasons, small variations in Pr have no discernible influence on the fluid velocity and polymeric-stress components, Fig. 3-12. The activation-energy parameter, α, has similar effects to those of Br, see Fig. 3-13. The increase of fluid temperature with increasing α as illustrated in Fig. 3-13 can be directly linked to the increase of nanofluid thermal-conductivity, κ_{nf}, with increasing α, see Fig. 3-14.

Fig. 3-15 illustrates the required increase in fluid velocity with increased pressure driving-force.

The behaviour of fluid temperature with variations in the exothermic-reaction parameter δ_1 is similar to that with respect to Br given the linkages of these parameters to the heat sources, see Fig. 3-16. The major difference is that the fluid temperature increases linearly with increasing Br whereas the fluid temperature increases exponentially with increasing δ_1, see [82]. The possibility of thermal runway phenomena therefore looms large with regards to increases in δ_1 due to exponential temperature growth. Indeed, for large values of the exothermic-reaction parameter δ_1, the steady

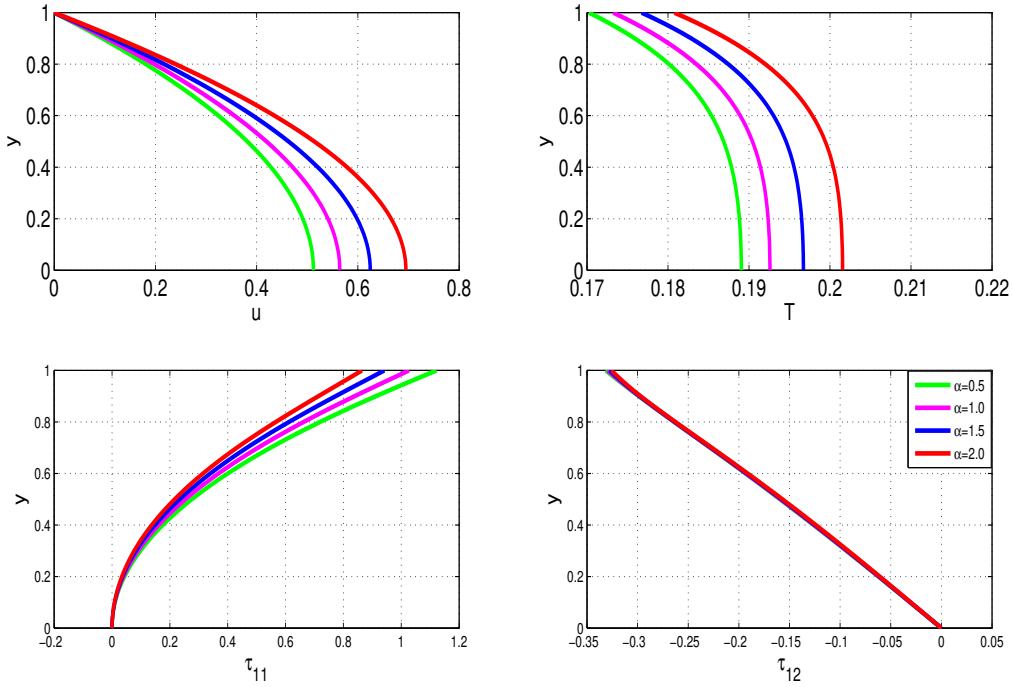

Fig. 3-13 Response of flow quantities to variations in α, where $\delta_1 = 0.001$.

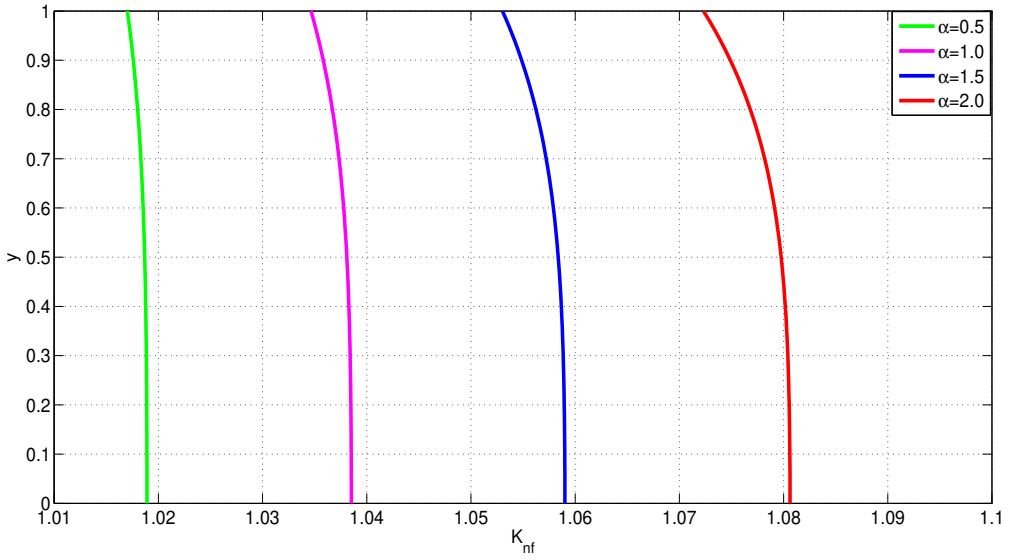

Fig. 3-14 Response of nanofluid thermal-conductivity, κ_{nf}, to variations in α.

state solutions would not be attainable - the solutions would blow up in finite time, see Fig. 3-17.

The respective behaviour of flow quantities with variations in the viscoelastic parameters, γ and De, are illustrated in Fig. 3-18 and Fig. 3-19 respectively.

As expected, the polymeric (viscoelastic) stresses increase with increasing De.

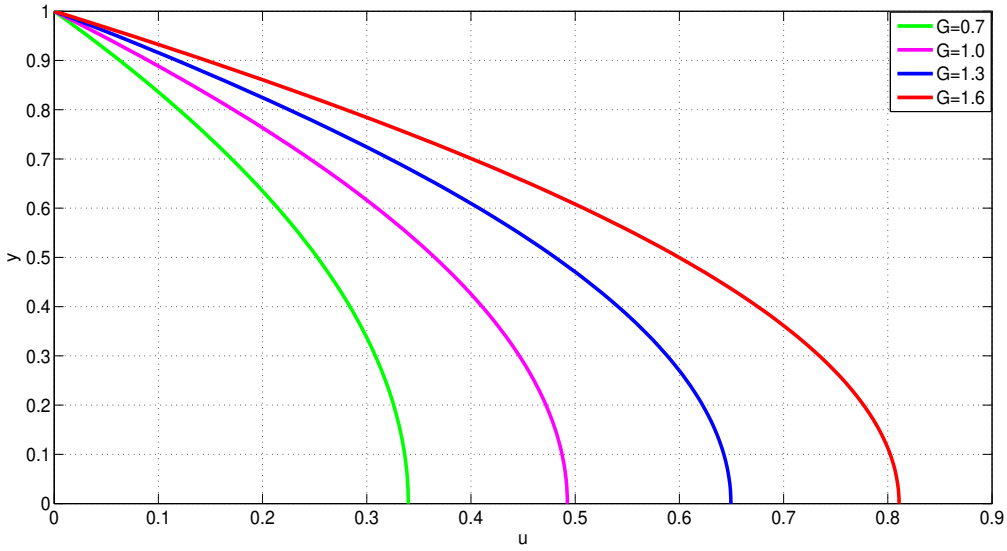

Fig. 3-15 Effects of variations in pressure driving force on fluid velocity.

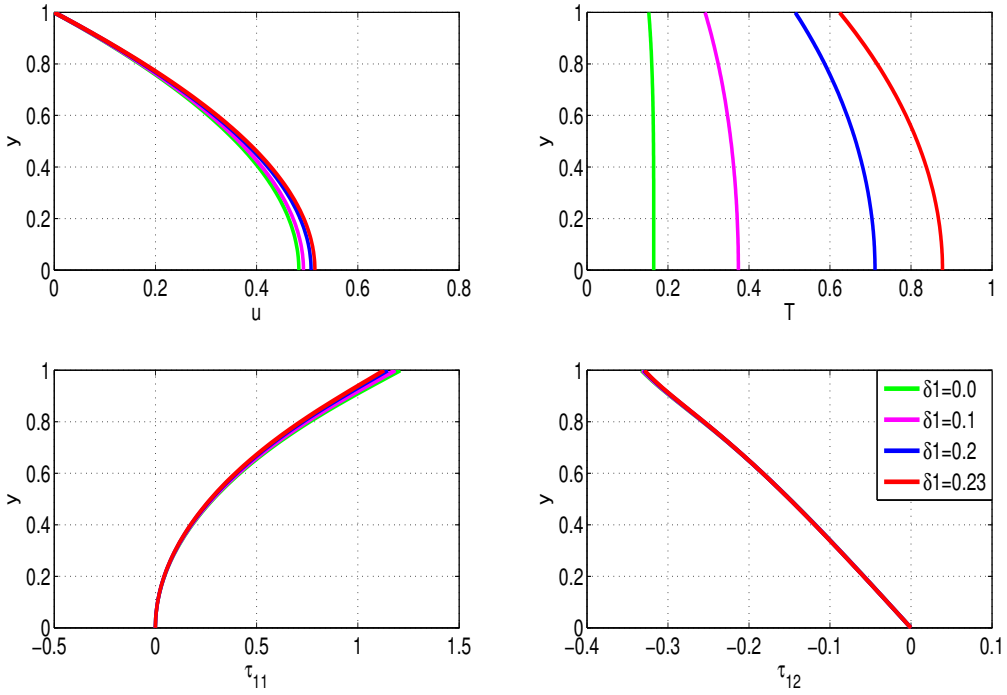

Fig. 3-16 Response of flow quantities to variations in δ_1.

It is also noticed, as expected, that the fluid temperature increases with increasing γ given the dominance of entropic heat dissipation (over energetic heat storage) for larger values of γ.

The heat exchange between the ambient environment, the channels walls, and the nanofluid is related to the Biot number Bi, see Eq. (3-16). Enhanced convective cooling at the channel walls is directly related to higher Bi. The cooled walls in turn

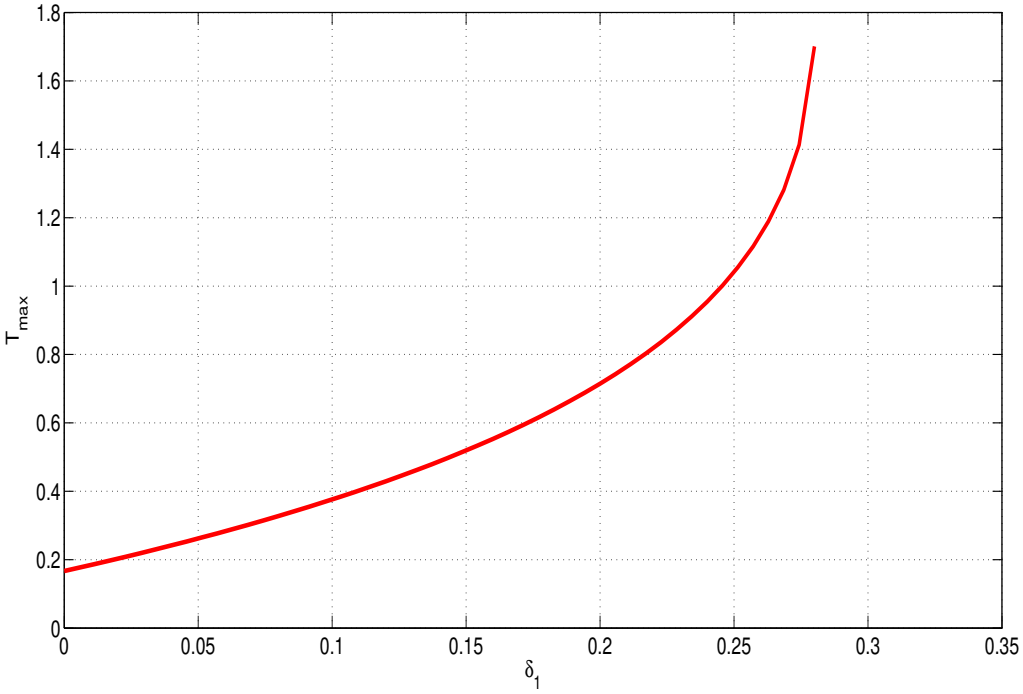

Fig. 3-17 Finite time blow-up of fluid temperature for large value of δ_1.

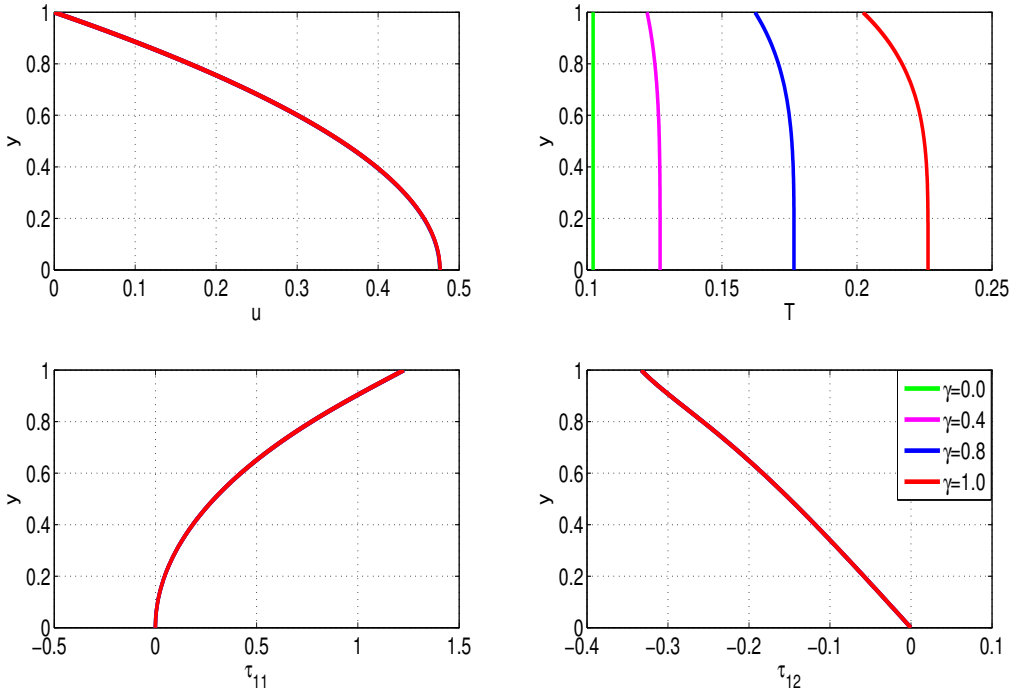

Fig. 3-18 Response of flow quantities to variations in γ.

lead to lower nanofluid temperatures in the bulk flow. Fig. 3-20 therefore illustrates, as expected, the decrease in (bulk) nanofluid temperature with increasing Bi.

The nanofluid viscosity (at constant shear-rates) increases with increasing shear-

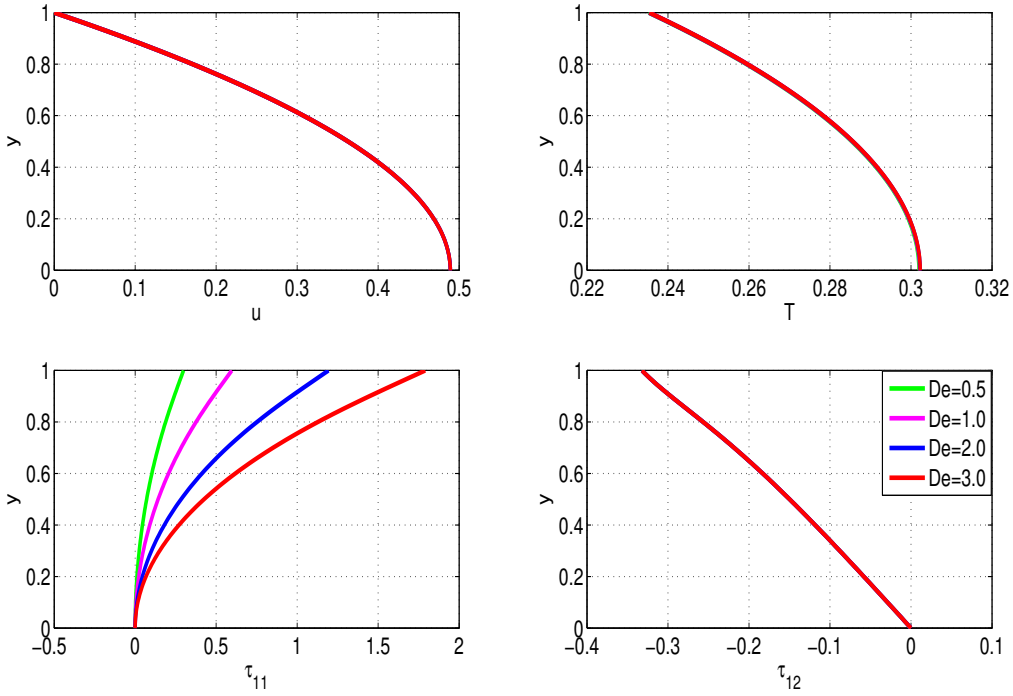

Fig. 3-19 Response of flow quantities to variations in De.

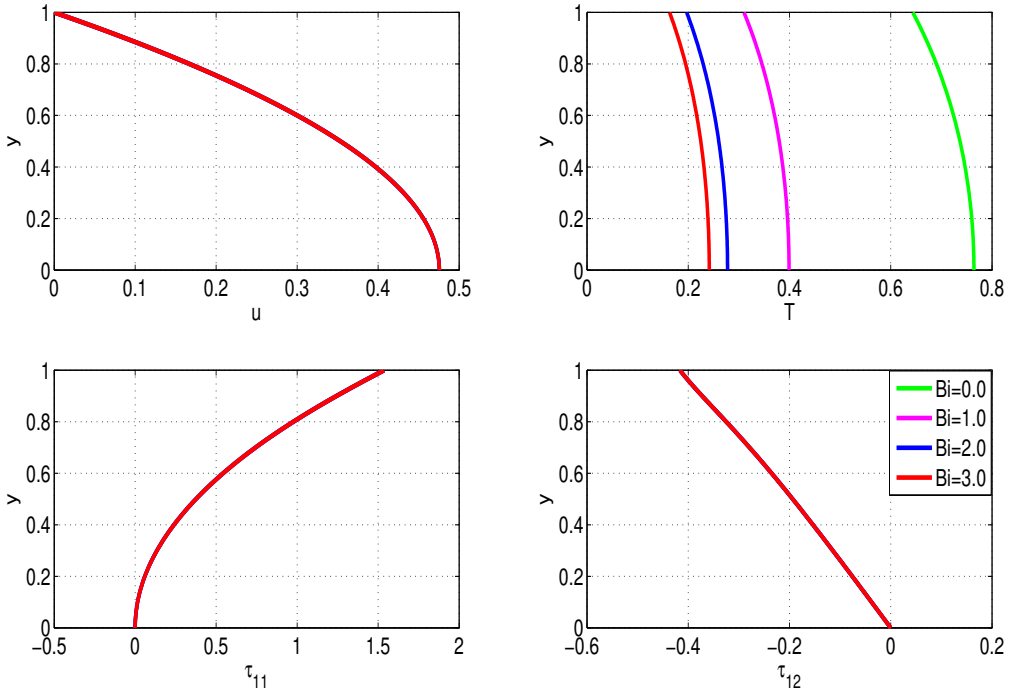

Fig. 3-20 Response of flow quantities to variations in Bi.

thinning parameter, m. An increase in m therefore increases resistance to flow (due to the higher viscosity) and hence leads to a decrease in fluid velocity as shown in Fig. 3-21. A decrease in both the fluid temperature and the polymeric stresses with

increasing m is also noticed.

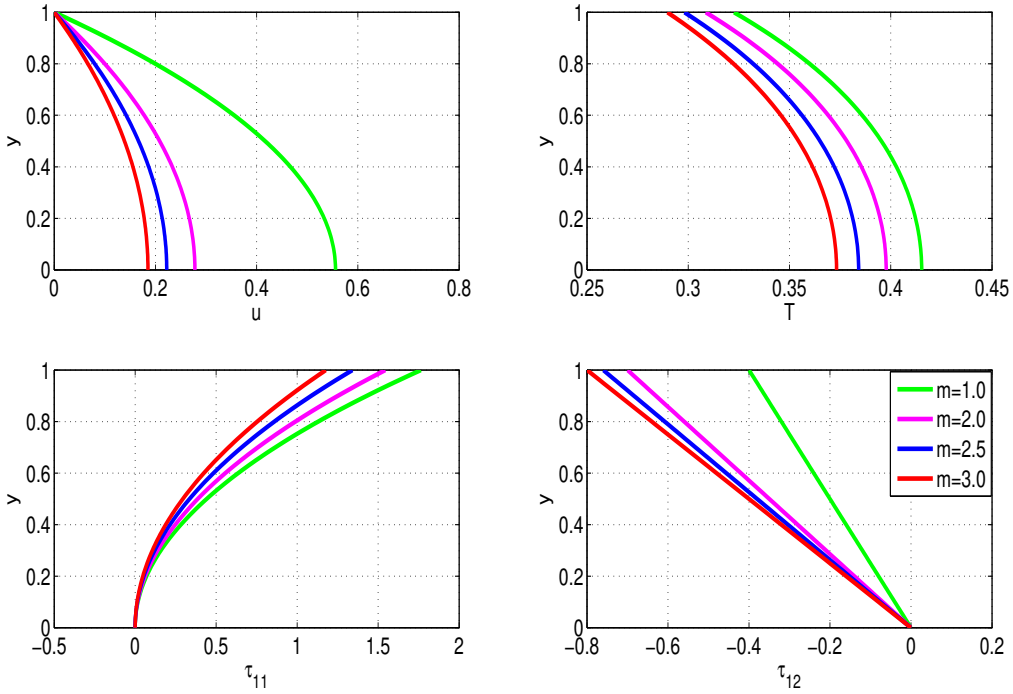

Fig. 3-21 Response of flow quantities to variations in m.

3.5 Concluding Remarks

The investigation employed efficient and convergent semi-implicit numerical and computational algorithms based on the finite difference methods to analyze the non-isothermal, pressure-driven, channel-flow of a generalized-viscoelastic-fluid-based nanofluid (GVFBN) subject to convective cooling at the channel boundaries. The assumed mathematical model is based on a single-phase (constant concentration) nanofluid mixture in which the nanoparticles are homogeneously mixed with the generalized-viscoelastic-fluid base. The research results are explored in qualitative (graphical) detail illustrating the effects of the variations of the fundamental embedded parameters on the flow quantities, specifically; the fluid velocity, fluid temperature, and polymer-stresses. The results demonstrate that those parameters which only directly couple to the energy equation (but are otherwise indirectly coupled to the momentum and stress-constitutive equations, say via the viscosities and relaxation times) would only show prominent effects on nanofluid temperature but not on the fluid velocity or the polymer stresses. The results also demonstrate, as in the literature on exothermic flows, that the values of exothermic-reaction parameter must be carefully controlled as large values would lead to thermal runway phenomena. The present results are consistent with the existing literature and additionally add novel new contributions to non-isothermal and pressure-driven channel flow of GVFBN under convective cooling conditions.

Acknowledgements

The authors would like to extend their sincere gratitude to National Research Foundation (NRF) for providing financial support to publish this work.

Chapter 4 Computational analysis of shear-banding in simple-shear-flow of viscoelastic-fluid-based nanofluids subject to exothermic reactions[1]

ABSTRACT

We investigate the shear-banding phenomena in non-isothermal simple-shear-flow of a viscoelastic-fluid-based nanofluid (VFBN) subject to exothermic reactions. The polymeric (viscoelastic) behaviour of the VFBN is modelled via the Giesekus constitutive equation, with appropriate adjustments to incorporate both the non-isothermal and nanoparticle effects. Nahme-type laws are employed to describe the temperature dependence of the VFBN viscosities and relaxation times. Arrhenius theory is used for the modelling and incorporation of exothermic reactions. The VFBN is modelled as a single-phase homogeneous-mixture and hence the effects of the nanoparticles is based on the volume-fraction parameter. Efficient numerical schemes based on semi-implicit finite-difference-methods are employed in MATLAB for the computational solution of the governing systems of partial differential equations. The fundamental fluid-dynamical and thermodynamical phenomena such as shear-banding, thermal-runaway, and heat-transfer-rate (HTR) enhancement are explored under relevant conditions. Important novel results of industrial significance are observed and demonstrated. Firstly, under shear-banding conditions of the Giesekus-type VFBN model, we observe remarkable HTR and Therm-C enhancement in the VFBN as compared, to NFBN. Specifically, the results demonstrate that the VFBN are less susceptible to thermal runaway than are NFBN. Additionally, the results illustrate that the reduced susceptibility of the Giesekus-type VFBN to thermal-runaway phenomena is further enhanced under shear-banding conditions, in particular when the nanofluid becomes increasingly polymeric. Increased polymer-viscosity is used as the most direct proxy for measuring the increase in the polymeric nature of the fluid.

[1]The contents of this chapter are from khan et.al [141]

4.1 Introduction

Research into the enhancement of heat-transfer-rate (HTR) and thermal-conductivity (Therm-C) characteristics of nanofluids has gained wide contemporary traction, see for example [20, 36, 92–98, 100–106, 109, 110, 135–138]. The evidence of the efficacy of nanofluids (formed from mixtures of metallic-nanoparticles and base-fluids such as water or oil) in HTR and Therm-C enhancement is now widespread, commonly accepted, and hence such nanofluids are now extensively used for these purposes. Similar investigations have been conducted on the use of various, natural and synthetic, fluid properties for the enhancement of certain characteristic that are desirable for applications. Fluid viscoelasticity has indeed received wide attention in this regard specifically for the improvement of certain industrial, domestic, and medical applications. Such widespread use of the viscoelastic (polymeric) fluids, for the improvement and enhancement of, say, HTR and Therm-C, emulsion-polymerization, drag-reduction, etc. can be found for example in [82, 86–88, 92, 110, 112, 116, 117, 119, 135, 139, 142–144].

The present study extends the investigations in [92] to the conditions of shear-banding. Specifically, the current investigation explores the novel contributions of shear-banding phenomena to HTR and Therm-C enhancement. Alternatively and additionally, the current investigation extends the studies in [88], [119] , and [86] (all of which focused on the flow be-haviour and thermodynamics of particle-free viscoelastic fluids) to nanofluids, specifically VFBN modeled by the Giesekus constitutive model. The study in [88] investigates shear-banding phenomena using the Rolie-Poly two-fluid viscoelastic constitutive model and the investigations in [119] and [86] employ the Johnson-Segalman viscoelastic constitutive model.

Shear-banding phenomena in shear-flow of viscoelastic fluids represents observable and physical discontinuities in the shear-rate profiles of the flow-velocity and finds wide industrial and domestic application, say in emulsion-polymerization and drop break-up [144]. The main mechanism for shear-banding in [88] falls under the category of what are termed flow-induced inhomogeneities. On the other hand, the mechanism for shear-banding in [119] and [86]falls under the category of constitutive instabilities. The researchers in [88] however demonstrated that their finite-volume-method (FVM) based numerical and computational algorithms (implemented on the OpenFOAM software) were capable of reproducing the shear-banding characteristics via either mechanism, using the Johnson-Segalman, Giesekus, and Rolie-Poly viscoelastic constitutive models. Shear-banding phenomena has been observed in

the shear-flow of polymeric fluids of various types including, for example, worm-like micelle solutions [145, 146], polymer-solutions [147], foams [148], telechelic-polymers [149], granular-flows [150], soft-glasses [151], and polymer-melts [152].

The Chapter is structured as follows. Section 4.2 presents the physical and mathematical model. Section 4.3 outlines the numerical and computational algorithms. Section 4.4 lists the graphical and qualitative results. The concluding remarks are provided in Section 4.6.

4.2 Problem Formulation

We consider plane Couette-flow (simple-shear-flow) as depicted on the schematic in Fig. 4-1.

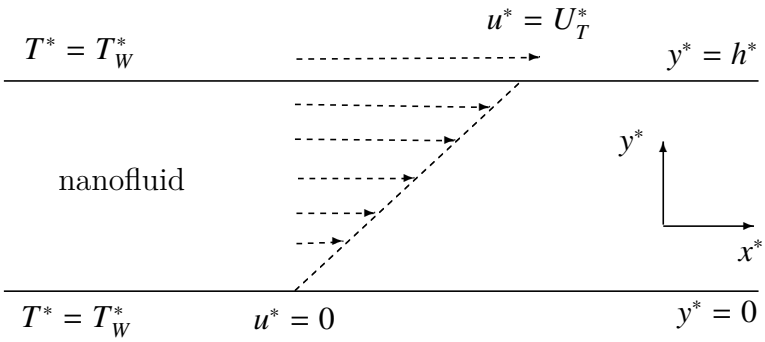

Fig. 4-1 Geometry of the model problem.

The variables appearing in Fig. 4-1 are the velocity field, $u(t, y)$, the temperature field, $T(t, y)$, the time ,t, and the 2D Cartesian space coordinates, $x = (x, y)$.

4.2.1 Model assumptions

- We assume the flow of a VFBN in a channel of infinite longitudinal extent. We therefore assume that the flow is fully developed in the x-direction and hence that flow quantities are independent of x. This allows us to focus attention on the primary effects of shear-banding on HTR and Therm-C enhancement without the complications of 2D (or indeed 3D) computations.
- We assume that the shear-banding is driven by constitutive instabilities via the Giesekus viscoelastic constitutive model. The exact mechanisms of shear-banding, whether via constitutive instabilities or via flow inhomogeneities, are still areas of active research. Indeed, even for shear-banding via constitutive instabilities, at least two viscoelastic constitutive models have been advanced. None of these considerations however detract from the primary

aim to investigate the broader effects of shear-banding on HTR and Therm-C enhancement.

- We assume spherical nanoparticles that are homogeneously mixed with the base-fluid. The size, shape, distribution, orientation, etc. of the nanoparticles is still a wide open areas with regards to investigating the optimal conditions for HTR and Therm-C enhancement. None of these considerations however detract from the primary aim to investigate the broader effects of nanoparticles on HTR and Therm-C enhancement.

4.2.2 Dimensionless governing equations

The development of the governing equations for the VFBN is adapted from Eqs. (2-1 - 2-10). Using the notation of Eqs. (2-11, 2-12), the relevant equations in dimensionless form are,

$$\nabla \cdot \boldsymbol{u} = 0, \tag{4-1}$$

$$\mathrm{Re}_{nf}\,\frac{D\boldsymbol{u}}{Dt} = -\mathrm{Re}_{nf}\,\nabla p + \nabla\cdot(\boldsymbol{\sigma}), \tag{4-2}$$

$$\mathrm{Pe}_{nf}\,\frac{DT}{Dt} = -\nabla\cdot\left(\kappa_{nf}\,\nabla T\right) + \mathrm{Br}\,Q_D + \delta_1\,\exp\left(\frac{T}{1+\alpha T}\right), \tag{4-3}$$

$$\boldsymbol{\tau} + \varepsilon\,\boldsymbol{\tau}^2 + \mathrm{De}\,\bar{\lambda}(T)\left[\overset{\nabla}{\boldsymbol{\tau}} - \boldsymbol{\tau}\,\frac{D}{Dt}\left(\ln\left(1+\alpha T\right)\right)\right] = \frac{\eta_p(T)}{(\sqrt{1-\phi})^5}\,\boldsymbol{S}, \tag{4-4}$$

with,

$$Q_D = \gamma\boldsymbol{S}:\boldsymbol{\tau} + (1-\gamma)\frac{\boldsymbol{\eta}_s(T)}{(\sqrt{1-\phi})^5}\,\boldsymbol{S}:\boldsymbol{S}, \tag{4-5}$$

$$\eta_s(T) = (1-\beta)\,\exp(-\alpha\,T), \quad (\eta_s)_{nf} = \frac{\eta_s(T)}{(\sqrt{1-\phi})^5}, \tag{4-6}$$

$$\eta_p(T) = \beta\,e^{(-\alpha\,T)}, \quad (\eta_p)_{nf} = \frac{\eta_p(T)}{(\sqrt{1-\phi})^5}, \tag{4-7}$$

$$\eta = \eta_s(T) + \eta_p(T), \quad \eta_{nf} = \frac{\eta}{(\sqrt{1-\phi})^5}, \tag{4-8}$$

$$\bar{\lambda}(T) = \frac{1}{1+\alpha\,T}\,\exp(-\alpha\,T), \tag{4-9}$$

$$\kappa_{nf} = \frac{\kappa_s + (1-\chi)\kappa_f - (\chi-1)\phi(\kappa_f-\kappa_s)}{\kappa_s + (1-\chi)\kappa_f + \phi(\kappa_f-\kappa_s)}\,(1+\alpha\,A_2\,T). \tag{4-10}$$

Where

$$\boldsymbol{\sigma} = \boldsymbol{\tau} + (\eta_s)_{nf}\,\boldsymbol{S}, \quad \boldsymbol{S} = \nabla\boldsymbol{u} + (\nabla\boldsymbol{u})^T . \tag{4-11}$$

The non-dimensional variables and dimensionless parameters used in Eqs. (4-1- 4-11) are defined in the Nomenclature at the end of the article. In particular, p is the pressure field, ε is the Giesekus non-linear parameter, $\boldsymbol{\sigma}$ is the Total-stress tensor, $\boldsymbol{S}$ is the rate of deformation tensor, $\boldsymbol{\tau}$ is the polymer-stress tensor, $(\eta_s)_{nf}$ is the solvent-viscosity for the nanofluid, $(\eta_p)_{nf}$ is the polymer-viscosity for the nanofluid, $(\eta)_{nf}$ is the total-viscosity for the nanofluid, $()_{nf}$ is the thermal-conductivity for the nanofluid, α is the activation-energy parameter, β is the polymer to total-viscosity ratio, Br is the Brinkman-number, δ_1 is the Frank-Kamenetskii parameter, De is the Deborah-number, Pr is the Prandtl-number, Pe is the Peclet-number, Re is the Reynolds-number, and the subscript $()_{nf}$ represent nanofluid. Each os the nanofluid quantities, $()_{nf}$, is obtained as a linear combination of the contributions from the solid nanoparticles, $()_s$, and the base-fluid, $()_f$;

$$()_{nf} = \phi()_s + (1-\phi)()_f.$$

The notations ∇ and $\frac{D}{Dt}$ represent the usual gradient and material-derivative operators respectively.

4.2.3 Initial and boundary conditions

The following initial and boundary conditions apply,

$$u(0,y) = 0, \quad T(0,y) = 0, \quad \boldsymbol{\tau}(0,y) = 0, \quad \text{for} \quad 0 \le y \le 1, \tag{4-12}$$

$$u(t,0) = 0, \quad T(t,0) = 0, u(t,1) = 0, \qquad T(t,1) = 0, \quad \text{for} \quad t \ge 0. \tag{4-13}$$

4.3 Numerical and computational algorithms

The semi-implicit numerical scheme for the longitudinal velocity component is,

$$\mathrm{Re}_{nf}\frac{u^{(n+1)} - u^{(n)}}{\Delta t} = \mathrm{Re}_{nf}\,G + \frac{\partial}{\partial y}\tau_{12}^{(n)} + \left((\eta_s)_{nf}^{(n)}\frac{\partial^2}{\partial y^2}u^{(n+\xi)} + \frac{\partial}{\partial y}u^{(n)}\frac{\partial}{\partial y}(\eta_s)_{nf}^{(n)}\right), \tag{4-14}$$

where

$$u^{(n+\xi)} = \xi u^{(n+1)} + (1-\xi)u^{(n)}.$$

The longitudinal velocity therefore updates in time to $u^{(n+1)}$ via,

$$-r_1 u_{j-1}^{(n+1)} + (\mathrm{Re}_{nf} + 2r_1) u_j^{(n+1)} - r_1 u_{j+1}^{(n+1)} = \mathrm{Re}_{nf}\, G + \mathrm{Re}_{nf}\, u_j^{(n)} + \Delta t \frac{\partial}{\partial y}\tau_{12}^{(n)} + (1-\xi)\,\Delta t\,(\eta_s)_{nf}^{(n)} \frac{\partial^2}{\partial y^2} u^{(n)} + (1-\beta)\,\Delta t \frac{\partial}{\partial y} u^{(n)} \frac{\partial}{\partial y}(\eta_s)_{nf}^{(n)}, \quad (4\text{-}15)$$

where

$$r_1 = \xi\,(\eta_s)_{nf}^{(n)} \frac{\Delta t}{\Delta y^2}.$$

A similar semi-implicit numerical scheme for the temperature is,

$$\mathrm{Pe}_{nf} \frac{\partial T}{\partial t} = \kappa_{nf}^{(n)} \frac{\partial^2}{\partial y^2} T^{(n+\xi)} + \frac{\partial}{\partial y} T^{(n)} \frac{\partial}{\partial y} \kappa_{nf}^{(n)} + \mathrm{Br}\, Q_D^{(n)} + \delta_1 \exp\left(\frac{T^{(n)}}{1+\alpha\, T^{(n)}}\right). \quad (4\text{-}16)$$

leading to,

$$-r_2 T_{j-1}^{(n+1)} + (\mathrm{Pe}_{nf} + 2r_2) T_j^{(n+1)} - r_2 T_{j+1}^{(n+1)} = \mathrm{Pe}_{nf}\, T_j^{(n)} + (1-\xi)\,\Delta t\, \kappa_{nf} \frac{\partial^2}{\partial y^2} T^{(n)} + \Delta t \frac{\partial}{\partial y} T^{(n)} \frac{\partial}{\partial y} \kappa_{nf}^{(n)} + 2(1-\gamma)\Delta t\, \mathrm{Br}\, (\eta_s)_{nf}^{(n)} \left(\frac{\partial}{\partial y} u^{(n)}\right)^2 + 2\Delta t\, \mathrm{Br}\, \gamma\, \tau_{12}^{(n)} \frac{\partial}{\partial y} u^{(n)}, \quad (4\text{-}17)$$

where

$$r_2 = \xi\, \kappa_{nf} \frac{\Delta t}{\Delta y^2}.$$

Finally, the semi-implicit numerical scheme for the polymeric-stress is,

$$\boldsymbol{\tau}^{(n+\xi)} + \varepsilon\,(\boldsymbol{\tau}^2)^{(n)} + \mathrm{De}\, \bar{\lambda}^{(n)} \frac{\boldsymbol{\tau}^{(n+1)} - \boldsymbol{\tau}^{(n)}}{\Delta t} = \text{explicit terms..}$$

This leads to the direct solution,

$$(\mathrm{De}\, \bar{\lambda}^{(n)} + \xi\, \Delta t)\, \boldsymbol{\tau}^{(n+1)} = \text{explicit terms.} \quad (4\text{-}18)$$

where the respective explicit terms are,

$$[\mathrm{De}\, \bar{\lambda}^{(n)} - (1-\xi)\Delta t]\, \tau_{11}^{(n)} + \Delta t\, \mathrm{De}\, \bar{\lambda}^{(n)} \left[\tau_{12}^{(n)} \frac{\partial}{\partial y} u^{(n)} + \tau_{11}^{(n)} \frac{\partial}{\partial y} \log\left(1+\alpha T^{(n)}\right)\right] - \varepsilon\, \Delta t\, (\tau_{11}^2 + \tau_{12}^2), \quad (4\text{-}19)$$

$$[\mathrm{De}\, \bar{\lambda}^{(n)} - (1-\xi)\Delta t]\, \tau_{12}^{(n)} + \Delta t\, \mathrm{De}\, \bar{\lambda}^{(n)} \left[\tau_{22}^{(n)} \frac{\partial}{\partial y} u^{(n)} + \tau_{12}^{(n)} \frac{\partial}{\partial y} \log\left(1+\alpha T^{(n)}\right)\right] + \Delta t\, (\eta_p)_{nf} \frac{\partial}{\partial y} u^{(n)} - \varepsilon\, \Delta t\, (\tau_{11}\tau_{12} + \tau_{12}\tau_{22}), \quad (4\text{-}20)$$

$$[\mathrm{De}\, \bar{\lambda}^{(n)} - (1-\xi)\Delta t]\, \tau_{22}^{(n)} + \Delta t\, \mathrm{De}\, \bar{\lambda}^{(n)}\, \tau_{22}^{(n)} \frac{\partial}{\partial y} \log\left(1+\alpha T^{(n)}\right) - \varepsilon\, \Delta t\, (\tau_{12}^2 + \tau_{22}^2). \quad (4\text{-}21)$$

4.4 Graphical and qualitative results

Unless otherwise indicated, the following list of default values will be assumed for the various quantities and parameters,

$$\alpha = 0.01,\ \mathrm{Br} = 1,\ \mathrm{Re} = 1,\ \mathrm{Pr} = 1,\ \mathrm{De} = 2,\ \gamma = 0.5,\ \beta = 0.2,\ \Delta y = 0.01,$$
$$\Delta t = 0.01,\ t = 50,\ \delta_1 = 0.5,\ \zeta = 1,\ \phi = 0.04,\ \varepsilon = 0.5,\ A_2 = 0.2,\ \chi = 3. \qquad (4\text{-}22)$$

4.4.1 Time development of steady smooth solutions

Figs. 4-2 - 4-5 show the development (in time) of flow quantities until steady states are reached. Specifically, Fig. 2 illustrates the transient development of nanofluid velocity, u, and nanofluid temperature, T. The fluid flow is driven by shear forces acting longitudinally on the upper wall. Initially the bulk fluid is at rest. We notice from Fig. 4-2, as required, that the fluid velocity develops steadily in time from the initial state until the linear shear flow profile is achieved. Similarly, the fluid temperature is initially at zero throughout the flow geometry. As the flow develops in time, the exothermic reactions and mechanical dissipation processes taking place in the bulk flow lead to inevitable temperature increases in the bulk fluid. The channel walls are otherwise maintained at isothermal temperatures. We therefore notice from Fig. (4-2), as expected, that the bulk flow temperature gradually increases in time until steady state parabolic temperature profiles are reached

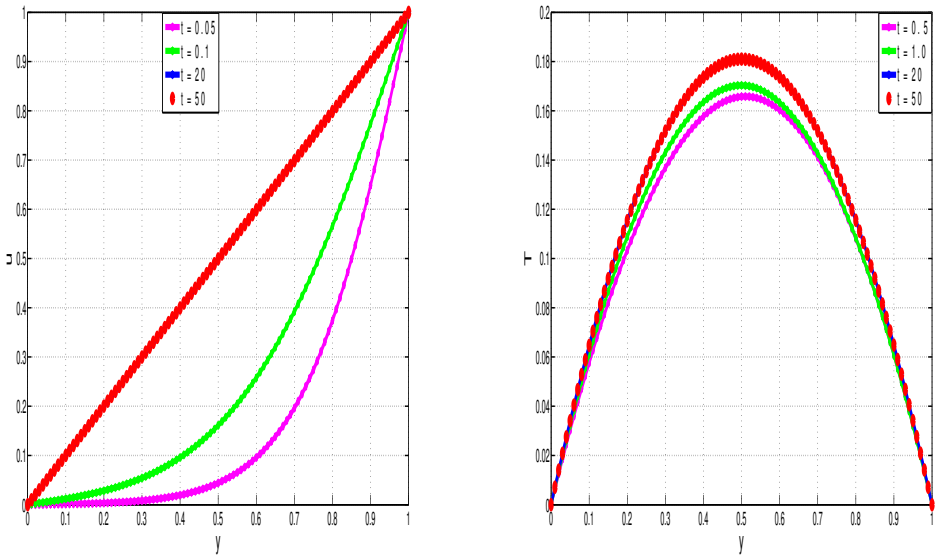

Fig. 4-2 Development of steady velocity and temperature profiles.

Figs. 4-2 and 4-3 show the time development of polymer stresses, $\tau_{11}, \tau_{22}, \tau_{12}$, and hence also of the second normal stress difference $N_1 = \tau_{11} - \tau_{22}$ N1 = 11 − 22.

As with the velocity and temperature profiles we notice that the polymer-stresses converge to fixed (reproducible) steady state solutions. The fixed (reproducibility) nature of the converged steady solutions is specifically illustrated in Fig. 4-5 where the same converged values are obtained irrespective of the subsequent time of additional computation. For example, once the solutions converge to steady state at, time t= 20, then extending the computations to say, time t = 100, will not change (qualitatively and quantitatively) the steady solutions.

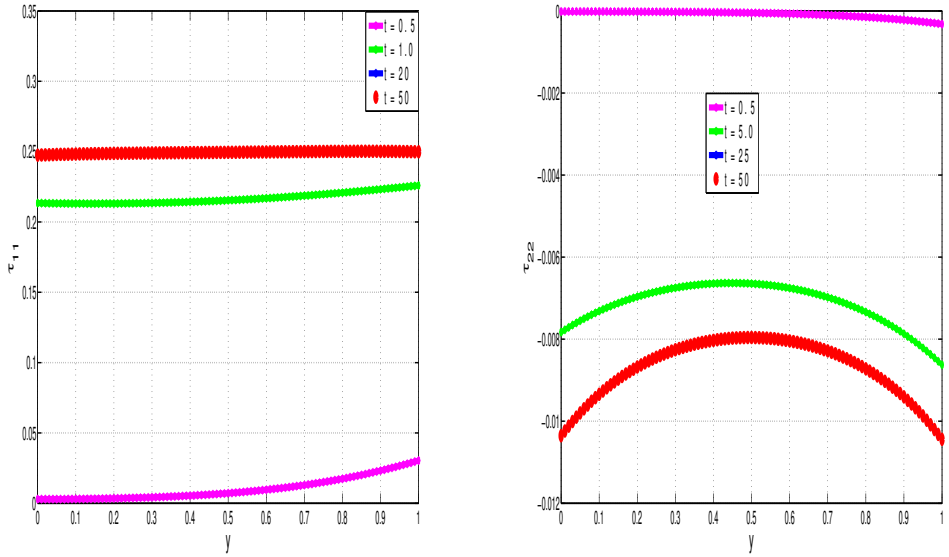

Fig. 4-3 Development of steady diagonal stress profiles.

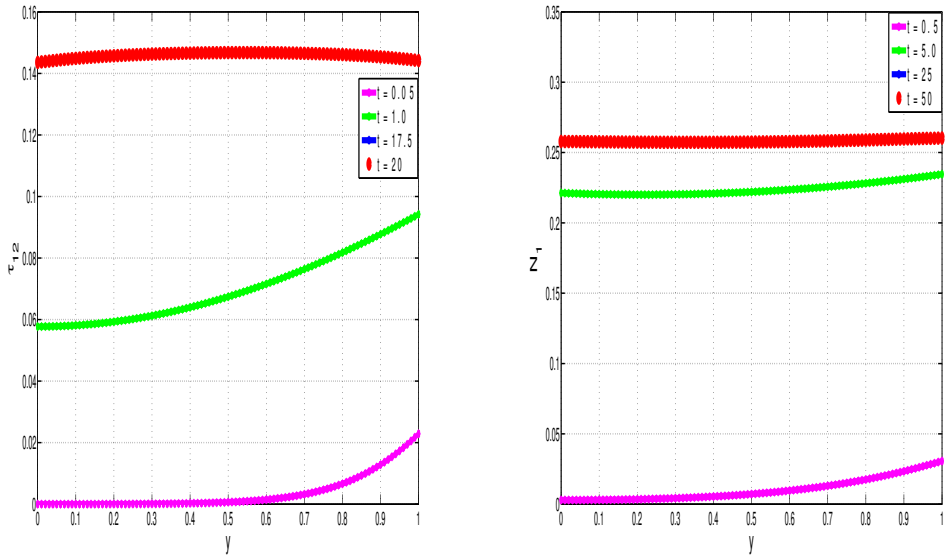

Fig. 4-4 Development of steady τ_{12} and N_1 profiles.

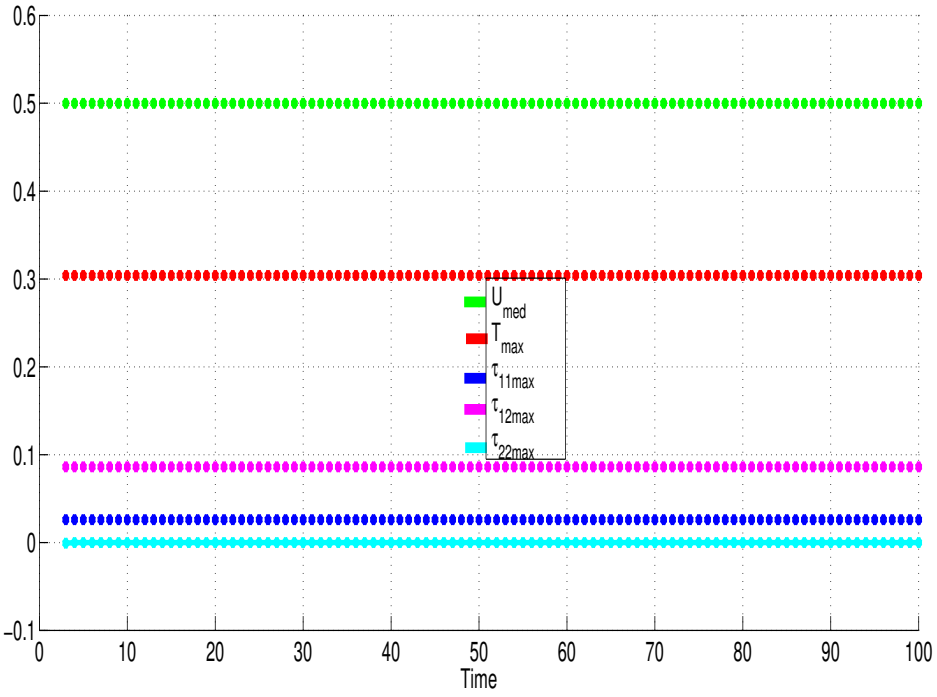

Fig. 4-5 Development of steady maximum flow profiles.

4.4.2 Mesh-size and time-step and convergence

Figs. 4-6 and 4-7 demonstrate, as required, that our numerical algorithms are independent of both mesh size and time-step. Specifically, the computational algorithms efficiently reproduce the expected solutions for a broad range of mesh-sizes and time-steps.

4.4.3 Development of Shear-banding

As noted in the introduction, shear-banding phenomena in shear-flow of viscoelastic fluids represents observable and physical discontinuities in the shear-rate profiles of the flow-velocity. Shear-banding phenomena has been observed in the shear-flow of polymeric fluids of various types including, for example, worm-like micelle solutions, polymer-solutions, foams, telechelic-polymers, granular-flows, soft-glasses, and polymer-melts.

As also noted in the introduction, there are two main scientifically agreed mechanisms for shear-banding, namely flow-induced inhomogeneities and constitutive instabilities. The Rolie-Poly viscoelastic constitutive model has been developed to explain shear-banding phenomena via flow-induced inhomogeneities.

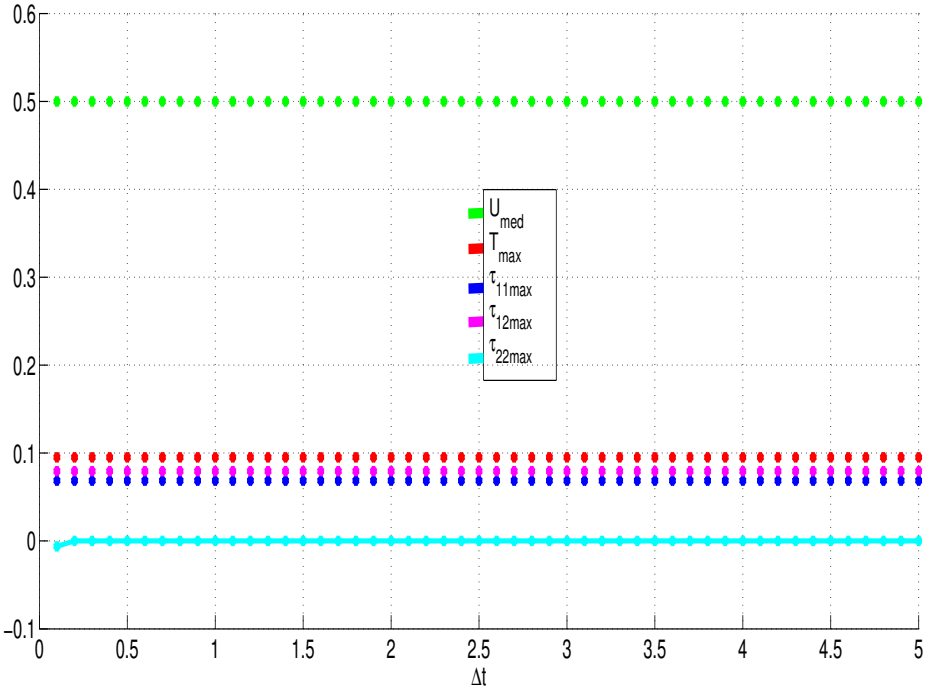

Fig. 4-6 Dependence of solutions on time step size.

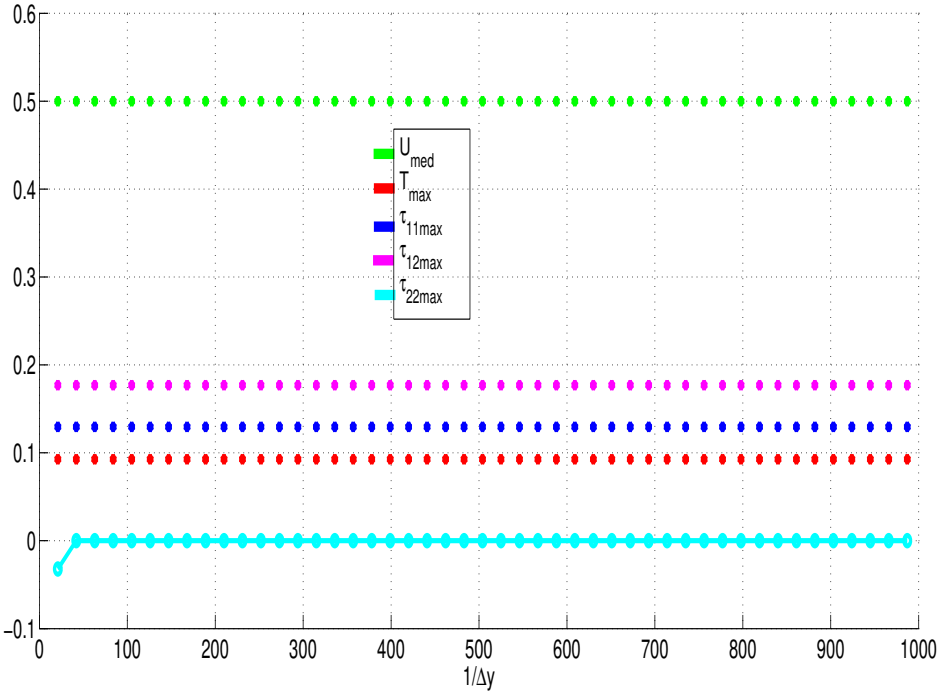

Fig. 4-7 Dependence of solutions on mesh size.

The Johnson-Segalman and Giesekus viscoelastic constitutive models allow for the mechanisms of shear-banding phenomena via constitutive instabilities if certain values of the viscoelastic material-parameters are taken.

Specifically, when $\beta = 0.95$ and $\varepsilon = 2$ in the Giesekus constitutive model, we note that the steady solutions exhibit shear-banding phenomena, see Fig. 4-8.

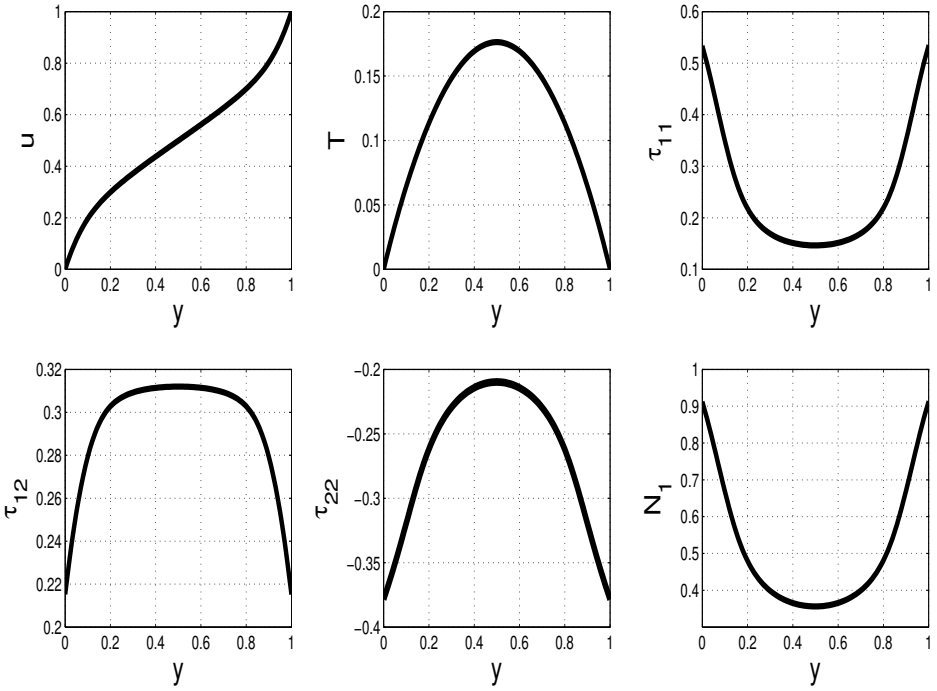

Fig. 4-8 Development of shear-bands for the Giesekus model with $\beta = 0.95$, $\varepsilon = 2$.

As already indicated, and as in [86], the shear-banding phenomena depicted in Fig. 4-8 is linked to the viscoelastic parameters, specifically the polymer-to-total-viscosity ratio (β) and the Giesekus nonlinear parameter (ε) in the present study. In [86] the shear-banding was linked to (β) and the Johnson-Segalman parameter. Taking $\varepsilon = 0$ reduces the Giesekus viscoelastic constitutive model to the Oldroyd-B model which is not capable of exhibiting shear-banding as illustrated in Fig. 4-9. Similarly, varying the values of β shows that the onset and prevalence of shear-banding is linked to higher values of β, as long as the value of ε is high enough, see Fig. 4-10

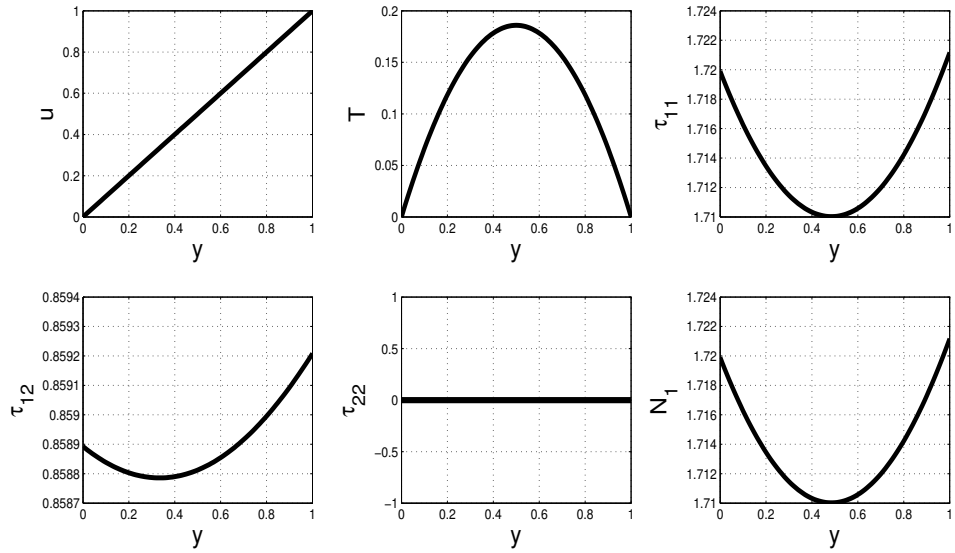

Fig. 4-9 Absence of shear-bands for Oldroyd-B model with $\beta = 0.95$, $\varepsilon = 0$.

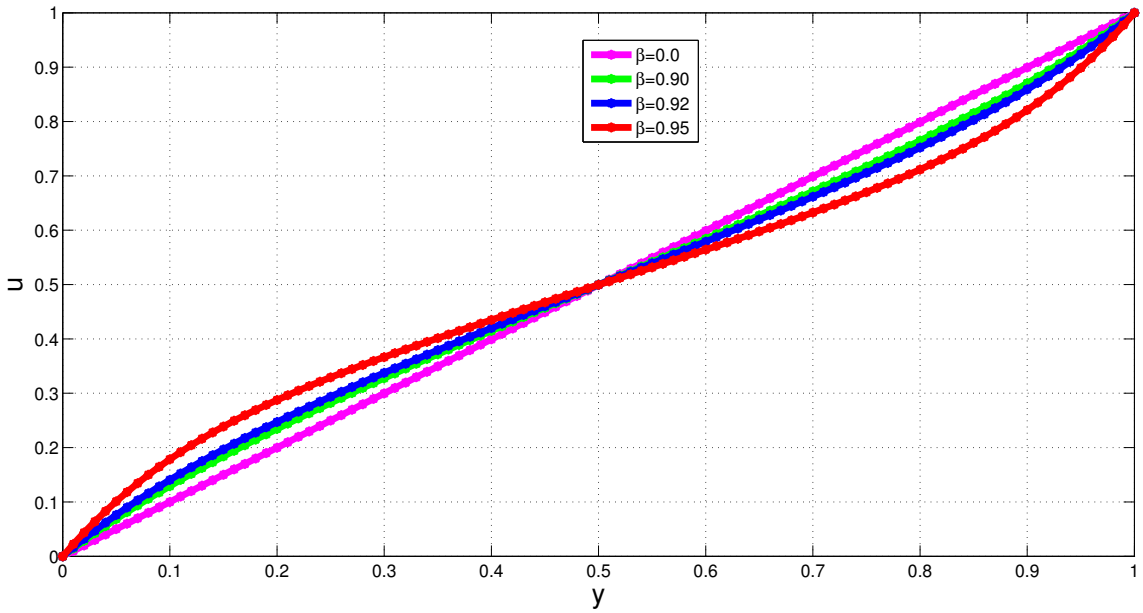

Fig. 4-10 Development of shear-banding with increasing β where $\varepsilon = 2$.

The phenomena of shear-banding via constitutive instabilities is extensively investigated in [86] using the Johnson-Segalman viscoelastic constitutive model. In particular, it is conclusively demonstrated in [86] that shear-banded solutions are essentially weak solutions of the governing partial differential equations for viscoelastic fluid flow and alsothat an infinite number of possible such solutions exist for any set of shear-banding material-parameters. However, the results in [86] illustrate that for each such set of shear-banding material-parameter values, the computational results will always reproduce the same unique (albeit weak) solution! The unique selected shear-rate path has been scientifically explained using the concept of stress diffusion as demonstrated in [87].

Figs. 4-11 and 4-12 illustrate the transient development of steady shear-banded solutions, demonstrating, as in [86, 87] the robustness and reproducibility of the shear-banded solutions.

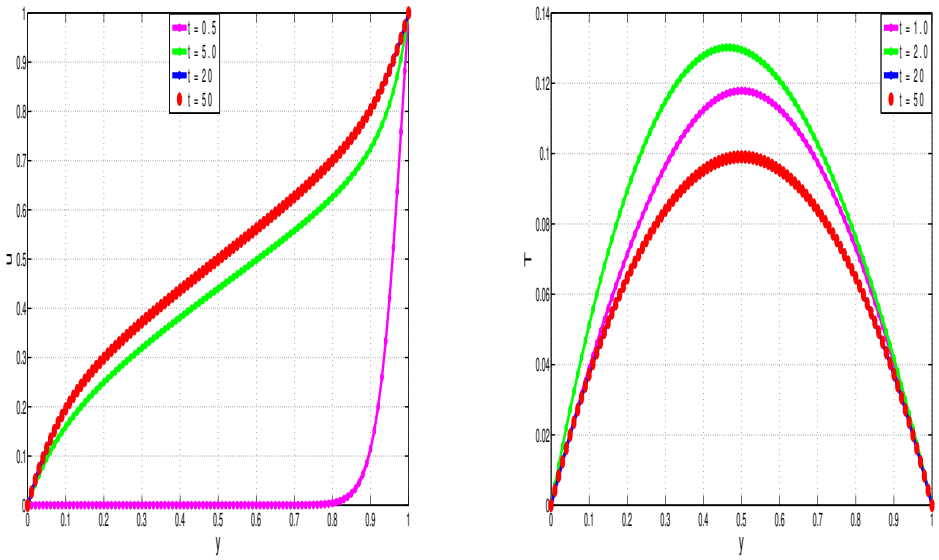

Fig. 4-11 Development of steady velocity and temperature profiles with $\beta = 0.95$, $\varepsilon = 2$.

4.4.4 Thermal runway

In industrial applications involving exothermic reaction, it is fundamental to ensure thermal stability and avoid thermal-runaway phenomena. Thermal run-away can be demonstrated by increasing the values of the exothermic-reaction parameter, δ_1. Fig. 4-13 illustrates the effects of δ_1 on the steady-state VFBN velocity and temperature, specifically the drastic increase of temperature with increasing δ_1.

Fig. 4-14 gives a comparative illustration of the thermal-runaway phenomena for Newtonian-fluid-based and viscoelastic-fluid-based nanofluids, i.e. NFBN and

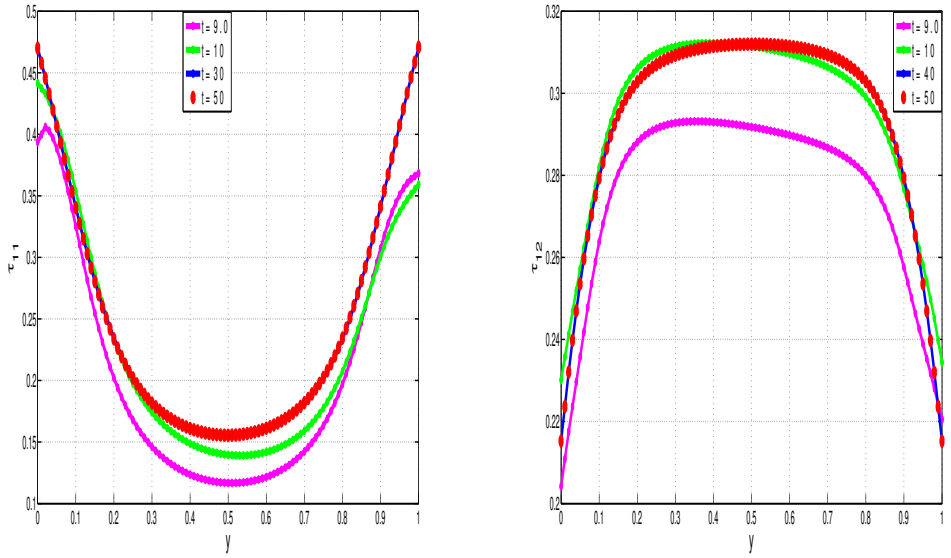

Fig. 4-12 Development of steady polymeric-stress profiles with $\beta = 0.95$, $\varepsilon = 2$.

VFBN. The results for the Giesekus type VFBN computations are consistent with those in [82] which are based on the particle-free Oldroyd-B fluid computations. In particular, our results demonstrate that NFBN are more susceptible to thermal-runaway than are the VFBN. This is consistent with the results in [82]. Essentially, the current results and those in [82] demonstrate that fluid viscoelasticity fundamentally acts to reduce large temperature build- ups in the exothermic shear-flow setup and hence can be used to mitigate against rapid and finite-time temperature blow-up, i.e. thermal-runaway. The present study will additionally demonstrate that shear-banding phenomena can further enhance these favourable HTR characteristics of viscoelastic fluids, thus extending the scope of the investigations in [82, 92].

4.5 Parameter dependence of solutions under shear-banding conditions

The dependence of thermal-runaway on δ_1 and that of shear-banding on β and ε have already been illustrated.

We now demonstrate more generally the sensitivity of the flow variables (solutions) to variations in these and other embedded parameters under shear-banding conditions, i.e. $\beta = 0.95$, $\varepsilon = 2$.

Fig. 4-15 shows the dependence of the VFBN temperature field and thermal-conductivity on nanoparticle volume-fraction, ϕ. As expected, both the VFBN temperature and thermal- conductivity increase with increasing ϕ. This is clear expected since the higher the con- centration of heat-conducting nanoparticles (i.e. higher ϕ) the higher the corresponding Therm-C capabilities of the resultant nanofluid and

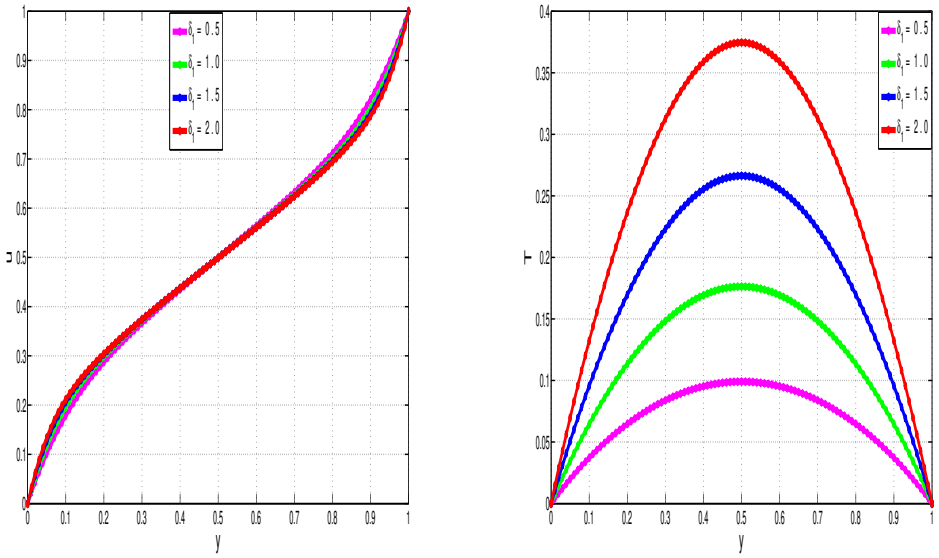

Fig. 4-13 Variation of velocity and temperature profiles with δ_1 where $\beta = 0.95$, $\varepsilon = 2$.

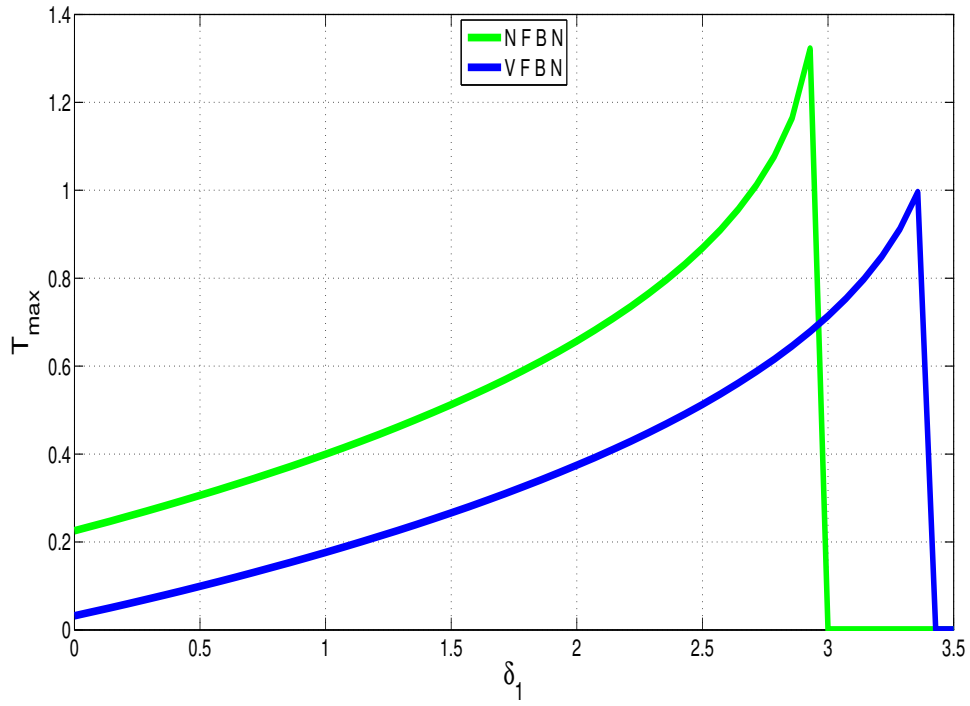

Fig. 4-14 Exponential increase of temperature with δ_1 for various nanofluids where $\beta = 0.95$, $\varepsilon = 2$.

hence also the higher the temperatures in the nanofluid. Fig. 4-16 shows the dependence of the VFBN velocity and temperature on the Brinkman number, Br. Being directly proportional to the heat-sources in the energy equation, increases in the Brinkman number, Br, would correspondingly increase the fluid temperature. Fig. 4-16 also illustrates that the Brinkman number would not affect the shear-banded

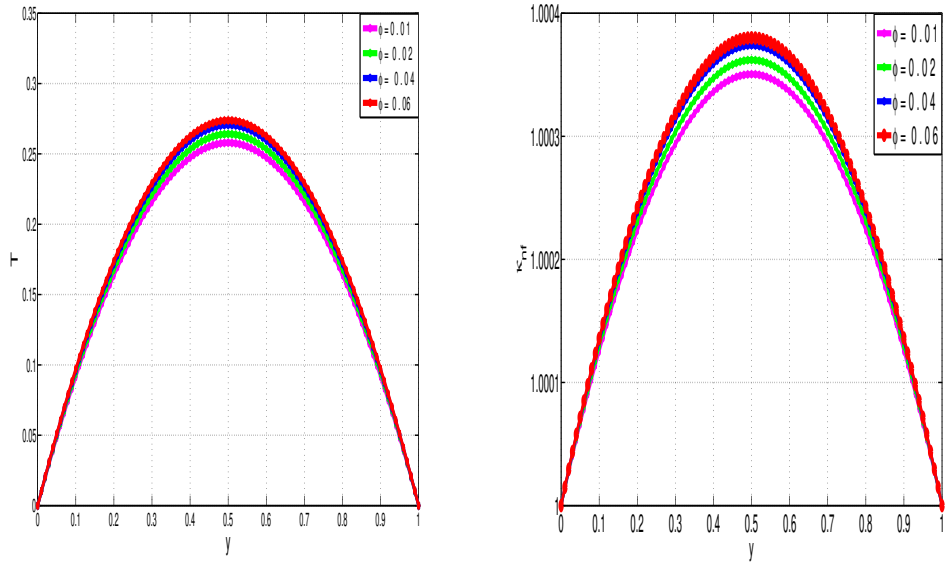

Fig. 4-15 Sensitivity of VFBN temperature and thermal-conductivity to variations in φ.

nature of the velocity profile.

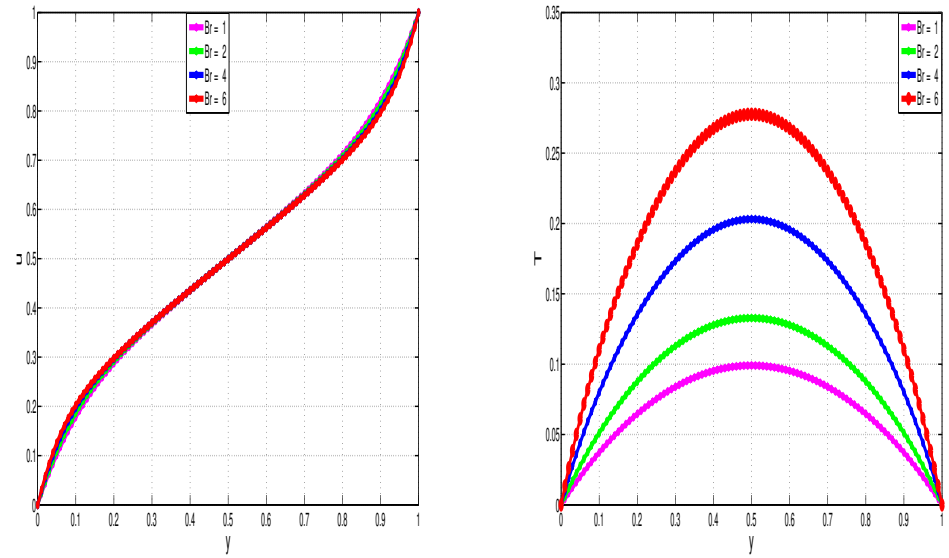

Fig. 4-16 Sensitivity of VFBN velocity and temperature to variations in Br.

As with the thermal-runaway analysis presented earlier (see Figs. 4-13 and 4-14) as well as the comparative literature, say [82, 86], Fig. 4-17 shows, as expected, that the VFBNs are more resistant to temperature increases that NFBN.

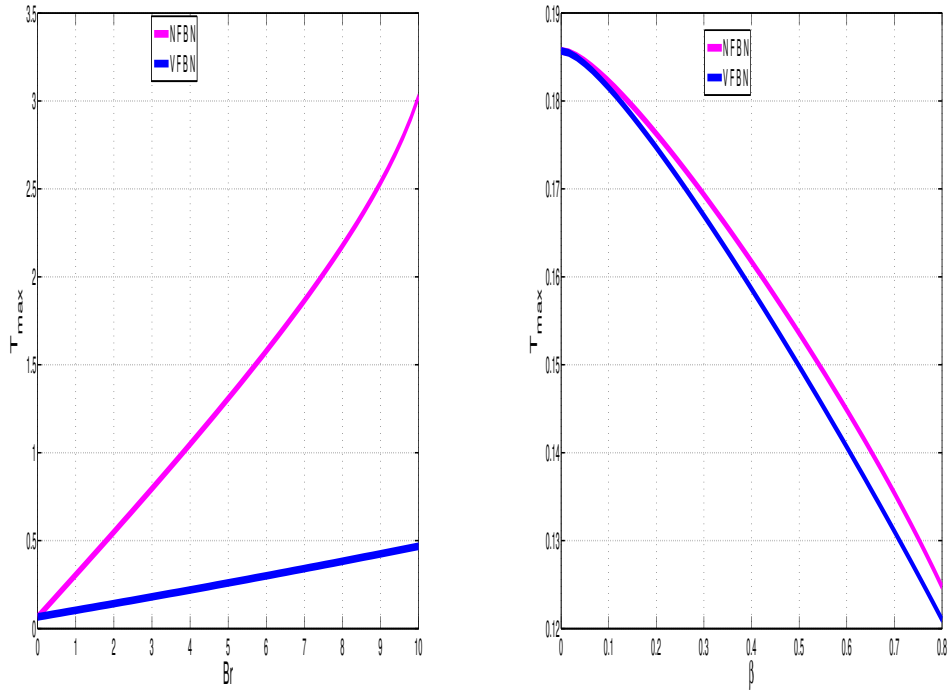

Fig. 4-17 Comparative dependence of nanofluid temperature on Br and β.

Fig. 4-16 additionally shows, as already expected, that the nanofluid temperature increases with increasing Br but decreases with increasing polymer viscosity, β. This further illustrates the viability of viscoelasticity (for which the polymer viscosity is a proxy) in dampening unwanted temperature increases and temperature blow-ups. As in [82], Fig. 4-16 shows that the increase of temperature with respect to Br is linear for viscoelastic flow as opposed to the exponential increase observed with respect to δ_1. This therefore means that increases in Br are not expected to lead to thermal-runaway in shear-flow of VFBN.

We conclude by demonstrating the expected increase of both the VFBN temperature and thermal-conductivity with increasing activation-energy parameter, α, see Fig. 4-18. As would be logically expected, the higher the activation-energy strength, the faster the exothermic-reaction processes and hence also the higher the nanofluid thermal-conductances and obtainable temperatures as illustrated in Fig. 4-18.

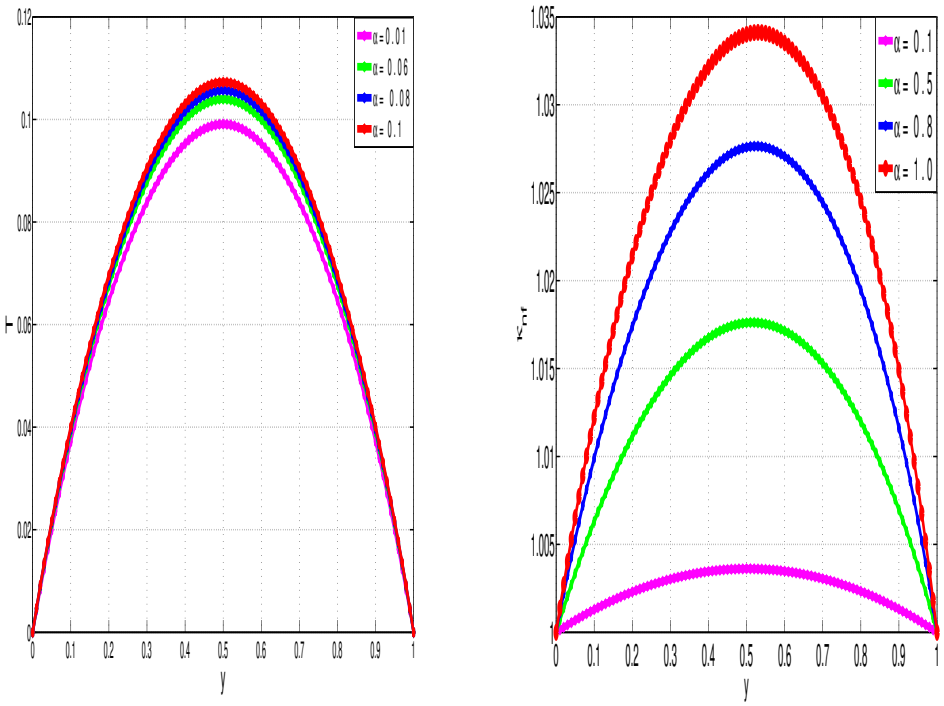

Fig. 4-18 Sensitivity of VFBN temperature and thermal-conductivity to variations in α.

4.6 Concluding Remarks

We employed a versatile and convergent numerical and computational algorithm, based on semi-implicit finite-difference-methods to study the shear-banding and thermal-runaway characteristics of VFBN which use Gisekus base-fluids. We observed remarkable HTR and Therm-C enhancement in the VFBN under shear-banding conditions of the material parameters. Specifically, we demonstrated that the VFBN are less susceptible to thermal runaway than NFBN and other types of nanofluids and that this reduced suspeptibility to thermal-runaway phenomena is further enhanced under shear-banding conditions - in particular, under increased polymer-viscosity conditions.

Acknowledgements

The authors would like to extend their sincere gratitude to National Research Foundation (NRF) for providing financial support to publish this work.

Chapter 5 Computational analysis of non-isothermal dynamics of gravity driven flow of viscoelastic-fluid-based nanofluids down an inclined plane[1]

abstract

The paper explores the gravity-driven flow of viscoelastic-fluid-based nanofluids (VFBN) along an inclined plane under non-isothermal conditions and convective cooling on the free surface. Newton's law of cooling is invoked for the convective heat-exchange with the ambient and at the free surface. The Giesekus viscoelastic constitutive model, with appropriate modifications to account for non-isothermal effects, is employed to describe the polymeric effects. The unsteady and coupled non-linear Partial Differential Equations (PDEs) describing the model problem are obtained and solved via efficient semi-implicit numerical-schemes based on the Finite Difference Methods (FDM). The computational solution algorithms are implemented in the MATLAB software. The responses of the flow variables to variations in the various fundamental flow parameters are explored graphically and discussed qualitatively. Specifically, the novel responses (of the VFBN velocity, VFBN temperature, VFBN thermal-conductivity, and VFBN polymeric-stresses) to variations in the volume-fraction of embedded nanoparticles are illustrated. Such novel responses of the VFBN flow variables to variations in nanoparticle volume fraction provide the main framework for the fundamental contributions of this study.

[1]The contents of this chapter are from khan et.al [153]

5.1 Introduction

Dispersion of highly conductive tiny metallic particles within a fluid (Such as water, oil, etc.) is the most obvious and effective method of improving/enhancing the heat-transfer-rate (HTR) characteristics and thermal-conductivity properties of the fluid. The size and texture of the metallic particles is clearly fundamental, large particles can lead to sedimentation, clogging, etc. while coarse-grained particles can cause abrasion, etc. For these reasons, nanometer-size particles (nanoparticles) are used [20, 36, 92–106, 110, 131, 135–138, 141]
As in the cited references, we use the term nanofluid to describe the suspension of nanoparticles in a base fluid. A variety of industrial applications (say to heating and cooling) and medical applications (chemotherapy, etc.) of nanofluids are well documented in the cited references. Noting the fundamental importance of the rheology of the base-fluid to the contemporary applications of nanofluids, the studies, in [92, 131, 141] focus attention on non-Newtonian (specifically polymeric) base-fluids under various flow conditions. The widespread importance of non-Newtonian fluids, both the Generalized Newtonian Fluids (GNF) as well as the polymeric (viscoelastic) fluids, in contemporary application is quite clear, see for example [82, 88, 92, 110, 112, 116, 117, 119, 131, 135, 139, 141–144]

The current study builds on the investigations in [92, 131, 141] and extends these investigation to free-surface, gravity-driven, thin-film flows with convective heat exchange at the free-surface. Additionally and alternatively, the current work extends the combined (particle-free) fluid-dynamics studies in [82] and [112] to the inclusion of nanoparticles and hence to nanofluid-dynamics.

The following sequence is adopted in the paper. Section 5.2 outlines the description of the physical and mathematical models. The development and implementation of the numerical and computational algorithms as well as the fundamental efficacy and convergence tests of the computational methodologies are given in Section 5.3. The main results are presented graphically and discussed qualitatively in Section 5.4. Concluding remarks follow in section 5.5.

5.2 Problem Formulation

A schematic of the model problem is sketched in Fig. 5-1.

- A thin-film of nanofluid (VFBN) of height h^* (in the direction normal to inclined wall) flows down the inclined plane. The inclined wall/plane makes an angle θ with the horizontal.

- The x^*-axis is taken parallel to inclined wall and the y^*-axis is taken perpendicular to the inclined wall. The superscript (*) denotes dimensional variables and the remainder of the variables are otherwise similar to those described in chapter 2.

- The solid boundary (the inclined wall) is kept at a constant temperature T_w^* and we assume convective cooling at the free-surface following Newton's law of cooling.
- The motion of the fluid is exclusively gravity-driven and hence the pressure-gradient in the x^*-direction stays zero. Alternatively the pressure in the x^*-direction stays constant. Naturally, the pressure in the y^*-direction is non-constant increasing from atmospheric pressure at the free surface to the maximum pressure at the inclined wall.
- No-slip velocity boundary conditions are assumed along the rigid inclined wall. The velocity boundary conditions at the free-surface naturally also arise from the zero-shear-rate requirements.

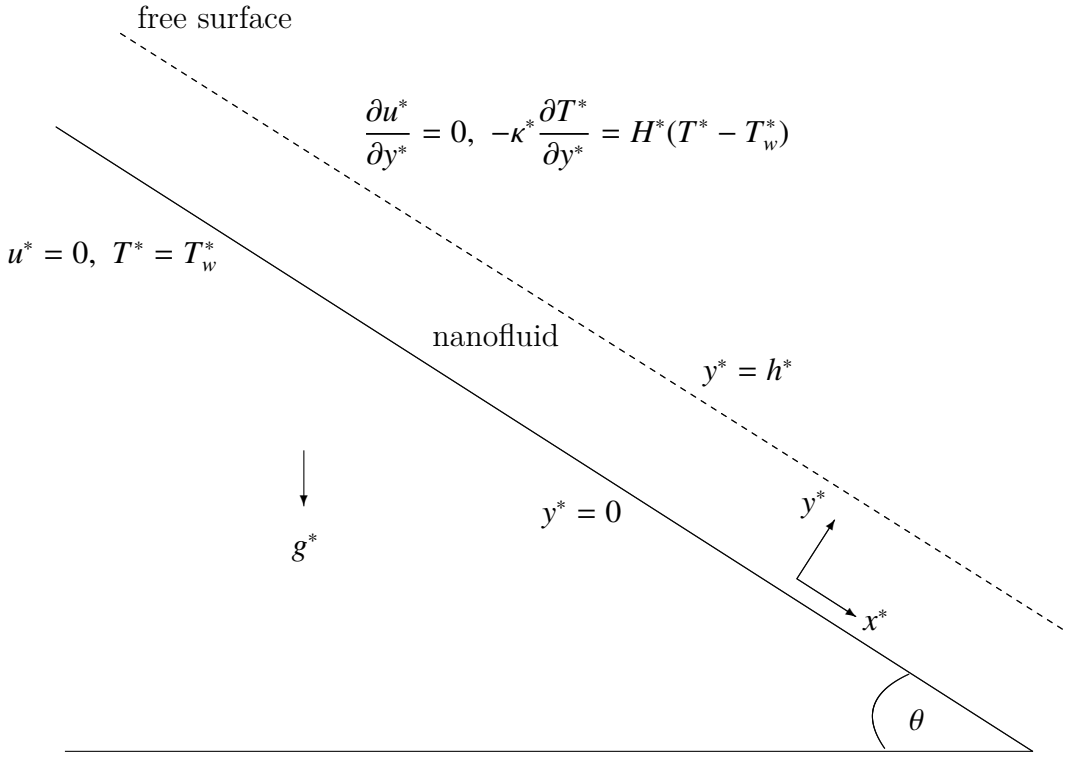

Fig. 5-1 Schematic of the model problem.

Following the notations of chapter 2 Eq.(2.11) and [112] the governing dimensional equations for the VFBN are,

$$\nabla^* \cdot \boldsymbol{u}^* = 0, \tag{5-1}$$

$$\rho_{nf}^* \frac{D\boldsymbol{u}^*}{Dt^*} = -\nabla^* p^* + \nabla^* \cdot (\boldsymbol{\sigma}^*) + \rho_{nf}^* g^* \boldsymbol{F}, \tag{5-2}$$

$$(\rho c_p)_{nf}^* \frac{DT^*}{Dt^*} = -\nabla^* \cdot \boldsymbol{\phi}_q^* + Q_D^* + r^*, \tag{5-3}$$

where g^* is the gravitational acceleration and $\boldsymbol{F} = (\sin\theta, -\cos\theta)$ denotes body forces. The term r^* denotes heat-sources, due to exothermic reaction(as discused in Chapter 2, 3,4) or thermal radiation. these terms will be neglected in this study as their effects have been comprehensively investigated in Chapters 2, 3 and 4.

Dimensionless parameters

The dimensionless parameters of interest are the; Reynolds number (Re), Brinkman number (Br), Deborah number (De), activation energy parameter (α), Prandtl number (Pr), Peclet number (Pe = Re · Pr), Grashof number (Gr), Biot number (Bi), and the ratio of the polymer to the total viscosity (β). These are defined as follows,

$$\beta = \frac{\eta_{p_\infty}^*}{\eta_\infty^*},\ \mathrm{De} = \frac{\lambda_\infty^* U_\infty^*}{h^*},\ \mathrm{Re} = \frac{\rho_f^* U_\infty^* h^*}{\eta_\infty^*},\ \mathrm{Pr} = \frac{c_{p_f}^* \eta_\infty^*}{\kappa_f^*},\ \mathrm{Br} = \frac{\eta_\infty^* U_\infty^{*\,2}}{\kappa_f^* \alpha T_W^*},$$

$$\mathrm{Re}_{nf} = \frac{\rho_{nf}}{\rho_f}\mathrm{Re},\ \mathrm{Pe}_{nf} = \frac{(\rho c_p)_{nf}}{(\rho c_p)_f}\mathrm{Pe},\ \alpha = \frac{R^* T_W^*}{E^*},\ \mathrm{Gr} = \frac{g^* h^*}{U_\infty^*},\ \mathrm{Bi} = \frac{H^* h^*}{k_0^*}, \tag{5-4}$$

The nanofluid quantities ($_{nf}$) result from linear combinations of the volume-fractions (φ) of the base-fluid ($_f$) and the nanoparticles ($_s$),

$$\rho_{nf} = \varphi \rho_s + (1-\varphi)\rho_f, \qquad (\rho c_p)_{nf} = \varphi (\rho c_p)_s + (1-\varphi)(\rho c_p)_f.$$

The resultant dimensionless equations are,

$$\nabla \cdot \boldsymbol{u} = 0, \tag{5-5}$$

$$\mathrm{Re}_{nf} \frac{D\boldsymbol{u}}{Dt} = -\mathrm{Re}_{nf} \nabla p + \nabla \cdot (\boldsymbol{\sigma}) + \mathrm{Re}_{nf}\,\mathrm{Gr}\,\boldsymbol{F}, \tag{5-6}$$

$$\mathrm{Pe}_{nf} \frac{DT}{Dt} = -\nabla \cdot \left(\kappa_{nf} \nabla T\right) + \mathrm{Br}\, Q_D, \tag{5-7}$$

$$\boldsymbol{\tau} + \varepsilon\,\boldsymbol{\tau}^2 + \mathrm{De}\,\bar{\lambda}(T)\left[\overset{\nabla}{\boldsymbol{\tau}} - \boldsymbol{\tau}\,\frac{D}{Dt}\left(\ln\left(1+\alpha T\right)\right)\right] = \frac{\eta_p(T)}{(\sqrt{1-\varphi})^5}\,\boldsymbol{S}. \tag{5-8}$$

The dimensionless dissipation term for the single-mode non-isothermal Giesekus model is,

$$Q_D = \gamma \boldsymbol{S} : \boldsymbol{\tau} + (1-\gamma)\frac{\boldsymbol{\eta}_s(T)}{(\sqrt{1-\varphi})^5}\,\boldsymbol{S} : \boldsymbol{S}. \tag{5-9}$$

The dimensionless (temperature-dependent) viscosities, relaxation-time and thermal-conductivity are,

$$\eta_s(T) = (1-\beta)\,\exp(-\alpha\,T), \quad (\eta_s)_{nf} = \frac{\eta_s(T)}{(\sqrt{1-\varphi})^5}, \tag{5-10}$$

$$\eta_p(T) = \beta\, e^{(-\alpha\,T)}, \quad (\eta_p)_{nf} = \frac{\eta_p(T)}{(\sqrt{1-\varphi})^5}, \tag{5-11}$$

$$\eta = \eta_s(T) + \eta_p(T), \quad \eta_{nf} = \frac{\eta}{(\sqrt{1-\varphi})^5}, \tag{5-12}$$

$$\bar{\lambda}(T) = \frac{1}{1+\alpha\,T}\,\exp(-\alpha\,T), \tag{5-13}$$

$$\kappa_{nf} = \frac{\kappa_s + (1-\aleph)\kappa_f - (\aleph-1)\varphi(\kappa_f-\kappa_s)}{\kappa_s + (1-\aleph)\kappa_f + \varphi(\kappa_f-\kappa_s)}\,(1+\alpha\,A_2\,T). \tag{5-14}$$

5.2.1 Initial and boundary conditions

The dimensionless initial- and boundary- conditions are,

$$u(0,y) = 0, \quad T(0,y) = 0, \quad \boldsymbol{\tau}(0,y) = 0, \quad 0 \le y \le 1, \tag{5-15}$$

$$u(t,0) = 0, \quad \frac{\partial}{\partial y}u(t,1) = 1, \quad T(t,0) = 0, \quad \frac{\partial}{\partial y}T(t,1) = -Bi\,T(t,1), \quad t \ge 0. \tag{5-16}$$

Due to the hyperbolic structure of the equations for the polymeric-stresses, their relevant boundary-conditions are reconstructed from the main flow, [112, 131].

5.3 Numerical Solution

The semi-implicit numerical algorithm for the velocity component is,

$$\mathrm{Re}_{nf}\frac{u^{(n+1)}-u^{(n)}}{\Delta t}=\frac{\partial}{\partial y}\tau_{12}^{(n)}+\left((\eta_s)_{nf}^{(n)}\frac{\partial^2}{\partial y^2}u^{(n+\xi)}+\frac{\partial}{\partial y}u^{(n)}\frac{\partial}{\partial y}(\eta_s)_{nf}^{(n)}\right)+\mathrm{Re}_{nf}\,\mathrm{Gr}\,\sin\theta, \tag{5-17}$$

where

$$u^{(n+\xi)}=\xi u^{(n+1)}+(1-\xi)u^{(n)}.$$

The velocity therefore updates at the new time-step, $u^{(n+1)}$, via,

$$\begin{aligned}-r_1u_{j-1}^{(n+1)}+(\mathrm{Re}_{nf}+2r_1)u_j^{(n+1)}-r_1u_{j+1}^{(n+1)}&=\mathrm{Re}_{nf}\,u_j^{(n)}+(1-\xi)\,\Delta t\,(\eta_s)_{nf}^{(n)}\frac{\partial^2}{\partial y^2}u^{(n)}\\&+\Delta t\frac{\partial}{\partial y}\tau_{12}^{(n)}+(1-\beta)\,\Delta t\,\frac{\partial}{\partial y}u^{(n)}\frac{\partial}{\partial y}(\eta_s)_{nf}^{(n)}+\Delta t\,\mathrm{Re}_{nf}\,\mathrm{Gr}\,\sin\theta,\end{aligned} \tag{5-18}$$

where

$$r_1=\xi\,(\eta_s)_{nf}^{(n)}\frac{\Delta t}{\Delta y^2}.$$

This represent a (diagonally-dominant) tri-diagonal linear algebraic system of equations. The discretized temperature equation is obtained similarly,

$$\mathrm{Pe}_{nf}\frac{\partial T}{\partial t}=\kappa_{nf}^{(n)}\frac{\partial^2}{\partial y^2}T^{(n+\xi)}+\frac{\partial}{\partial y}T^{(n)}\frac{\partial}{\partial y}\kappa_{nf}^{(n)}+\mathrm{Br}\,Q_D^{(n)}. \tag{5-19}$$

The temperature therefore updates at the new time-step, $T^{(n+1)}$, via,

$$\begin{aligned}-r_2T_{j-1}^{(n+1)}+(\mathrm{Pe}_{nf}+2r_2)T_j^{(n+1)}-r_2T_{j+1}^{(n+1)}&=\mathrm{Pe}_{nf}\,T_j^{(n)}+(1-\xi)\,\Delta t\,\kappa_{nf}\frac{\partial^2}{\partial y^2}T^{(n)}\\&+\Delta t\frac{\partial}{\partial y}T^{(n)}\frac{\partial}{\partial y}\kappa_{nf}^{(n)}+2(1-\gamma)\Delta t\,\mathrm{Br}\,(\eta_s)_{nf}^{(n)}\left(\frac{\partial}{\partial y}u^{(n)}\right)^2+2\Delta t\,\mathrm{Br}\,\gamma\,\tau_{12}^{(n)}\frac{\partial}{\partial y}u^{(n)},\end{aligned} \tag{5-20}$$

where

$$r_2=\xi\,\kappa_{nf}^{(n)}\frac{\Delta t}{\Delta y^2}.$$

The semi-implicit numerical scheme for the polymeric-stress, $\boldsymbol{\tau}$ is,

$$\boldsymbol{\tau}^{(n+\xi)}+\varepsilon\,(\boldsymbol{\tau}^2)^{(n)}+\mathrm{De}\,\bar{\lambda}^{(n)}\frac{\boldsymbol{\tau}^{(n+1)}-\boldsymbol{\tau}^{(n)}}{\Delta t}=\text{explicit terms.}$$

The solutions for the tensor components, $\tau_{11}^{(n+1)}$, $\tau_{12}^{(n+1)}$, and $\tau_{22}^{(n+1)}$ therefore follow directly,

$$(\mathrm{De}\,\bar{\lambda}^{(n)}+\xi\,\Delta t)\,\boldsymbol{\tau}^{(n+1)}=\text{explicit terms.} \tag{5-21}$$

The explicit terms for τ_{11}, τ_{12} and τ_{22} are respectively,

$$[\mathrm{De}\,\bar{\lambda}^{(n)}-(1-\xi)\Delta t]\,\tau_{11}^{(n)}+\Delta t\,\mathrm{De}\,\bar{\lambda}^{(n)}\left[\tau_{12}^{(n)}\frac{\partial}{\partial y}u^{(n)}+\tau_{11}^{(n)}\frac{\partial}{\partial y}\log\left(1+\alpha T^{(n)}\right)\right]$$

$$- \varepsilon \Delta t\,(\tau_{11}^2 + \tau_{12}^2), \tag{5-22}$$

$$[\mathrm{De}\,\bar{\lambda}^{(n)} - (1-\xi)\Delta t]\,\tau_{12}^{(n)} + \Delta t\,\mathrm{De}\,\bar{\lambda}^{(n)}\left[\tau_{22}^{(n)}\frac{\partial}{\partial y}u^{(n)} + \tau_{12}^{(n)}\frac{\partial}{\partial y}\log\left(1+\alpha T^{(n)}\right)\right] + \Delta t\,(\eta_p)_{nf}\,\frac{\partial}{\partial y}u^{(n)} - \varepsilon\,\Delta t\,(\tau_{11}\tau_{12} + \tau_{12}\tau_{22}), \tag{5-23}$$

$$[\mathrm{De}\,\bar{\lambda}^{(n)} - (1-\xi)\Delta t]\,\tau_{22}^{(n)} + \Delta t\,\mathrm{De}\,\bar{\lambda}^{(n)}\,\tau_{22}^{(n)}\frac{\partial}{\partial y}\log\left(1+\alpha T^{(n)}\right) - \varepsilon\,\Delta t\,(\tau_{12}^2 + \tau_{22}^2). \tag{5-24}$$

5.4 Results

Graphical results are presented for the velocity (u), temperature (T), polymeric-stress components ($\tau_{11}, \tau_{12}, \tau_{22}$), using the below list of default values,

$$\alpha = 0.01,\ \mathrm{Br} = 1,\ \mathrm{Re} = 1,\ \mathrm{Pr} = 1,\ \mathrm{Gr} = 1,\ \mathrm{Bi} = 1,\ \mathrm{De} = 2,\ \gamma = 0.5,\ \beta = 0.2,\ \Delta y = 0.01,$$
$$\Delta t = 0.1,\ t = 50,\ \zeta = 1,\ \theta = 45,\ \varphi = 0.04,\ \varepsilon = 1,\ A_2 = 0.2,\ \aleph = 3. \tag{5-25}$$

5.4.1 Time devolvement of steady solutions

The time development of flow variables from the initial states until steady solutions are reached is illustrated in Figs. 5-2 and 5-3.

5.4.2 Time-step and mesh-size convergence

Figs. 5-4, 5-5, 5-6, and 5-7 illustrate, as required, that our computational algorithms are independent of both time-step and mesh size. Specifically, the algorithms efficiently produce the required solutions for a wide range of expected time-steps and mesh-sizes.

5.4.3 Code validation

A similar investigation to the current one was conducted in [112] using the Oldroyd-B constitutive model and in the absence of nanoparticles. The Oldroyd-B model is obtained from Giesekus model by taking $\varepsilon = 0$. The absence of nanoparticles reduce to $\varphi = 0$. The study in [112] therefore used the ordinary Oldroyd-B constitutive model with constant thermal-conductivity, $A_2 = 0$. By taking $\varepsilon = 0, \varphi = 0, A_2 = 0$ in our current model, our VFBN results reduce to those for a normal viscoelastic (Oldroyd-B) fluid and are exactly the same as those in [112].

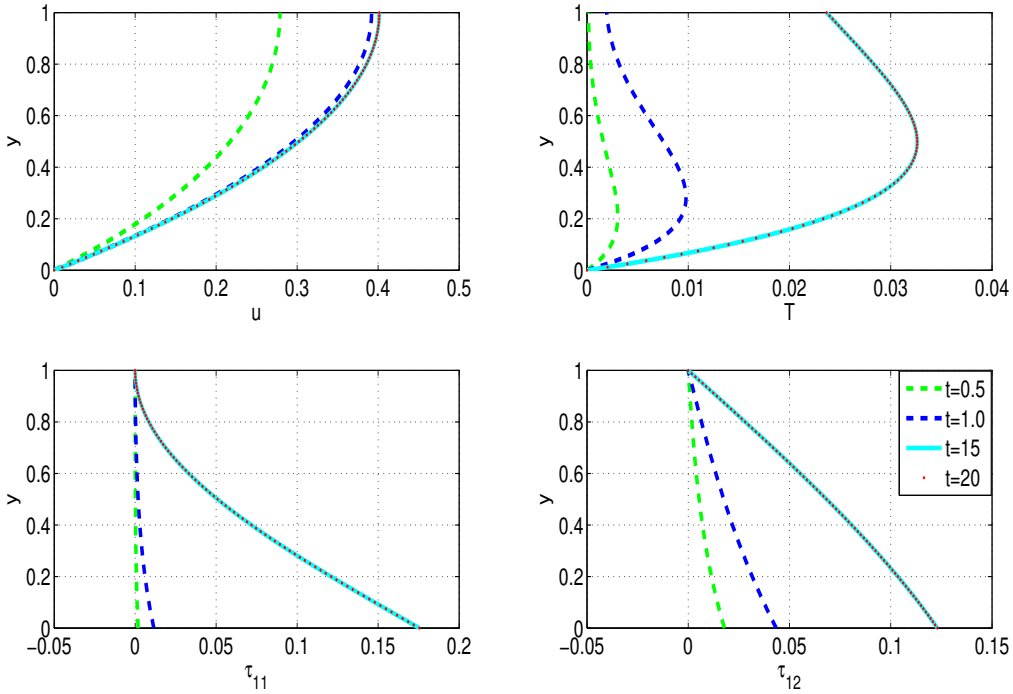

Fig. 5-2 Transient development of profiles to steady state with $\Delta t = 0.05$

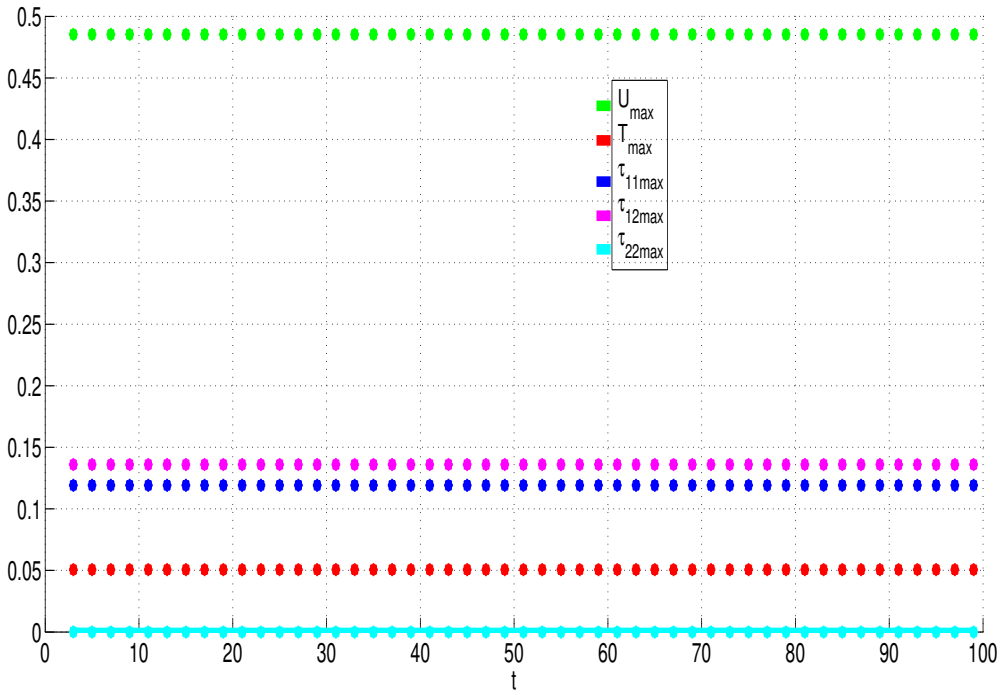

Fig. 5-3 Time development of maximum flow quantities to steady state.

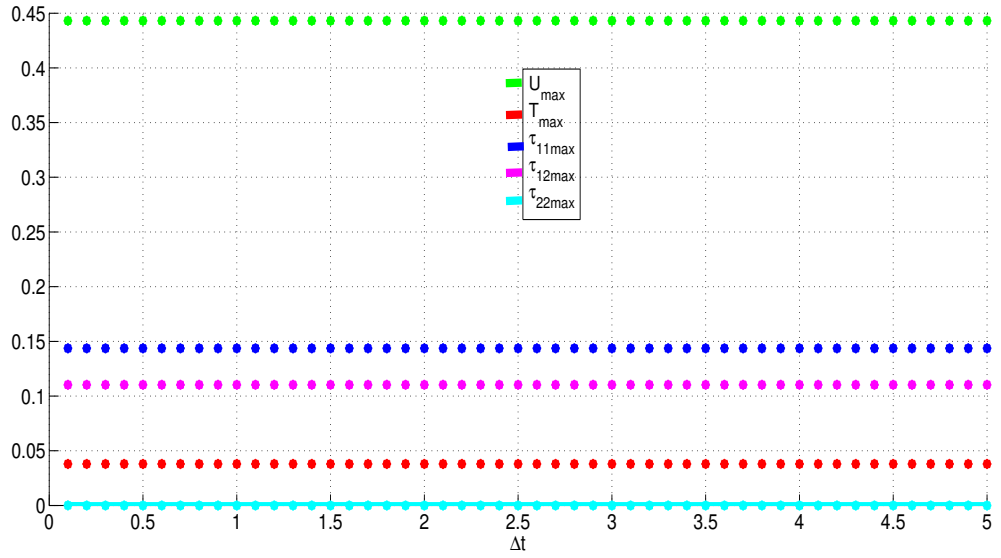

Fig. 5-4 Time-step independence of maximum solutions

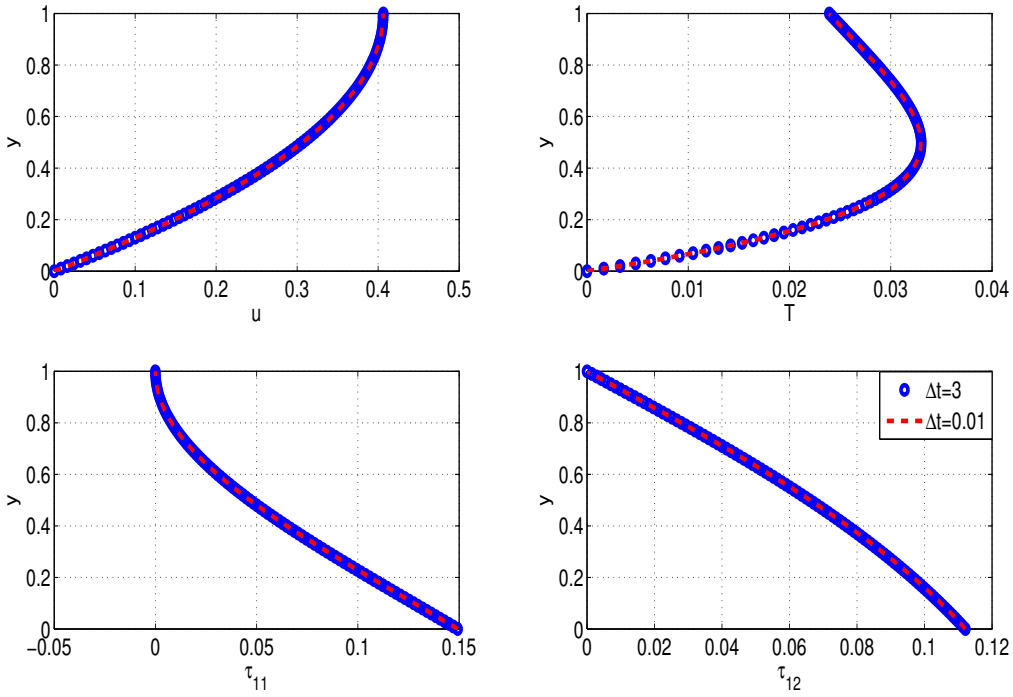

Fig. 5-5 Time-step independence of solutions.

5.4.4 Sensitivity of solutions to embedded parameters

We present a representative sample of the behaviour of flow quantities with variations in the embedded parameters. The response of the VFBN thermal-conductivity to variations in φ is illustrated in Fig. 5-8. As expected, the VFBN thermal-conductivity increases with increasing φ.

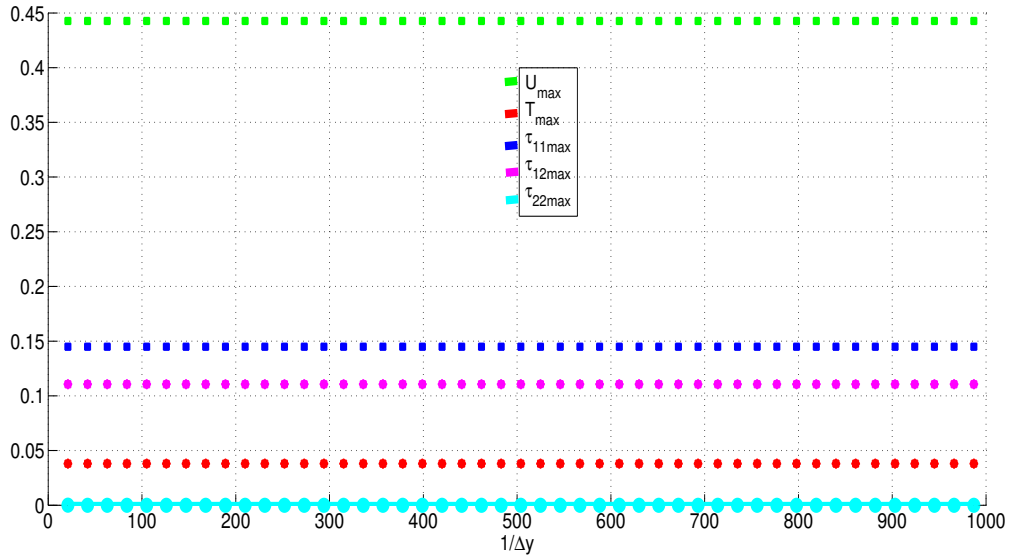

Fig. 5-6 Mesh-size independence of maximum solutions.

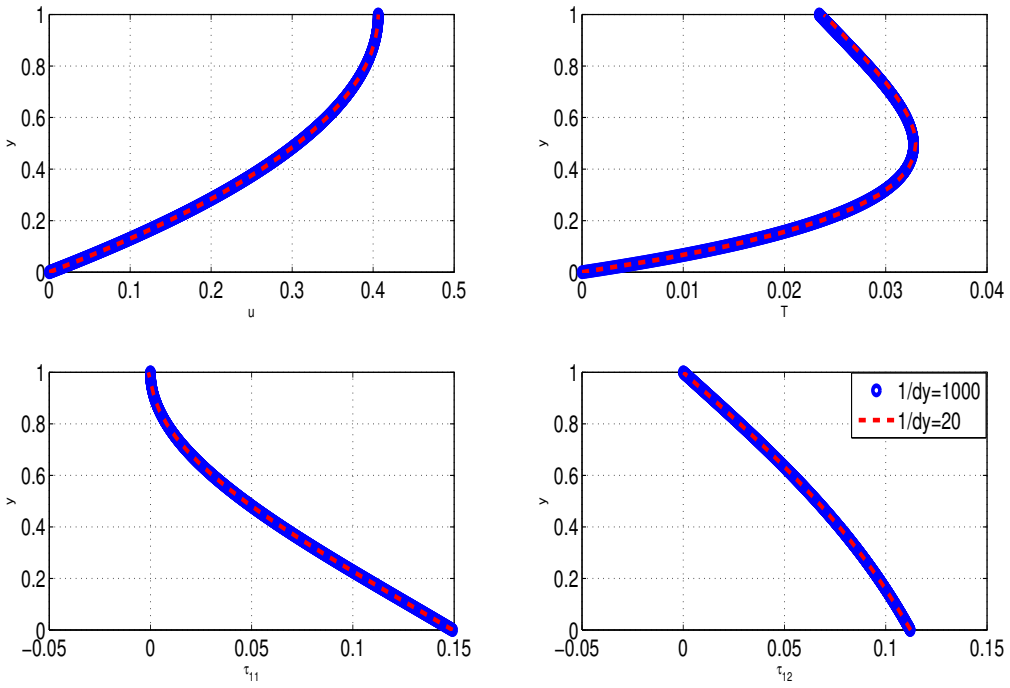

Fig. 5-7 Mesh-size independence of solutions.

It naturally therefore follows that the VFBN temperature increases with increasing φ. This expected response of the VFBN temperature to variations in φ is illustrated in Fig. 5-9. With increasing temperatures comes a reduction in viscosity and hence we expect the VFBN velocity to increase with increasing VFBN temperature. This expected increase of the VFBN velocity to variations in φ is also illustrated in Fig. 5-9. Lastly, Fig. 5-9 demonstrates an increase in the polymeric-stresses with increasing φ.

Similar responses (as with φ) of the VFBN thermal-conductivity to variations in both the thermal-conductivity parameter, A_2 and the activation-energy parameter, α are respectively illustrated in Figs. 5-10 and 5-11.

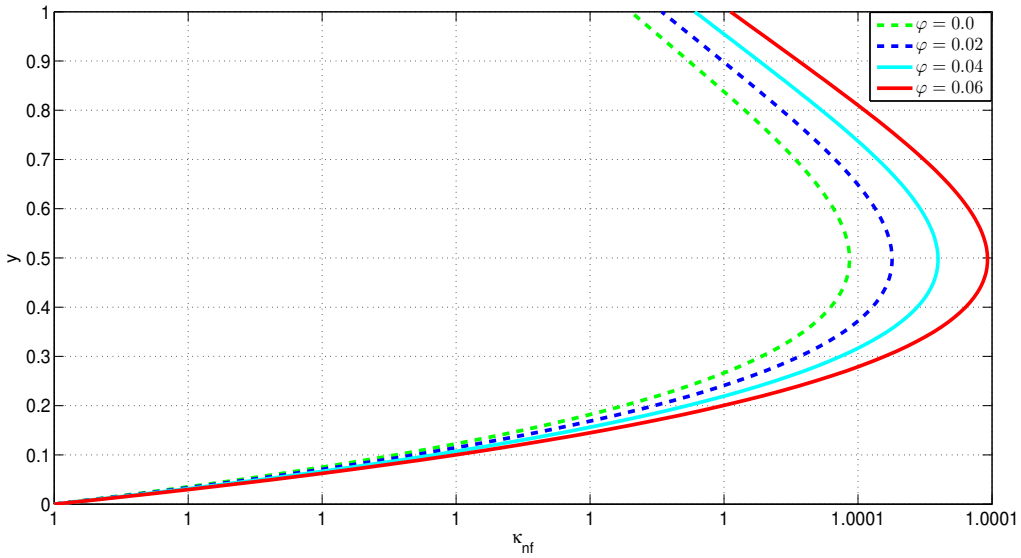

Fig. 5-8 Variation of VFBN thermal-conductivity with φ.

Fig. 5-12 shows the response of flow quantities to variations in the Prandtl number, Pr. In general, a high Prandtl number , Pr indicates that the fluid has a poor thermal conductivity, resulting in a thinner thermal boundary layer structure. In addition, when the amount of Pr increases, the thermal diffusion rate decreases. The VFBN thermal-conductivity (and hence also the VFBN temperature) are expected to decrease with increasing Pr. These expected results illustrated in Figs. 5-12 and 5-13 respectively.

The behaviour of VFBN relaxation time with variations in the Deborah number, De, is illustrated in Fig. 5-14. We notice that an increase in the Deborah number, De increases the elastic effects in the fluid, therefore the VFBN relaxation time increases with increasing De.

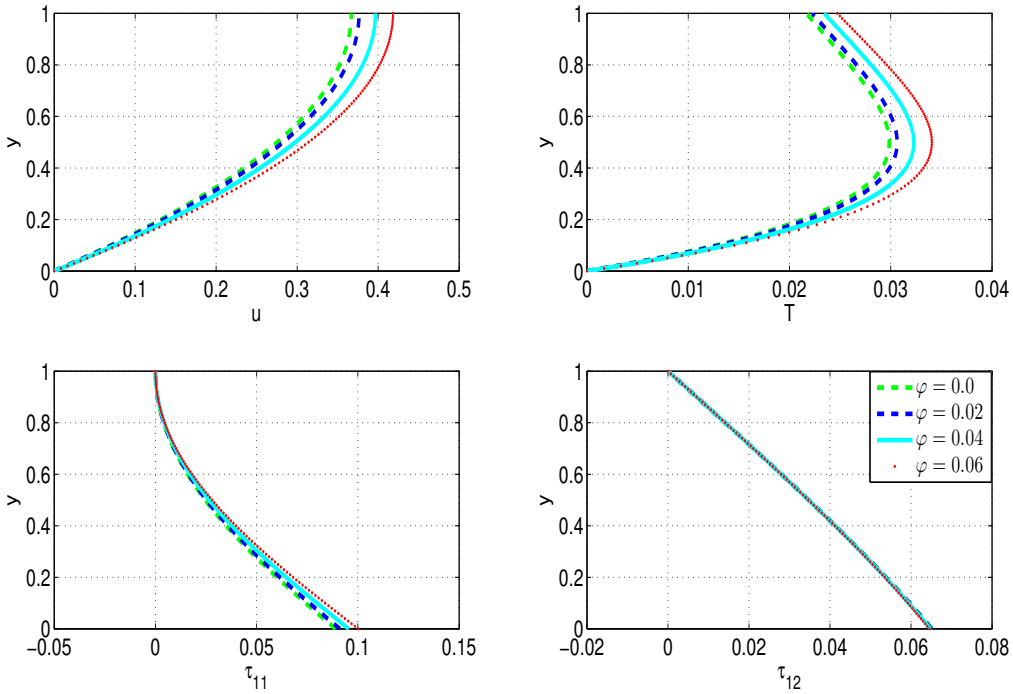

Fig. 5-9 Variation of VFBN flow quantities with φ.

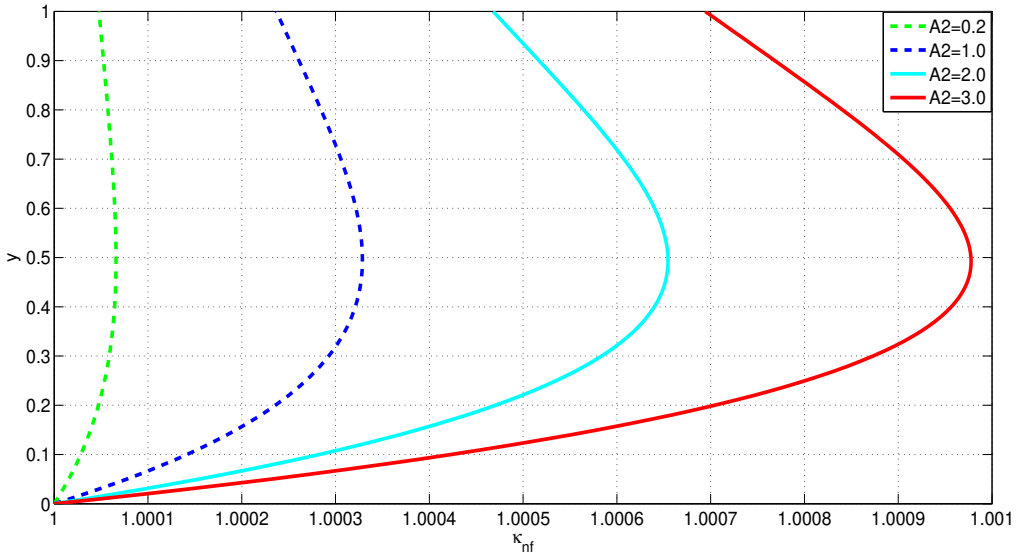

Fig. 5-10 Variation of VFBN thermal-conductivity with A_2.

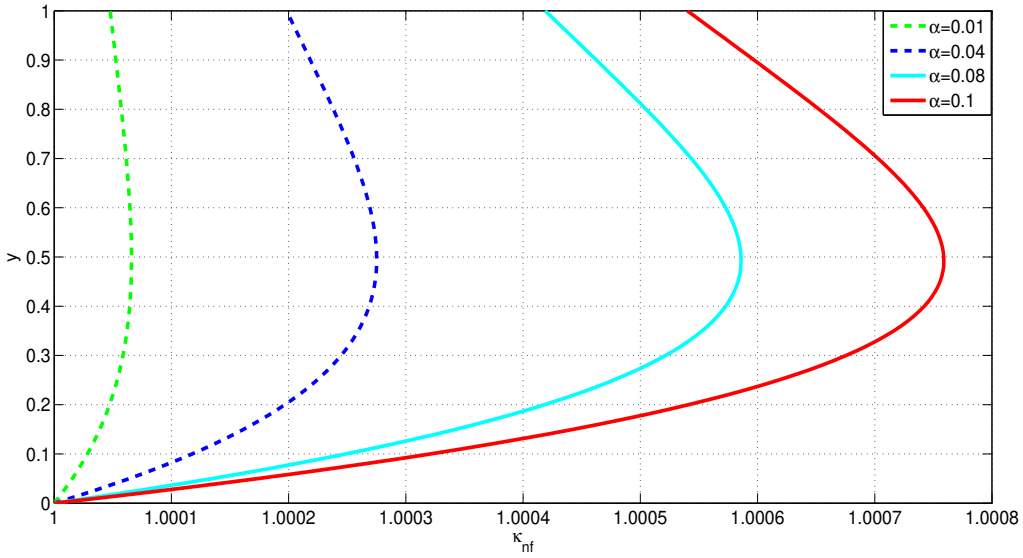

Fig. 5-11 Variation of VFBN thermal-conductivity with α.

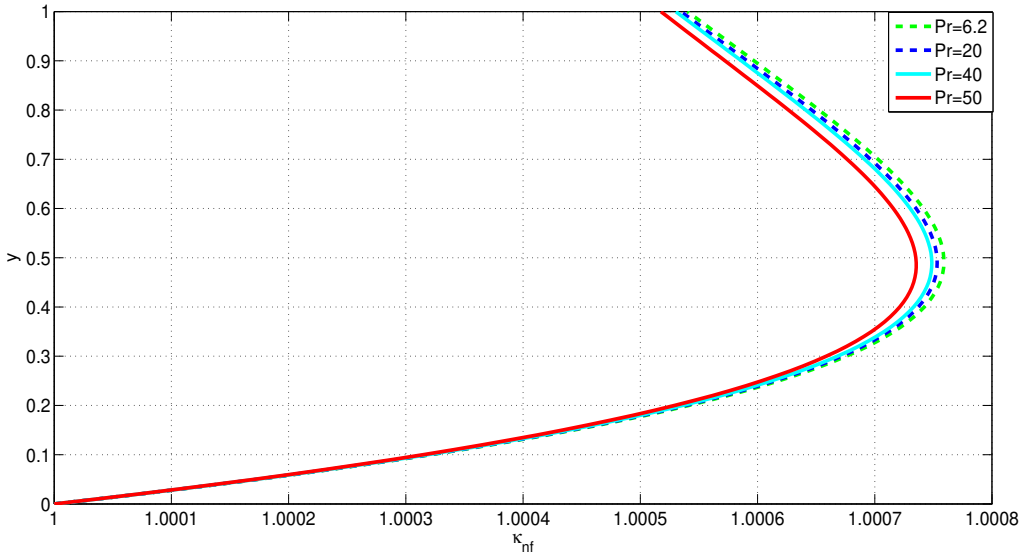

Fig. 5-12 Effects of Pr on VFBN thermal-conductivity.

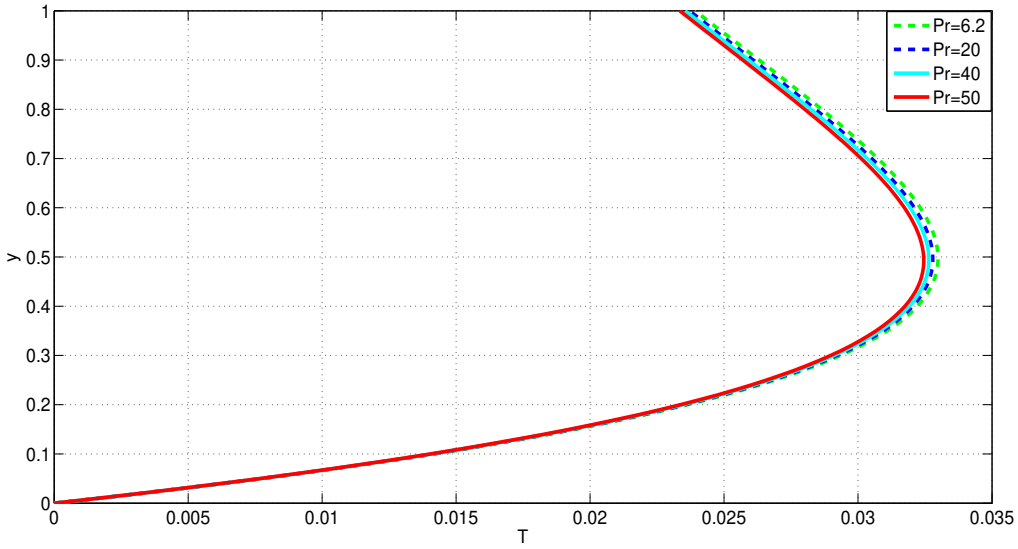

Fig. 5-13 Effects of Prandtl Number, Pr, on VFBN temperature.

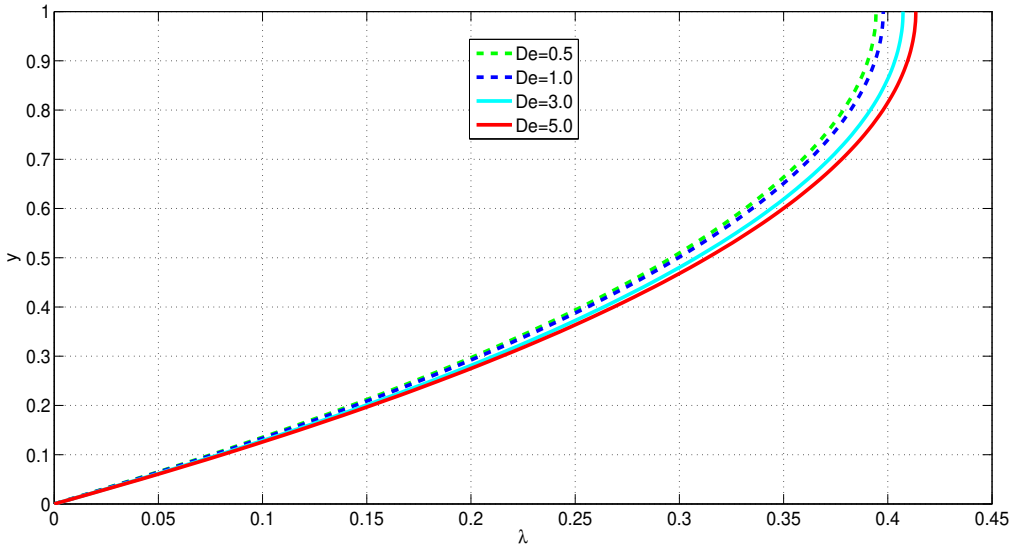

Fig. 5-14 Effects of De on VFBN relaxation time.

5.5 Concluding Remarks

Efficient semi-implicit numerical and computational algorithms, based on the finite difference methods, were employed to investigate the thermo-physical characteristics of a non-isothermal, gravity-driven flow of a thin-film, viscoelastic-fluid-based nanofluid (VFBN) flowing down an inclined plane subject to convective cooling at the free surface. The numerical and computational algorithms were checked for convergence in both space and time and were also positively validated against the results in the existing literature. A single-phase nanofluid model, in which metallic nanoparticles of spherical shape are homogenously mixed (ensuring non-sedimentation) to a viscoelastic base fluid of the Giesekus type, was adopted. The results illustrate that the volume-fraction of the embedded nanoparticles play fundamental roles in the fluid-dynamical and thermo-physical properties of the VFBN. Specifically, the VFBN thermal-conductivity, VFBN temperature, VFBN velocity, and VFBN polymeric stresses (in particular, the first normal stress difference) all increase with increasing nanoparticles volume-fraction. The results are of fundamental importance to heating and cooling applications, specifically to heat-transfer-rate (HTR) enhancement via nanoparticles and nanofluidics.

Chapter 6 Conclusions

This thesis focuses on computational analysis of generalized viscoelastic fluid based nanofluids (GVFBNs) and viscoelastic fluid based nanofluids (VFBNs) flows using single-phase homogeneous approach, under different physical and geometrical conditions. In particular, four nanofluids flow problems motivated by relevant industrial applications are considered. This final chapter provides a summary of the goals and objectives presented in the beginning chapters of this thesis.

Our first study (chapter 2) limits attention to Couette-type flow whose stress behaviour is described by reduced generalized non-isothermal Oldroyd-B model from generalized non-isothermal Gieskus model with suitable adjustment to incorporate the nanopartilces. We conduct numerical investigations on the combined effects of wall no-slip and isothermal conditions on the resulting shear driven flow between two parallel plates. The nanofluid temperature, thermal conductivity and viscoelasticity are shown to increase with increase of nanoparticles concentration. The study further investigates the relationship between the thermal loading properties and the corresponding viscoelasticity of the nanofluids. Higher nanofluid viscoelasticity has been shown to lead to higher susceptibility to temperature increase (thermal runaway phenomena). In particular, susceptibility order for different types of nanofluids is Newtonian-fluid-based nanofluids (NFBNs), Generalized-Newtonian-fluid-based nanofluids (GNFBNs), Viscoelastic-fluid-based nanofluids (VFBNs) and Generalized-viscoelastic-fluid-based nanofluids (GVFBNs). These findings are notably similar to those found in the literature without the use of nanoparticles.

In a related second study (chapter 3), again the stress behaviour is described by reduced generalized non-isothermal Oldroyd-B model from generalized non-isothermal Gieskus model with suitable adjustment to incorporate the nanoparticles. This time we conduct the numerical investigations on the combined effects of wall no-slip and symmetric convective heat exchange with the ambient conditions on the resulting pressure driven channel flow. The addition of nanoparticles has the same effect on nanofluid velocity, temperature, thermal conductivity and viscoelasticity as studied in chapter 2.

The appearance of instability, represented by shear bands, has been observed experimentally in the flow of certain complex fluids whose behavior under stress can be described by viscoelastic constitutive correlations. Chapter (4) is about to the flow of VFB nanofluids in a channel described by one of these constitutive models,

the non-isothermal Gieskus model. We conduct numerical study on the combined effect of wall no-slip and isothermal conditions on shear driven flow of Gieskus type nanofluids. Strong shear banding phenomena was observed for certain parameter values. The fluid temperature and thermal conductivity has been shown to increase with the increase of nanoparticles, as the wall slides, under shear banding conditions. Under relevant conditions of wall slip and shear banding, the study further illustrates the relationships between VFBNs viscoelasticity and the respective thermal loading properties. In particular, it has been shown that the higher viscoelasticity of VFBNs leads to lower values of the critical exothermic reaction parameter, thereby leading to rise susceptibility to thermal runaway phenomena. In other words we can say that viscoelastic fluid based nanofluids possess better thermal loading properties as compared to Newtonian based nanofluids.

In the final chapter 5, Computational analysis of the dynamics of Viscoelastic-fluid-based nanofluids (VFBNs) subject to Gravity Driven flow was carried out, whose stress behaviour is governed by non-isothermal Gieskus model. Again it was observed that the nanofluid temperature and thermal conductivity increases with the increase of nanoparticles concentration and activation energy parameter. Our results also show an inverse relationship between temperature and Deborah number De. The computational results were also compared without nanoparticles results in literature by reducing Gieskus model to Oldroyd-B model. These results are particularly consistent with those reported in the literature.

The above presented problems have been modeled mathematically using complex couple and nonlinear Partial Differential Equations (PDEs) and the stress equations were modeled using the non-isothermal Giesekus model (an extension of non-isothermal Oldroyd-B model). There are different numerical methods (like Finite Element, Finite Volume etc.) in literature to solve this type of equations, however, in this thesis these equations were solved using the semi-implicit finite difference method as discussed in chapter one, which was found to be unconditionally stable and efficient numerically. This is because it is capable of combining the stability of the implicit method with the accuracy of the method. Also, implementing Crank-Nicolson scheme on implicit terms increases stability. The algorithm has been tested for space and time convergence.

Future work

These presented problems could be extended to hybrid nanofluids. For the same problems to model the viscoelasticity of nanofluids apart from non-isothermal

Gieskus model we can use, Johnson-Segalman (JS), Diffusive Johnson-Segalman (DJS) and Phan-Thien-Tanner constitutive models. We can also use second and third grade fluids as a base fluids.

References

1 H. Masuda, A. Ebata, and K. Teramae, "Alteration of thermal conductivity and viscosity of liquid by dispersing ultra-fine particles. dispersion of al2o3, sio2 and tio2 ultra-fine particles," 1993.

2 S. U. Choi and J. A. Eastman, "Enhancing thermal conductivity of fluids with nanoparticles," tech. rep., Argonne National Lab., IL (United States), 1995.

3 S. U. Choi, "Nanofluids: from vision to reality through research," Journal of Heat transfer, vol. 131, no. 3, 2009.

4 E. B. Elçioğlu, "Experimental and theoretical investigations on alumina-water nanofluid viscosity with statistical analysis," Master's thesis, Middle East Technical University, 2013.

5 S. Choi, Z. G. Zhang, W. Yu, F. Lockwood, and E. Grulke, "Anomalous thermal conductivity enhancement in nanotube suspensions," Applied physics letters, vol. 79, no. 14, pp. 2252–2254, 2001.

6 S. Kakaç and A. Pramuanjaroenkij, "Review of convective heat transfer enhancement with nanofluids," International journal of heat and mass transfer, vol. 52, no. 13-14, pp. 3187–3196, 2009.

7 J. A. Eastman, U. Choi, S. Li, L. Thompson, and S. Lee, "Enhanced thermal conductivity through the development of nanofluids," MRS Online Proceedings Library (OPL), vol. 457, 1996.

8 S. K. Das, S. U. Choi, W. Yu, and T. Pradeep, Nanofluids: science and technology. John Wiley & Sons, 2007.

9 G. Liang and I. Mudawar, "Review of single-phase and two-phase nanofluid heat transfer in macro-channels and micro-channels," International Journal of Heat and Mass Transfer, vol. 136, pp. 324–354, 2019.

10 W. Yu and H. Xie, "A review on nanofluids: preparation, stability mechanisms, and applications," Journal of nanomaterials, vol. 2012, 2012.

11 C.-H. Lo, T.-T. Tsung, and L.-C. Chen, "Shape-controlled synthesis of cu-based nanofluid using submerged arc nanoparticle synthesis system (sanss)," Journal of Crystal Growth, vol. 277, no. 1-4, pp. 636–642, 2005.

12 A. Gakare, "A review on nanofluids: Preparation and applications," Nano Trends-A Journal of Nano Technology & Its Applications, vol. 21, pp. 21–35, 2019.

13 O. Mahian, L. Kolsi, M. Amani, P. Estellé, G. Ahmadi, C. Kleinstreuer, J. S. Marshall, M. Siavashi, R. A. Taylor, H. Niazmand, et al., "Recent advances in modeling and simulation of nanofluid flows-part i: Fundamentals and theory," Physics reports, vol. 790, pp. 1–48, 2019.

14 F. Achard, "James clerk maxwell, a treatise on electricity and magnetism, (1873)," in Landmark Writings in Western Mathematics 1640-1940, pp. 564–587, Elsevier, 2005.

15 R. L. Hamilton and O. Crosser, "Thermal conductivity of heterogeneous two-component systems," Industrial & Engineering chemistry fundamentals, vol. 1, no. 3, pp. 187–191, 1962.

16 V. D. Bruggeman, "Berechnung verschiedener physikalischer konstanten von heterogenen substanzen. i. dielektrizitätskonstanten und leitfähigkeiten der mischkörper aus isotropen substanzen," Annalen der physik, vol. 416, no. 7, pp. 636–664, 1935.

17 Y. Xuan, Q. Li, and W. Hu, "Aggregation structure and thermal conductivity of nanofluids," AIChE Journal, vol. 49, no. 4, pp. 1038–1043, 2003.

18 C.-J. Yu, A. Richter, A. Datta, M. Durbin, and P. Dutta, "Molecular layering in a liquid on a solid substrate: an x-ray reflectivity study," Physica B: Condensed Matter, vol. 283, no. 1-3, pp. 27–31, 2000.

19 W. Yu and S. Choi, "The role of interfacial layers in the enhanced thermal conductivity of nanofluids: a renovated maxwell model," Journal of nanoparticle research, vol. 5, no. 1, pp. 167–171, 2003.

20 S. E. B. Maiga, S. J. Palm, C. T. Nguyen, G. Roy, and N. Galanis, "Heat transfer enhancement by using nanofluids in forced convection flows," International journal of heat and fluid flow, vol. 26, no. 4, pp. 530–546, 2005.

21 K. Khanafer and K. Vafai, "A critical synthesis of thermophysical characteristics of nanofluids," International journal of heat and mass transfer, vol. 54, no. 19-20, pp. 4410–4428, 2011.

22 C. Ho, W. Liu, Y. Chang, and C. Lin, "Natural convection heat transfer of alumina-water nanofluid in vertical square enclosures: An experimental study," International Journal of Thermal Sciences, vol. 49, no. 8, pp. 1345–1353, 2010.

23 H. Ş. Aybar, M. Sharifpur, M. R. Azizian, M. Mehrabi, and J. P. Meyer, "A review of thermal conductivity models for nanofluids," Heat Transfer Engineering, vol. 36, no. 13, pp. 1085–1110, 2015.

24 M. Saqib, I. Khan, S. Shafie, and A. Qushairi, "Recent advancement in thermopgycial properties of nanofluids and hybrid nanofluids: An overview," City Univ. Int. J. Comput. Anal, vol. 3, no. 2, pp. 16–25, 2019.

25 A. Einstein, "Eine neue bestimmung der molekuldimensionen," Ann. Phys., vol. 34, pp. 591–592, 1911.

26 H. C. Brinkman, "The viscosity of concentrated suspensions and solutions," The Journal of chemical physics, vol. 20, no. 4, pp. 571–571, 1952.

27 S. Hussain, S. E. Ahmed, and T. Akbar, "Entropy generation analysis in mhd mixed convection of hybrid nanofluid in an open cavity with a horizontal channel containing an adiabatic obstacle," International Journal of Heat and Mass Transfer, vol. 114, pp. 1054–1066, 2017.

28 U. Farooq, M. I. Afridi, M. Qasim, and D. Lu, "Transpiration and viscous dissipation effects on entropy generation in hybrid nanofluid flow over a nonlinear radially stretching disk," Entropy, vol. 20, no. 9, p. 668, 2018.

29 P. K. Singh, K. Anoop, T. Sundararajan, and S. K. Das, "Entropy generation due to flow and heat transfer in nanofluids," International Journal of Heat and Mass Transfer, vol. 53, no. 21-22, pp. 4757–4767, 2010.

30 O. Mahian, A. Kianifar, C. Kleinstreuer, A.-N. Moh' d A, I. Pop, A. Z. Sahin, and S. Wongwises, "A review of entropy generation in nanofluid flow," International Journal of Heat and Mass Transfer, vol. 65, pp. 514–532, 2013.

31 R. B. Mansour, N. Galanis, and C. T. Nguyen, "Effect of uncertainties in physical properties on forced convection heat transfer with nanofluids," Applied Thermal Engineering, vol. 27, no. 1, pp. 240–249, 2007.

32 M. Akbari, N. Galanis, and A. Behzadmehr, "Comparative analysis of single and two-phase models for cfd studies of nanofluid heat transfer," International Journal of Thermal Sciences, vol. 50, no. 8, pp. 1343–1354, 2011.

33 J. Buongiorno, "Convective transport in nanofluids," 2006.

34 Y. Xuan and W. Roetzel, "Conceptions for heat transfer correlation of nanofluids," International Journal of heat and Mass transfer, vol. 43, no. 19, pp. 3701–3707, 2000.

35 S. E. B. Maïga, C. T. Nguyen, N. Galanis, and G. Roy, "Heat transfer behaviours of nanofluids in a uniformly heated tube," Superlattices and Microstructures, vol. 35, no. 3-6, pp. 543–557, 2004.

36 G. Roy, C. T. Nguyen, and P.-R. Lajoie, "Numerical investigation of laminar flow and heat transfer in a radial flow cooling system with the use of nanofluids," Superlattices and Microstructures, vol. 35, no. 3-6, pp. 497–511, 2004.

37 G. Saha and M. C. Paul, "Investigation of the characteristics of nanofluids flow and heat transfer in a pipe using a single phase model," International Communications in Heat and Mass Transfer, vol. 93, pp. 48–59, 2018.

38 H. Demir, A. Dalkilic, N. Kürekci, W. Duangthongsuk, and S. Wongwises, "Numerical investigation on the single phase forced convection heat transfer characteristics of tio2 nanofluids in a double-tube counter flow heat exchanger," International Communications in Heat and Mass Transfer, vol. 38, no. 2, pp. 218–228, 2011.

39 P. K. Namburu, D. K. Das, K. M. Tanguturi, and R. S. Vajjha, "Numerical study of turbulent flow and heat transfer characteristics of nanofluids considering variable properties," International journal of thermal sciences, vol. 48, no. 2, pp. 290–302, 2009.

40 M. K. Moraveji, M. Darabi, S. M. H. Haddad, and R. Davarnejad, "Modeling of convective heat transfer of a nanofluid in the developing region of tube flow with fluid dynamics," International communications in heat and mass transfer, vol. 38, no. 9, pp. 1291–1295, 2011.

41 O. Manca, S. Nardini, and D. Ricci, "A numerical study of nanofluid forced convection in ribbed channels," Applied Thermal Engineering, vol. 37, pp. 280–292, 2012.

42 M. Ahmed, M. Yaseen, and M. Yusoff, "Numerical study of convective heat transfer from tube bank in cross flow using nanofluid," Case studies in thermal engineering, vol. 10, pp. 560–569, 2017.

43 R. S. Vajjha, D. K. Das, and P. K. Namburu, "Numerical study of fluid dynamic and heat transfer performance of al2o3 and cuo nanofluids in the flat tubes of a radiator," International Journal of Heat and fluid flow, vol. 31, no. 4, pp. 613–621, 2010.

44 S. Z. Heris, M. N. Esfahany, and G. Etemad, "Numerical investigation of nanofluid laminar convective heat transfer through a circular tube," Numerical Heat Transfer, Part A: Applications, vol. 52, no. 11, pp. 1043–1058, 2007.

45 S. Özerinç, A. G. Yazıcıoğlu, and S. Kakaç, "Numerical analysis of laminar forced convection with temperature-dependent thermal conductivity of nanofluids and thermal dispersion," International journal of thermal sciences, vol. 62, pp. 138–148, 2012.

46 A. Mokmeli and M. Saffar-Avval, "Prediction of nanofluid convective heat transfer using the dispersion model," International Journal of Thermal Sciences, vol. 49, no. 3, pp. 471–478, 2010.

47 K. Khanafer, K. Vafai, and M. Lightstone, "Buoyancy-driven heat transfer enhancement in a two-dimensional enclosure utilizing nanofluids," International journal of heat and mass transfer, vol. 46, no. 19, pp. 3639–3653, 2003.

48 M. S. Mojarrad, A. Keshavarz, and A. Shokouhi, "Nanofluids thermal behavior analysis using a new dispersion model along with single-phase," Heat and mass transfer, vol. 49, no. 9, pp. 1333–1343, 2013.

49 M. Bahiraei and S. M. Hosseinalipour, "Thermal dispersion model compared with euler-lagrange approach in simulation of convective heat transfer for nanoparticle suspensions," Journal of dispersion science and technology, vol. 34, no. 12, pp. 1778–1789, 2013.

50 J.-C. Yang, F.-C. Li, W.-H. Cai, H.-N. Zhang, and B. Yu, "On the mechanism of convective heat transfer enhancement in a turbulent flow of nanofluid investigated by dns and analyses of pod and fsp," International Journal of Heat and Mass Transfer, vol. 78, pp. 277–288, 2014.

51 M. Ameri, M. Amani, and P. Amani, "Thermal performance of nanofluids in metal foam tube: Thermal dispersion model incorporating heterogeneous distribution of nanoparticles," Advanced Powder Technology, vol. 28, no. 10, pp. 2747–2755, 2017.

52 M. Bahiraei and S. I. Vasefi, "A novel thermal dispersion model to improve prediction of nanofluid convective heat transfer," Advanced Powder Technology, vol. 25, no. 6, pp. 1772–1779, 2014.

53 F. Akbaridoust, M. Rakhsha, A. Abbassi, and M. Saffar-Avval, "Experimental and numerical investigation of nanofluid heat transfer in helically coiled tubes at constant wall temperature using dispersion model," International Journal of Heat and Mass Transfer, vol. 58, no. 1-2, pp. 480–491, 2013.

54 S. Kumar, S. K. Prasad, and J. Banerjee, "Analysis of flow and thermal field in nanofluid using a single phase thermal dispersion model," Applied Mathematical Modelling, vol. 34, no. 3, pp. 573–592, 2010.

55 M. Bahiraei and S. M. Hosseinalipour, "Accuracy enhancement of thermal dispersion model in prediction of convective heat transfer for nanofluids considering the effects of particle migration," Korean Journal of Chemical Engineering, vol. 30, no. 8, pp. 1552–1558, 2013.

56 F. Garoosi, L. Jahanshaloo, M. M. Rashidi, A. Badakhsh, and M. E. Ali, "Numerical simulation of natural convection of the nanofluid in heat exchangers using a buongiorno model," Applied Mathematics and Computation, vol. 254, pp. 183–203, 2015.

57 F. Garoosi, S. Garoosi, and K. Hooman, "Numerical simulation of natural convection and mixed convection of the nanofluid in a square cavity using buongiorno model," Powder technology, vol. 268, pp. 279–292, 2014.

58 M. A. Sheremet and I. Pop, "Conjugate natural convection in a square porous cavity filled by a nanofluid using buongiorno' s mathematical model," International Journal of Heat and Mass Transfer, vol. 79, pp. 137–145, 2014.

59 N. Shehzad, A. Zeeshan, R. Ellahi, and K. Vafai, "Convective heat transfer of nanofluid in a wavy channel: Buongiorno's mathematical model," Journal of Molecular Liquids, vol. 222, pp. 446–455, 2016.

60 S. Nadeem, A. Khan, and S. Saleem, "A comparative analysis on different nanofluid models for the oscillatory stagnation point flow," The European Physical Journal Plus, vol. 131, no. 8, pp. 1–14, 2016.

61 L. Fan and C. Zhu, "Dense-phase fluidized beds," Principles of gas-solid flows, pp. 371–420, 1998.

62 D. Gidaspow, Multiphase flow and fluidization: continuum and kinetic theory descriptions. Academic press, 1994.

63 Z. Zhang and Q. Chen, "Comparison of the eulerian and lagrangian methods for predicting particle transport in enclosed spaces," Atmospheric environment, vol. 41, no. 25, pp. 5236–5248, 2007.

64 P. K. Singh, P. Harikrishna, T. Sundararajan, and S. K. Das, "Experimental and numerical investigation into the hydrodynamics of nanofluids in microchannels," Experimental Thermal and Fluid Science, vol. 42, pp. 174–186, 2012.

65 Y. Sato, E. Deutsch, and O. Simonin, "Direct numerical simulations of heat transfer by solid particles suspended in homogeneous isotropic turbulence," International journal of heat and fluid flow, vol. 19, no. 2, pp. 187–192, 1998.

66 N. Aziz, "Mhd boundary layer flow of williamson nanofluid with the effect of cattaneo-christov heat flux," 2018.

67 S. Rostami, S. Aghakhani, A. Hajatzadeh Pordanjani, M. Afrand, G. Cheraghian, H. F. Oztop, and M. S. Shadloo, "A review on the control parameters of natural convection in different shaped cavities with and without nanofluid," Processes, vol. 8, no. 9, p. 1011, 2020.

68 F. Irgens, Rheology and non-newtonian fluids, vol. 190. Springer, 2014.

69 H. A. Barnes, J. F. Hutton, and K. Walters, An introduction to rheology, vol. 3. Elsevier, 1989.

70 O. Hassager, "Rheology: An historical perspective. by ri tanner & k. walters. elsevier, 1998. 268 pp. hardback: Isbn 0-444-829458. nlg 368 or us

192.50.*paperback* : *Isbn*0 – 444 – 829466.*nlg*225*orus*114.," Journal of Fluid Mechanics, vol. 446, pp. 409–410, 2001.

71 C. J. Seeton, "Viscosity-temperature correlation for liquids," in International Joint Tribology Conference, vol. 42592, pp. 131–142, 2006.

72 P. J. Halley and M. E. Mackay, "Chemorheology of thermosets—an overview," Polymer Engineering & Science, vol. 36, no. 5, pp. 593–609, 1996.

73 P. C. Mishra, S. Mukherjee, S. K. Nayak, and A. Panda, "A brief review on viscosity of nanofluids," International nano letters, vol. 4, no. 4, pp. 109–120, 2014.

74 I. E. Ireka, "Computational analysis of non-isothermal flow of non-newtonian fluids," 2015.

75 R. P. Chhabra, "Non-newtonian fluids: an introduction," in Rheology of complex fluids, pp. 3–34, Springer, 2010.

76 R. W. Fox, A. T. McDonald, and J. W. Mitchell, Fox and McDonald's introduction to fluid mechanics. John Wiley & Sons, 2020.

77 A. H. P. Skelland, "Non-newtonian flow and heat transfer(book on quantitative relationships for non- newtonian systems, considering classification and fluid behavior of materials with anomalous flow properties)," NEW YORK, JOHN WILEY AND SONS, INC., 1967. 469 P, 1967.

78 E. A. Avallone, T. Baumeister III, and A. Sadegh, Marks' standard handbook for mechanical engineers. McGraw-Hill Education, 2007.

79 R. B. Bird, C. F. Curtiss, R. C. Armstrong, and O. Hassager, Dynamics of polymeric liquids, volume 2: Kinetic theory. Wiley, 1987.

80 A. Lacey, "Diffusion models with blow-up," Journal of and applied mathematics, vol. 97, no. 1-2, pp. 39–49, 1998.

81 T. Chinyoka, "dynamics of a thermally decomposable viscoelastic lubricant under shear," Journal of Fluids Engineering, vol. 130, no. 12, 2008.

82 T. Chinyoka, "Comparative response of newtonian and non-newtonian fluids subjected to exothermic reactions in shear flow," International journal of applied and computational mathematics, vol. 7, no. 3, pp. 1–19, 2021.

83 T. Chinyoka and O. D. Makinde, "Numerical analysis of the transient and non-isothermal channel flow of a third-grade fluid with convective cooling," Engineering Transactions, vol. 68, no. 4, pp. 335–351, 2020.

84 M. David, "Modelling of shear banding in viscoelastic fluids via the giesekus model," 2018.

85 M.-A. Fardin, B. Lasne, O. Cardoso, G. Grégoire, M. Argentina, J.-P. Decruppe, and S. Lerouge, "Taylor-like vortices in shear-banding flow of giant micelles," Physical review letters, vol. 103, no. 2, p. 028302, 2009.

86 T. Chinyoka, "Suction-injection control of shear banding in non-isothermal and exothermic channel flow of johnson-segalman liquids," Journal of fluids engineering, vol. 133, no. 7, 2011.

87 I. Ireka and T. Chinyoka, "Non-isothermal flow of a johnson–segalman liquid in a lubricated pipe with wall slip," Journal of Non-Newtonian Fluid Mechanics, vol. 192, pp. 20–28, 2013.

88 J. G. Abuga and T. Chinyoka, "Numerical study of shear banding in flows of fluids governed by the rolie-poly two-fluid model via stabilized finite volume methods," Processes, vol. 8, no. 7, p. 810, 2020.

89 S. CHAPRA and R. P. Canale, "Numerical methods for engineers: with programing and software applications," 1998.

90 M. Davis, "Finite difference methods," MSc Course in Mathematics and Finance, Imperial College London, 2010.

91 T. Liszka and J. Orkisz, "The finite difference method at arbitrary irregular grids and its application in applied mechanics," Computers & Structures, vol. 11, no. 1-2, pp. 83–95, 1980.

92 I. Khan, T. Chinyoka, and A. Gill, "Computational analysis of the dynamics of generalized-viscoelastic-fluid-based nanofluids subject to exothermic-reaction in shear-flow," Journal of Nanofluids, vol. 11, pp. 487–499, 2022.

93 M. Sheikhpour, M. Arabi, A. Kasaeian, A. R. Rabei, and Z. Taherian, "Role of nanofluids in drug delivery and biomedical technology: Methods and applications," Nanotechnology, Science and Applications, vol. 13, p. 47, 2020.

94 K. V. Wong, Nanotechnology and energy. CRC Press, 2017.

95 Y. Xuan and Q. Li, "Heat transfer enhancement of nanofluids," International Journal of heat and fluid flow, vol. 21, no. 1, pp. 58–64, 2000.

96 J. A. Eastman, S. Choi, S. Li, W. Yu, and L. Thompson, "Anomalously increased effective thermal conductivities of ethylene glycol-based nanofluids containing copper nanoparticles," Applied physics letters, vol. 78, no. 6, pp. 718–720, 2001.

97 S. Lee, S.-S. Choi, S. Li, , and J. Eastman, "Measuring thermal conductivity of fluids containing oxide nanoparticles," 1999.

98 S. Özerinç, S. Kakaç, and A. G. Yazıcıoğlu, "Enhanced thermal conductivity of nanofluids: a state-of-the-art review," Microfluidics and Nanofluidics, vol. 8, no. 2, pp. 145–170, 2010.

99 Y. Xuan and Q. Li, "Investigation on convective heat transfer and flow features of nanofluids," J. Heat transfer, vol. 125, no. 1, pp. 151–155, 2003.

100 V. Terekhov, S. Kalinina, and V. Lemanov, "The mechanism of heat transfer in nanofluids: state of the art (review). part 1. synthesis and properties of nanofluids," Thermophysics and Aeromechanics, vol. 17, no. 1, pp. 1–14, 2010.

101 P. Keblinski, S. Phillpot, S. Choi, and J. Eastman, "Mechanisms of heat flow in suspensions of nano-sized particles (nanofluids)," International journal of heat and mass transfer, vol. 45, no. 4, pp. 855–863, 2002.

102 A. Behzadmehr, M. Saffar-Avval, and N. Galanis, "Prediction of turbulent forced convection of a nanofluid in a tube with uniform heat flux using a two phase approach," International journal of heat and fluid flow, vol. 28, no. 2, pp. 211–219, 2007.

103 M. Kalteh, A. Abbassi, M. Saffar-Avval, and J. Harting, "Eulerian–eulerian two-phase numerical simulation of nanofluid laminar forced convection in a microchannel," International journal of heat and fluid flow, vol. 32, no. 1, pp. 107–116, 2011.

104 S. Kondaraju, E. Jin, and J. Lee, "Investigation of heat transfer in turbulent nanofluids using direct numerical simulations," Physical Review E, vol. 81, no. 1, p. 016304, 2010.

105 L. S. Sundar, M. Naik, K. Sharma, M. Singh, and T. C. S. Reddy, "Experimental investigation of forced convection heat transfer and friction factor in a tube with fe3o4 magnetic nanofluid," Experimental Thermal and Fluid Science, vol. 37, pp. 65–71, 2012.

106 A. Sajadi and M. Kazemi, "Investigation of turbulent convective heat transfer and pressure drop of tio2/water nanofluid in circular tube," International Communications in Heat and Mass Transfer, vol. 38, no. 10, pp. 1474–1478, 2011.

107 B. A. Toms, "Some observations on the flow of linear polymer solutions through straight tubes at large reynolds numbers," Proc. of In. Cong. On Rheology, 1948, vol. 135, 1948.

108 F.-C. Li, Y. Kawaguchi, and K. Hishida, "Investigation on the characteristics of turbulence transport for momentum and heat in a drag-reducing surfactant solution flow," Physics of Fluids, vol. 16, no. 9, pp. 3281–3295, 2004.

109 Y. Qi, Y. Kawaguchi, R. N. Christensen, and J. L. Zakin, "Enhancing heat transfer ability of drag reducing surfactant solutions with static mixers and honeycombs," International Journal of Heat and Mass Transfer, vol. 46, no. 26, pp. 5161–5173, 2003.

110 J.-C. Yang, F.-C. Li, W.-W. Zhou, Y.-R. He, and B.-C. Jiang, "Experimental investigation on the thermal conductivity and shear viscosity of viscoelastic-fluid-based nanofluids," International Journal of Heat and Mass Transfer, vol. 55, no. 11-12, pp. 3160–3166, 2012.

111 Z.-H. Liu and L. Liao, "Forced convective flow and heat transfer characteristics of aqueous drag-reducing fluid with carbon nanotubes added," International Journal of Thermal Sciences, vol. 49, no. 12, pp. 2331–2338, 2010.

112 T. Chinyoka, S. Goqo, and B. Olajuwon, "Computational analysis of gravity driven flow of a variable viscosity viscoelastic fluid down an inclined plane," Computers & Fluids, vol. 84, pp. 315–326, 2013.

113 P. K. Kambhatla, O. Ojjela, and S. K. Das, "Viscoelastic model of ethylene glycol with temperature-dependent thermophysical properties," Journal of Thermal Analysis and Calorimetry, vol. 135, no. 2, pp. 1257–1268, 2019.

114 G. Peters, Thermorheological modelling of viscoelastic materials. In IUTAM Symposium on Numerical simulation of non-isothermal ow of viscoelastic liquids (pp. 21- 35). Springer, Dordrecht., 1995.

115 P. Wapperom and M. A. Hulsen, "Thermodynamics of viscoelastic fluids: the temperature equation," Journal of Rheology, vol. 42, no. 5, pp. 999–1019, 1998.

116 T. Chinyoka, "Viscoelastic effects in double-pipe single-pass counterflow heat exchangers," International journal for numerical methods in fluids, vol. 59, no. 6, pp. 677–690, 2009.

117 T. Chinyoka, "Computational dynamics of a thermally decomposable viscoelastic lubricant under shear," Journal of Fluids Engineering, vol. 130, no. 12, 2008.

118 H. Patel, S. Shah, R. Ahmed, and S. Ucan, "Effects of nanoparticles and temperature on heavy oil viscosity," Journal of Petroleum Science and Engineering, vol. 167, pp. 819–828, 2018.

119 I. Ireka and T. Chinyoka, "Analysis of shear banding phenomena in non-isothermal flow of fluids governed by the diffusive johnson–segalman model," Applied Mathematical Modelling, vol. 40, no. 5-6, pp. 3843–3859, 2016.

120 M. VeeraKrishna, G. Subba Reddy, and A. Chamkha, "Hall effects on unsteady mhd oscillatory free convective flow of second grade fluid through porous medium between two vertical plates," Physics of fluids, vol. 30, no. 2, p. 023106, 2018.

121 M. V. Krishna, K. Jyothi, and A. J. Chamkha, "Heat and mass transfer on unsteady, magnetohydrodynamic, oscillatory flow of second-grade fluid through a porous medium between two vertical plates, under the influence of fluctuating heat source/sink, and chemical reaction," International Journal of Fluid Mechanics Research, vol. 45, no. 5, 2018.

122 A. I. Alsabery, M. A. Ismael, E. Gedik, A. J. Chamkha, and I. Hashim, "Transient nanofluid flow and energy dissipation from wavy surface using magnetic field and two rotating cylinders," Computers & Mathematics with Applications, vol. 97, pp. 329–343, 2021.

123 S. HAZARIKA, S. AHMED, and A. J. CHAMKHA, "Analysis of platelet shape al2o3 and tio2 on heat generative hydromagnetic nanofluids for the base fluid c2h6o2 in a vertical channel of porous medium," Walailak Journal of Science and Technology (WJST), vol. 18, no. 14, pp. 21424–19, 2021.

124 A. J. Chamkha, A. Dogonchi, and D. Ganji, "Magneto-hydrodynamic flow and heat transfer of a hybrid nanofluid in a rotating system among two surfaces in the presence of thermal radiation and joule heating," AIP Advances, vol. 9, no. 2, p. 025103, 2019.

125 J. Raza, F. Mebarek-Oudina, A. Chamkha, et al., "Multidiscipline modeling in materials and structures," Materials and Structures, vol. 15, no. 4, pp. 737–757, 2019.

126 A. J. Chamkha, "Non-darcy fully developed mixed convection in a porous medium channel with heat generation/absorption and hydromagnetic effects," Numerical Heat Transfer, Part A Applications, vol. 32, no. 6, pp. 653–675, 1997.

127 A. J. Chamkha, "On laminar hydromagnetic mixed convection flow in a vertical channel with symmetric and asymmetric wall heating conditions," International Journal of Heat and Mass Transfer, vol. 45, no. 12, pp. 2509–2525, 2002.

128 A. J. Chamkha, "Unsteady laminar hydromagnetic fluid–particle flow and heat transfer in channels and circular pipes," International Journal of Heat and Fluid Flow, vol. 21, no. 6, pp. 740–746, 2000.

129 T. Chinyoka, Y. Renardy, M. Renardy, and D. Khismatullin, "Two-dimensional study of drop deformation under simple shear for oldroyd-b liquids," Journal of Non-Newtonian Fluid Mechanics, vol. 130, no. 1, pp. 45–56, 2005.

130 Y. Renardy, M. Renardy, D. Khismatullin, and T. Chinyoka, "A viscoelastic vof-prost code for the study of drop deformation," in APS Division of Fluid Dynamics Meeting Abstracts, vol. 57, pp. MB–008, 2004.

131 I. Khan, T. Chinyoka, and A. Gill, "Dynamics of non-isothermal pressure-driven flow of generalized viscoelastic-fluid-based nanofluids in a channel," Mathematical Problems in Engineering, vol. 2022, ID 9080009, p. 17, 2022, https://doi.org/10.1155/2022/9080009.

132 I. Animasaun, S.-J. Yook, T. Muhammad, and A. Mathew, "Dynamics of ternary-hybrid nanofluid subject to magnetic flux density and heat source or sink on a convectively heated surface," Surfaces and Interfaces, vol. 28, p. 101654, 2022.

133 X. Sun, I. L. Animasaun, K. Swain, N. A. Shah, A. Wakif, and P. O. Olanrewaju, "Significance of nanoparticle radius, inter-particle spacing, inclined magnetic field, and space-dependent internal heating: The case of chemically reactive water conveying copper nanoparticles," ZAMM-Journal of Applied Mathematics and Mechanics/Zeitschrift für Angewandte Mathematik und Mechanik, p. e202100094, 2021.

134 K. V. Wong and O. De Leon, "Applications of nanofluids: current and future," in Nanotechnology and Energy, pp. 105–132, Jenny Stanford Publishing, 2017.

135 F.-C. Li, J.-C. Yang, W.-W. Zhou, Y.-R. He, Y.-M. Huang, and B.-C. Jiang, "Experimental study on the characteristics of thermal conductivity and shear viscosity of viscoelastic-fluid-based nanofluids containing multiwalled carbon nanotubes," Thermochimica Acta, vol. 556, pp. 47–53, 2013.

136 C. Kleinstreuer and Y. Feng, "Experimental and theoretical studies of nanofluid thermal conductivity enhancement: a review," Nanoscale research letters, vol. 6, no. 1, pp. 1–13, 2011.

137 M. Chandrasekar and S. Suresh, "Determination of heat transport mechanism in aqueous nanofluids using regime diagram," Chinese Physics Letters, vol. 26, no. 12, p. 124401, 2009.

138 Z. Xiao-Feng and G. Lei, "Effect of multipolar interaction on the effective thermal conductivity of nanofluids," Chinese Physics, vol. 16, no. 7, p. 2028, 2007.

139 T. Chinyoka, "Poiseuille flow of reactive phan–thien–tanner liquids in 1d channel flow," Journal of Heat Transfer, vol. 132, no. 11, 2010.

140 E. R. El-Zahar, A. Algelany, and A. M. Rashad, "Sinusoidal natural convective flow of non-newtonian nanoliquid over a radiative vertical plate in a saturated porous medium," IEEE Access, vol. 8, pp. 136131–136140, 2020.

141 I. Khan, T. Chinyoka, and A. Gill, "Computational analysis of shear banding in simple shear flow of viscoelastic fluid-based nanofluids subject to exothermic reactions," Energies, vol. 15, no. 5, p. 1719, 2022.

142 J. Abuga and T. Chinyoka, "Benchmark solutions of the stabilized computations of flows of fluids governed by the rolie-poly constitutive model," Journal of Physics Communications, vol. 4, no. 1, p. 015024, 2020.

143 T. Chinyoka, "Modeling of cross-flow heat exchangers with viscoelastic fluids," Nonlinear Analysis: Real World Applications, vol. 10, no. 6, pp. 3353–3359, 2009.

144 T. Chinyoka, Numerical simulation of stratified flows and droplet deformation in two-dimensional shear flow of Newtonian and viscoelastic fluids. PhD thesis, Virginia Polytechnic Institute and State University, 2004.

145 J. Garcı, O. Manero, F. Bautista, J. Puig, et al., "Inhomogeneous flows and shear banding formation in micellar solutions: Predictions of the bmp model," Journal of Non-Newtonian Fluid Mechanics, vol. 179, pp. 43–54, 2012.

146 Y. Kim, A. Adams, W. H. Hartt, R. G. Larson, and M. J. Solomon, "Transient, near-wall shear-band dynamics in channel flow of wormlike micelle solutions," Journal of Non-Newtonian Fluid Mechanics, vol. 232, pp. 77–87, 2016.

147 L. Hilliou and D. Vlassopoulos, "Time-periodic structures and instabilities in shear-thickening polymer solutions," Industrial & engineering chemistry research, vol. 41, no. 25, pp. 6246–6255, 2002.

148 A. Kabla and G. Debrégeas, "Local stress relaxation and shear banding in a dry foam under shear," Physical review letters, vol. 90, no. 25, p. 258303, 2003.

149 J. Billen, M. Wilson, and A. R. Baljon, "Shear banding in simulated telechelic polymers," Chemical Physics, vol. 446, pp. 7–12, 2015.

150 D. M. Mueth, G. F. Debregeas, G. S. Karczmar, P. J. Eng, S. R. Nagel, and H. M. Jaeger, "Signatures of granular microstructure in dense shear flows," Nature, vol. 406, no. 6794, pp. 385–389, 2000.

151 W. M. Holmes, P. T. Callaghan, D. Vlassopoulos, and J. Roovers, "Shear banding phenomena in ultrasoft colloidal glasses," Journal Of Rheology, vol. 48, no. 5, pp. 1085–1102, 2004.

152 Y. Fang, G. Wang, N. Tian, X. Wang, X. Zhu, P. Lin, G. Ma, and L. Li, "Shear inhomogeneity in poly (ethylene oxide) melts," Journal of Rheology, vol. 55, no. 5, pp. 939–949, 2011.

153 I. Khan, T. Chinyoka, and A. Gill, "Computational-analysis of the non-isothermal dynamics of gravity-driven flows of viscoelastic-fluid-based nanofluids down an inclined plane," Fluid Dynamics & Materials Processing, In press, 2022.

154 T. Chinyoka, S. Goqo, and B. Olajuwon, "analysis of gravity driven flow of a variable viscosity viscoelastic fluid down an inclined plane," Computers & Fluids, vol. 84, pp. 315–326, 2013.

155 K. V. Wong and O. De Leon, "Applications of nanofluids: current and future," Advances in mechanical engineering, vol. 2, p. 519659, 2010.